

5-1-2019

The Development of a Viscoelastic Ellipsoidal Model for use in Measuring Plantar Tissue Material Properties during Walking

Jessica Lee DeBerardinis
deberardinis.jessica@gmail.com

Follow this and additional works at: <https://digitalscholarship.unlv.edu/thesesdissertations>



Part of the [Biomedical Engineering and Bioengineering Commons](#), [Engineering Science and Materials Commons](#), [Materials Science and Engineering Commons](#), and the [Mechanical Engineering Commons](#)

Repository Citation

DeBerardinis, Jessica Lee, "The Development of a Viscoelastic Ellipsoidal Model for use in Measuring Plantar Tissue Material Properties during Walking" (2019). *UNLV Theses, Dissertations, Professional Papers, and Capstones*. 3593.

<https://digitalscholarship.unlv.edu/thesesdissertations/3593>

This Dissertation is protected by copyright and/or related rights. It has been brought to you by Digital Scholarship@UNLV with permission from the rights-holder(s). You are free to use this Dissertation in any way that is permitted by the copyright and related rights legislation that applies to your use. For other uses you need to obtain permission from the rights-holder(s) directly, unless additional rights are indicated by a Creative Commons license in the record and/or on the work itself.

This Dissertation has been accepted for inclusion in UNLV Theses, Dissertations, Professional Papers, and Capstones by an authorized administrator of Digital Scholarship@UNLV. For more information, please contact digitalscholarship@unlv.edu.

THE DEVELOPMENT OF A VISCOELASTIC ELLIPSOIDAL MODEL FOR USE IN MEASURING
PLANTAR TISSUE MATERIAL PROPERTIES DURING WALKING

By

Jessica Lee DeBerardinis

Bachelor of Science – Biomedical Engineering

University of Utah

2012

A dissertation submitted in partial fulfillment
of the requirements for the

Doctor of Philosophy – Mechanical Engineering

Department of Mechanical Engineering

Howard R. Hughes College of Engineering

The Graduate College

University of Nevada, Las Vegas

May 2019



Dissertation Approval

The Graduate College
The University of Nevada, Las Vegas

April 11, 2019

This dissertation prepared by

Jessica Lee DeBerardinis

entitled

The Development of a Viscoelastic Ellipsoidal Model for Use in Measuring Plantar
Tissue Material Properties during Walking

is approved in partial fulfillment of the requirements for the degree of

Doctor of Philosophy – Mechanical Engineering
Department of Mechanical Engineering

Mohamed B. Trabia, Ph.D.
Examination Committee Co-Chair

Kathryn Hausbeck Korgan, Ph.D.
Graduate College Dean

Janet S. Dufek, Ph.D.
Examination Committee Co-Chair

Jaeyun Moon, Ph.D.
Examination Committee Member

Woosoon Yim, Ph.D.
Examination Committee Member

Brendan O'Toole, Ph.D.
Examination Committee Member

Julia Freedman Silvernail, Ph.D.
Graduate College Faculty Representative

Abstract

Introduction: The mechanical characteristics of the plantar tissues during walking is not well understood as most of the current research focuses on testing specific plantar regions in cadavers or while the feet of the participants are raised. In this work, it is hypothesized that a viscoelastic geometric ellipsoid model used to assess multiple structures of the foot would be accurate and robust. This model would be participant-specific and applicable to the entire stance phase of gait.

Methods: The proposed viscoelastic ellipsoid model would represent several key anatomical areas: Heel, Posterior Midfoot, Anterior Midfoot, Metatarsals 1-2, Metatarsals 3-5, Toe 1, Toe 2, and Toes 3-5. The ellipsoid model required measurement of force and contact area simultaneously. This was done using pressure-measuring insoles (Medilogic ®, Schönefeld, Germany), worn by multiple, college-aged participants. The insole force and area data were used to optimize the model for each participant as the material properties and geometry of each participant's foot will differ.

Results: The results of the model application was able to show that the ellipsoid model was fairly successful in producing the ground reaction force during walking. Further, the ellipsoid model was able to characterize stiffness and damping results, that were different for all the plantar regions. These results were also different from previous research that used data from mechanical tests and experiments where the participant's foot was static.

Conclusion: The viscoelastic ellipsoidal model was able to reproduce ground reaction force and determine the unique mechanical characteristics for each plantar region. Future uses of the model will be with clinical data collected from persons with plantar diseases, which could lead to predictions and preventions of plantar disease.

I would like to dedicate this work to my family, friends, and advisors.

I will forever be grateful for their support.

Table of Contents

<u>Abstract</u>	iii
<u>Table of Contents</u>	v
<u>List of Tables</u>	ix
<u>List of Figures</u>	xi
1. <u>Introduction</u>	1
1.1. <i>Background</i>	1
1.2. <i>Models for the Mechanical Characteristics of Plantar Tissues</i>	3
1.2.1. <i>Linear plantar tissue material models</i>	4
1.2.2. <i>Nonlinear plantar tissue material models: Load-deformation</i>	5
1.2.3. <i>Nonlinear plantar tissue material models: Hysteresis</i>	7
1.2.4. <i>Nonlinear plantar tissue material models: Nonlinear spring-damper</i>	8
1.2.5. <i>Nonlinear plantar tissue material models: Quasi-linear, viscoelastic</i>	9
1.2.6. <i>Nonlinear plantar tissue material models: Hyperelastic</i>	11
1.2.7. <i>Nonlinear plantar tissue material models: Visco-hyperelastic</i>	14
1.2.8. <i>Nonlinear plantar tissue material models: Varying contact area</i>	15
1.3. <i>Research hypothesis</i>	17
1.4. <i>Research Objectives</i>	18
2. <u>Viscoelastic ellipsoidal model of plantar soft tissues</u>	19
2.1. <i>Ellipsoid model placement and description</i>	19

2.2.	<i>Ellipsoid model kinematics</i>	22
2.3.	<i>Ellipsoid Model Kinetics</i>	24
2.4.	<i>Relating Ellipsoid deformation to contact area</i>	25
2.5.	<i>Final model</i>	27
3.	<u>The use of pressure-measuring insoles to assess ground reaction force and contact area</u>	29
3.1.	<i>Pressure-measuring insoles</i>	29
3.2.	<i>Using the insoles to collect walking data</i>	31
3.3.	<i>Pre-processing the insole data</i>	34
3.3.1.	<i>Determining the times of stance phase</i>	34
3.3.2.	<i>Using an adaptive threshold to pre-process the sensor data</i>	36
3.4.	<i>Determining vertical ground reaction force using pressure-measuring insoles</i>	39
3.5.	<i>Determining plantar contact area using pressure-measuring insoles</i>	41
3.6.	<i>Summary</i>	43
4.	<u>Determining the elliptical contact area</u>	44
4.1.	<i>Fitting an ellipse to the contact areas</i>	44
4.1.1.	<i>Case 1 – Isolated active area(s)</i>	44
4.1.2.	<i>Case 2 – Active area forming a rectangle</i>	46
4.1.3.	<i>Case 3 – Active area forming an irregular shape</i>	47
4.1.4.	<i>Case 4 – Active sensor forming an irregular shape with large aspect ratio</i> ...	50

4.2.	<i>Performance assessment</i>	52
4.2.1.	<i>Results of performance assessment</i>	53
4.2.2.	<i>Discussion of the performance assessment.</i>	56
5.	<u>Application of ellipsoid model on each region of the foot</u>	57
5.1.	<i>Insole data preprocessing</i>	57
5.1.1.	<i>Preprocessing the area-time curve</i>	57
5.1.2.	<i>Preprocessing the force-time curve</i>	58
5.2.	<i>Identification of the plantar tissue model of each participant</i>	59
5.2.1.	<i>Objective function and model penalty</i>	59
5.2.2.	<i>Determining boundaries for each anatomical region</i>	61
5.2.3.	<i>Nonlinear multivariate identification</i>	61
5.3.	<i>Results of model application</i>	62
5.3.1.	<i>Comparing the model output to experimental ground reaction forces.</i>	63
5.3.2.	<i>Plantar tissue model variable results</i>	66
5.4.	<i>Discussion of plantar tissue model application results</i>	68
6.	<u>Conclusion and future work</u>	70
	<u>Appendix A. Sensor Maps of Medilogic Pressure-Measuring Insoles</u>	74
	<u>Appendix B - Sensor Maps of Medilogic Pressure-Measuring Insoles</u>	75
	<u>Appendix C – IRB Approval of Protocol #724468-5.</u>	81
	<u>Appendix D - Boundary Method used for Verification of Neighbors</u>	83

<u>Appendix E - Ellipse fitting method</u>	84
<u>Appendix F – Results of Ellipse Fitting for Participant 112, Trial 1 – Left Foot</u>	85
<u>Appendix G – Results of Ellipse Fitting for Participant 112, Trial 1 – Right Foot</u>	112
<u>Appendix H – Variable boundaries used for model optimization</u>	143
<u>Appendix I – Variable and NRMSE results from model application</u>	151
<u>References</u>	157
<u>Curriculum Vitae</u>	164

List of Tables

Table 1. The number of sensors in each insole size.....	30
Table 2. The threshold (percentage of the maximum summed bits) used for each insole size (Lidstone et al., 2019).....	37
Table 3. The number of occurrences that each of the Case methods was used for each anatomical area for each case. The Cases are as follows: Case 1 – there were only individual sensors; Case 2 – the sensor area was rectangular; Case 3 – the sensor area was irregularly shaped; and Case 4 – the sensor area formed a long shape.	54
Table 4. The normalized area results of Case 3. The ellipses fitted to the Neighbors method were compared to the validation method (Boundary).	55
Table 5. The NRMSE results of exemplar data from the right foot of a participant who wore size 37-38 insole.....	65
Table B. 1. The sensors for the insole size 35-36 grouped into anatomical regions.....	75
Table B. 2. The sensors for the insole size 37-38 grouped into anatomical regions.....	76
Table B. 3. The sensors for the insole size 39-40 grouped into anatomical regions.....	77
Table B. 4. The sensors for the insole size 41-42 grouped into anatomical regions.....	78
Table B. 5. The sensors for the insole size 43-44 grouped into anatomical regions.....	79
Table B. 6. The sensors for the insole size 45-46 grouped into anatomical regions.....	80
Table H. 1. The lower and upper bounds of the material variables.	143
Table I. 1. The ellipsoid variable results for each anatomical region of insole size 35-36. Shown as average (standard deviation).....	151
Table I. 2. The ellipsoid variable results for each anatomical region of insole size 37-38. Shown as average (standard deviation).....	152

Table I. 3. The ellipsoid variable results for each anatomical region of insole size 39-40. Shown as average (standard deviation)..... 153

Table I. 4. The ellipsoid variable results for each anatomical region of insole size 41-42. Shown as average (standard deviation)..... 154

Table I. 5. The ellipsoid variable results for each anatomical region of insole size 43-44. Shown as average (standard deviation)..... 155

Table I. 6. The ellipsoid variable results for each anatomical region of insole size 45-46. Shown as average (standard deviation)..... 156

List of Figures

Fig. 1. An anatomical representation of the foot with the rear foot, midfoot, and forefoot sections labeled. Additionally, the bones and anatomical structures are marked. Reprinted from Logan (2012), with permission from Elsevier. Anatomical identification has been added to original figure. 1

Fig. 2. An example of the placement of the ellipsoid models representing the foot. The ellipsoids are placed at the Heel (red), Posterior Midfoot (blue), Anterior Midfoot (green), Metatarsals 1-2 (black), Metatarsals 3-5 (purple), Toe 1 (pink), Toe 2 (orange), Toes 3-5 (gray)..... 20

Fig. 3. A dimensional representation of the ellipsoidal model. A , B , and C represented the major radii of the ellipsoid which is centered at the origin of X , Y , and Z . The total deformation is represented by d with δ representing the local deformation at coordinate (x,y) . The measures r_A and r_B are the radii of the contact area A_e 21

Fig. 4. The elliptical contact area A_e with radii r_A and r_B . The point (x,y) is the location of the local deformation and dA_e is the differential element of the contact area. 22

Fig. 5. (A) The Medilogic® left insole, Size 43-44. (B) The corresponding sensor map where each rectangle represents a single sensor. Image taken from DeBerardinis et al. (2018)..... 30

Fig. 6. A depiction of the sensors sorted into the anatomical regions for the size 37-38 insole (left foot)..... 31

Fig. 7. A flowchart detailing the methods to select the stance time (blue), use an adaptive threshold to identify active sensors (red), determine the ground reaction force (green), and determine the contact area (purple)..... 33

Fig. 8. Shown are several steps recorded by an insole during the walking protocol. The red points are the points selected from the swing phase in order to isolate the step. The time has been adjusted to start at zero. 35

Fig. 9. A step has been isolated from a walking task. Shown in red is the raw, summed bit data collected with the pressure-measuring insole. The blue dashed line shows the step returned to baseline by subtracting the average of the bit values before and after the step. The time has been adjusted to start at zero. 35

Fig. 10. The stance phase of the step was selected by considering only data between the times where the summed bits were measured to be above 142 bits (equivalent to the 40 N threshold for heel strike and toe off), which is marked with the red points. The support time has been adjusted to start at zero..... 36

Fig. 11. These two images show the sensors of the insole that were processed using the adaptive threshold. (A) Before the participant-specific threshold was applied. (B) After the participant-specific threshold was applied. In this example, the threshold is 5 bits, which was 0.2% of the maximum summed bits. The blue sensors seen are sensors considered active while the red sensors are considered inactive. It should be noted any sensor reading less than 5 bits was set to zero and thus, excluded from analysis. 38

Fig. 12. The results of applying the threshold to the insole data where the red is the zeroed summed bit data and blue is the summed bit data after a threshold was applied. In this example, the threshold is 5 bits, which was 0.2% of the maximum summed bits. This threshold only excludes a few sensors that have small bit values which explains the proximity of the raw data and the data processed with the threshold..... 39

Fig. 13. The ground reaction force for each anatomical area: (A) Heel, (B) Midfoot Posterior and Midfoot Anterior, (C) Metatarsals 1-2 and Metatarsals 3-5, (D) Toe 1, Toe 2, and Toes 3-5. 40

Fig. 14. The total ground reaction force calculated by summing the forces of each anatomical area: Heel, Midfoot Posterior, Midfoot Anterior, Metatarsals 1-2, Metatarsals 3-5, Toe 1, Toe 2, and Toes 3-5..... 41

Fig. 15. The contact area for each anatomical area: (A) Heel, (B) Midfoot Posterior and Midfoot Anterior, (C) Metatarsals 1-2 and Metatarsals 3-5, (D) Toe 1, Toe 2, and Toes 3-5. 42

Fig. 16. The total area and for each anatomical area: Heel, Midfoot Posterior , Midfoot Anterior, Metatarsals 1-2, Metatarsals 3-5, Toe 1, Toe 2, and Toes 3-5..... 43

Fig. 17. (A) The isolated sensor in the outermost row of the heel is an exception to Case 1 and would be included for analysis (encircled in yellow). The two other isolated sensors (one in the heel and one in midfoot posterior) would be excluded (encircled in white). (B) The isolated sensor in Toe 1 is an exception to Case 1 and would be included for analysis (encircled in green).
..... 45

Fig. 18. Example of fitting ellipse to rectangular area so that the ellipse area and the rectangle area are equal. Also shown are the rectangular dimensions and radii used in the equations..... 46

Fig. 19. An example of identifying the boundaries of the active sensors area. In the figure, yellow represented active sensors while gray represented the inactive neighboring sensors. The blue circles represent the points placed to identify the boundaries of the active sensors area. 48

Fig. 20. This is an example shape of how the method of Section 4.1.3. (or Case 3), seen in blue, and the *Boundary*, seen in orange, would choose points for ellipse fitting. It should be noted that the validation method does not consider divots whereas the method for Case 3 does consider the divots..... 49

Fig. 21. This is an example of how the ellipses would fit to the sample shape in Fig. 17 using the points chosen with Section 4.1.3. (or Case 3 seen in blue) or the *Boundary* (or the validation method seen in orange) methods. It should be noted the sensor area is 5.625 cm², the ellipse area from Case 3 is 5.9254 cm², and the ellipse area from the validation method is 6.5377 cm²..... 50

Fig. 22. Two examples of long shapes. (A) This example gives a ratio (Eq. 53) of 2.5 and (B) is an example gives a ratio (Eq. 53) of 0.4. In both cases, utilizing the path under Case 3 would result in errors during curve fitting and the methods of Case 4 would need to be used. 51

Fig. 23. An example of a long shape being fitted with an ellipse. It can be seen that the ellipse fitting method results in a poor fit, where the ellipse has an area of 126.51 cm² while the sensors have an area of 6.75 cm². 51

Fig. 24. An exemplar area-time curve for the showing the step-like raw (black line), the moving average smoothing the sharpness of the steps (red dotted line), and the 5th order polynomial fitted to the area (blue dashed line). 58

Fig. 25. An exemplar force-time curve for the heel showing the raw data (black line), and the 5th order polynomial fitted to the force (blue dashed line)..... 59

Fig. 26. An exemplar of curves showing the typical model output and experimental ground reaction force for each plantar region. These data were from the right foot of a participant wearing insole size 37-38. The graphs correspond to the following plantar regions: (a) Heel, (b) Posterior Midfoot, (c) Anterior Midfoot, (d) Metatarsals 1-2, (e) Metatarsals 3-5, (f) Hallux, (g) Toe 2, (h) Toes 3-5..... 63

Fig. 27. An exemplar of curves showing the combined model output, resulting from all of the individual anatomical areas summed together. This is compared to the total experimental ground reaction force. 64

Fig. 28. The NRMSE results for all anatomical regions and insole sizes. 65

Fig. 29. Averages and standard deviations for the plantar tissue model variables: (a) tissue thickness, (b) radius in x axis, (c) radius in y-axis, (d) radius in z-axis, (e) stiffness, (f) stiffness coefficient, (g) damping, and (h) damping coefficient. Values are displayed for each insole size and plantar region. 67

Fig. A.1. (A) Size 35-36 insole with 93 sensors. (B) Size 37-38 insole with 107 sensors. (C) Size 39-40 insole with 116 sensors. (D) Size 41-42 insole with 130 sensors. (E) Size 43-44 insole with 151 sensors. (F) Size 45-46 insole with 162 sensors 74

Fig. D. 1. This figure shows the steps used by the boundary function. (A) Alpha shapes in the form of circles are used to “scoop out” the 2D shape. (B) The Delaunay triangulation is used determine the border (in blue). These images are taken, with permission, from Amenta (2011). 83

Fig. H. 1. The upper (orange triangles) and lower (blue circles) bounds of the geometric variables for the Heel and all insole sizes: (a) tissue thickness (d_0), (b) radii in the x and y axis (A and B), and (c) radius in the z-axis (C). 144

Fig. H. 2. The upper (orange triangles) and lower (blue circles) bounds of the geometric variables for the Midfoot Posterior and Midfoot Anterior: (a) tissue thickness (d_0), (b) radii in the x and y axes (A and B), and (c) radius in the z-axis (C). The bounds are for all insole sizes..... 145

Fig. H. 3. The upper (orange triangles) and lower (blue circles) bounds of the geometric variables for the Metatarsals 1-2 and all insole sizes: (a) tissue thickness (d_0), (b) radii in the x and y axes (A and B), and (c) radius in the z-axis (C). 146

Fig. H. 4. The upper (orange triangles) and lower (blue circles) bounds of the geometric variables for the Metatarsals 3-5 and all insole sizes: (a) tissue thickness (d_0), (b) radii in the x and y axes (A and B), and (c) radius in the z-axis (C). 147

Fig. H. 5. The upper (orange triangles) and lower (blue circles) bounds of the geometric variables for the Hallux and all insole sizes: (a) tissue thickness (d_0), (b) radius in the x-axis (A), (c) radius in the y-axis (B), and (d) radius in the z-axis (C). 148

Fig. H. 6. The upper (orange triangles) and lower (blue circles) bounds of the geometric variables for the Toe 2 and all insole sizes: (a) tissue thickness (d_0), (b) radii in the x-axis (A), (c) radius in the y-axis (B), and (d) radius in the z-axis (C). 149

Fig. H. 7. The upper (orange triangles) and lower (blue circles) bounds of the geometric variables for the Toes 3-5 and all insole sizes: (a) tissue thickness (d_0), (b) radii in the x-axis (A), (c) radius in the y-axis (B), and (d) radius in the z-axis (C). 150

1. Introduction

1.1. *Background*

The human foot is comprised of bones, cartilage, and soft tissues such as skin, fat, muscle and tendons. The primary focus of this research will be on soft tissues comprising the sole of the foot, which will be referred to as plantar tissue or plantar soft tissue. The following terminology is used to describe the sections of the foot (Fig. 1):

- The rear foot – consisting of the heel area
- The midfoot – consisting of the arch of the foot and occupies the space between the heel and the metatarsal heads of the foot
- The forefoot – consisting of the metatarsal heads of the foot and the five toes

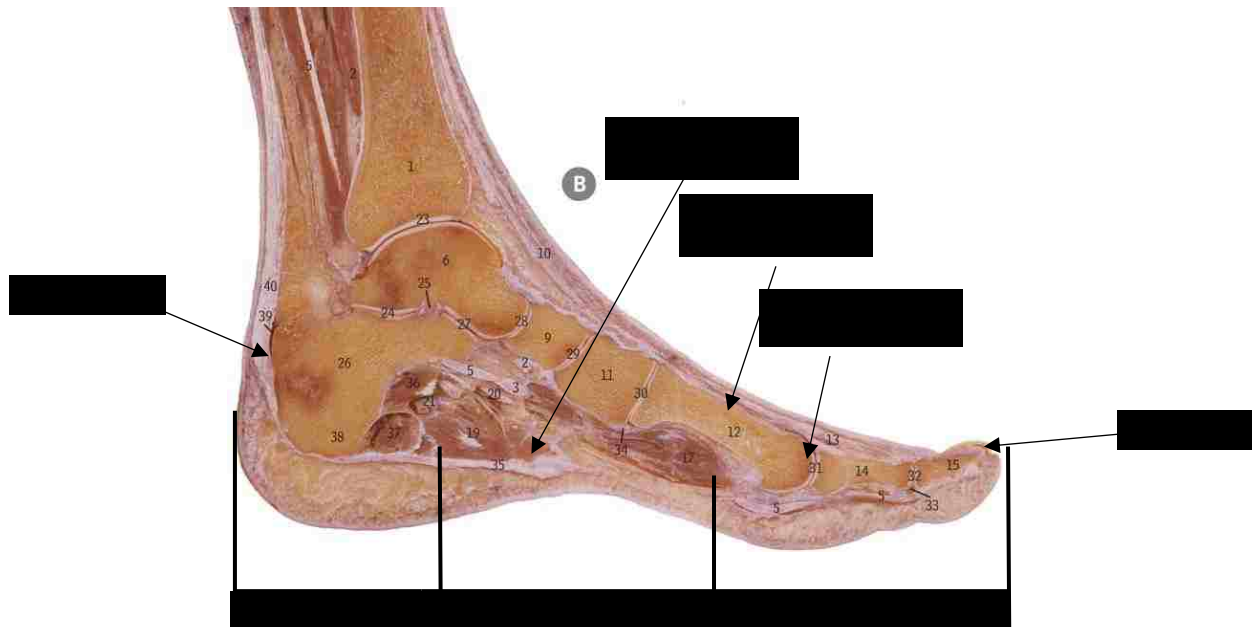


Fig. 1. An anatomical representation of the foot with the rear foot, midfoot, and forefoot sections labeled. Additionally, the bones and anatomical structures are marked. Reprinted from Logan (2012), with permission from Elsevier. Anatomical identification has been added to original figure.

Each of the above foot sections has unique functional structures, which causes its tissues to have different mechanical properties (Ker, 1996; Ledoux et al., 2005). The functional anatomy of each foot section, described by Sarrafian (1993) , are as follows:

- The rear foot tissue is comprised of a thick layer of subcutaneous connective tissue that forms pockets of fatty tissue. This structure allows the rear foot to absorb the shocks associated with the heel strike during walking or running.
- The midfoot plantar tissues have musculature and plantar fascia, which connect the calcaneus, the bone of the heel, and the metatarsals, the bones of the fore foot (Fig. 1). They maintain balance in response to changes in the environment and work with the other foot sections to absorb impacts and generate movement.
- The forefoot plantar tissues are comprised mainly of muscle and tendons, with small fat pads underneath the metatarsal heads and the toes. They are used to push off the ground, preparing the foot for the next step.

Healthy tissues typically tolerate the normal stresses of everyday activity without pain or injury. However, the American Podiatric Medical Association reported that up to 75% of Americans suffer from various foot ailments each year and approximately 50% reported foot pain (American Podiatric Medical Association and Kelton Research, 2009). Many diseases, such as diabetes and plantar fasciitis, affect the blood flow and tissue integrity of the foot, which can cause loss of sensation, ulceration, and other permanent damage (Alavi et al., 2014; Mithraratne et al., 2012; Pai and Ledoux, 2012). The progression of these diseases has been linked to changes in mechanical properties of the plantar tissues (Archer et al., 2006; Cavanagh et al., 1993; DeBerardinis et al., 2016; Levins and Skinner, 1998; Mithraratne et al., 2012; Pai and Ledoux, 2012). Specifically, research has suggested that mechanical properties such as stiffness or how

the tissue distributes loads could be used as predictors for injury and disease development (Naemi et al., 2016; Robinson et al., 2013). Therefore, understanding how the tissue responds to the loads can lead to a better understanding of gait mechanics, soft tissue function, and disease development and progression.

Much is still unknown about the mechanical characteristics of the plantar tissues. Measurement of these characteristics during walking using any direct measurement can change a person's gait (Selgrade and Chang, 2015). Developing a model, an indirect measurement, for the mechanical behavior of plantar tissues can help assess the mechanics of these tissues during walking. Additionally, using plantar tissue models reduces the number of experiments needed to examine how the mechanical properties of the tissue effect the kinetics and kinematics of gait. Many modeling methods have been developed to examine plantar tissues and they are normally tailored and validated against experimental kinematic and kinetics.

1.2. Models for the Mechanical Characteristics of Plantar Tissues

Many researchers have developed models to represent the mechanical behavior of plantar tissues, which were evaluated using experiments conducted on cadaveric or living tissue. In the following sections, a review is presented for several models including:

- Linear material models
- Nonlinear material models: Load-deformation
- Nonlinear material models: Hysteresis
- Nonlinear material models: Nonlinear spring-damper
- Nonlinear material models: Quasilinear and Viscoelastic
- Nonlinear material models: Hyperelastic

- Nonlinear material models: Visco-hyperelastic
- Nonlinear material models: Varying contact area

1.2.1. Linear plantar tissue material models

The simplicity of linear models encouraged several researchers to use them to model plantar tissues. Few of these researchers have examined the mechanical properties of plantar tissue using linear assumptions for spring-damper systems. One model used two linear springs and a linear damper to examine the stiffness and damping properties of the soft tissue (Klaesner et al., 2002). The coefficients of the model were determined using an indentation test performed on the heel and various metatarsal heads. It was found that the stiffness of the plantar tissue varied between locations, but the damping did not. Stebbins (2012) examined the material properties of the plantar soft tissue using a hydraulic loading device that was compatible with magnetic resonance imaging. In this experiment, the heel of a single participant was loaded and unloaded, creating a deformation-force curve. A linear fit was used to determine the stiffness of the tissue. Kwan et al., (2010) used an ultrasound probe and indented the heel and metatarsal heads of 60 older volunteers. A linear approximation was used to determine the stiffness of the soft tissue. It was found that all areas had an increase in stiffness with age. Zheng et al. (2012) designed a device to measure the mechanical properties of the tissue. Using an ultrasound indenter, the heels of 10 participants were indented with increasing loads corresponding to the participant's body weight. A linear regression was fitted to the resulting force-deformation curves to determine the stiffness of the heel tissue. They found that increased loads resulted in a decrease in tissue stiffness accompanied by a large variation in stiffness coefficients among participants. These studies show that the mechanical properties can be simplified to linear assumptions and vary between anatomical locations and participants.

Linear material models were proposed to examine the foot tissue during heel strike. For example, Yarnitzky et al. (2006) developed a two-dimensional structural model for the foot that utilized local finite element (FE) at the heel and medial metatarsal heads. The local analyses used a linear model of the tissue. This model was validated on the heel only. A study was performed for 18 participants by splitting the foot into two sections – lateral and medial – and focused on the push-off phase (Thomas et al., 2004). The linear soft tissue properties were determined using a hardness test. The tissue thickness of the modeled forefoot was varied to understand its effect on both normal and shear stresses, both of which increased as tissue thickness decreased. Fernandez et al. (2012) chose to vary the stiffness of the plantar tissue and examine the internal stresses of the tissue. The soft tissue was defined using a linear, pole-zero material law that set the material stiffness to be transversely isotropic. The stresses within the plantar tissue were examined at heel strike, midstance, and push-off. It was found that an increase in the plantar tissue stiffness led to an increased stress. Finally, Brown and McPhee, (2018) used volumetric ellipsoid contact models, defined by linear springs and dampers, to assess the heel, metatarsals, and hallux. The parameters of the models were optimized based on the motion capture analysis and center of pressure coordinates. The parameters were used to reproduce the plantar pressure and ground reaction force but the resulted in inaccuracy.

Linear plantar tissue models are simple and fast, especially within clinical applications. However, it has been shown that plantar tissues behave in a nonlinear fashion. Therefore, linear material models appear to be inaccurate beyond extremely light loads.

1.2.2. Nonlinear plantar tissue material models: Load-deformation

Load-deformation models allow for an assessment of nonlinear characteristics of the plantar tissue under loading. This approach, which was used solely on the heel in the following models,

applied a compressive load and the resulting deformation was recorded. Tong et al., (2003) studied the heel pad of persons who were healthy or diagnosed with diabetes or plantar heel pain. Participants had their heels loaded using an ultrasound probe attached to a force transducer, which measured the heel pad thickness as the load was applied. The stress-strain curve of all participants showed that the heel pad material was nonlinear, but the applied loads were lower than typical walking forces. Spears and Miller-Young, (2006) created a two-dimensional foot model where the parameters of a cadaveric heel tissue (with and without skin) were determined using indentation tests. The model was then validated against other force-displacement data in the literature (Aerts et al., 1995; Rome et al., 2001; Tong et al., 2003). It was found that the model overestimated the stiffness at lower strains but was accurate at higher strains. The results showed that the stiffness of the heel was dependent on the loading rate and the contact area of the indenter probe.

Many studies did not apply loads that were similar to those experienced during walking. To address this limitation, Wearing et al., (2014) examined the mechanical properties during heel strike. In this experiment, 16 healthy adults participated. Fluoroscopy and a pressure mat system were used to measure deformation and the force during heel strike, respectively. Results of this experiment also found that the stiffness increased as the load increased. Similarly, Telfer et al., (2014) examined the heel during walking. In their experiment, two types of heel orthotics were embedded with an ultrasound transducer. These orthotics were fitted into the shoes of 16 participants who walked on a treadmill. The pressure and deformation were synchronized, and it was found that this method was reliable in developing the functional geometry of the heel soft tissue and that specific orthotics can reduce the stiffness and pressure on the tissue.

The studies presented in this section suffered from being limited to the heel, which prevents the analysis of other sections of the foot and interactions between these sections. Furthermore, these experiments were not able to assess the unloading response of the tissues. This limits the analyses of plantar tissue as it has been shown that the unloading properties of the tissue differ from the loading properties (Ker, 1996; Pai and Ledoux, 2012; Trindade et al., 2014).

1.2.3. Nonlinear plantar tissue material models: Hysteresis

Hysteresis is a nonlinear phenomenon that describes a dynamic lag between the load and deformation of a material. The area between the loading and unloading curves on the force-displacement loop is related to the energy dissipated. Hysteretic material models require the measurement of deformation/strain and load/stress. Ker (1996) examined the effects of rest periods between single compression impacts on the energy loss and hysteresis of the tissue. Three calcaneal cadaver specimens were used: two specimens were tested at room temperature (approximately 20°C) and the third at body temperature. Testing consisted of loading the specimens cyclically to identify the hysteretic behavior of the tissues and the stiffness. It was found that energy loss had a positive linear relation to the logarithm of rest time and that each specimen had different stiffness values. Pai and Ledoux, (2012) examined the shear mechanical properties of soft tissue at multiple locations: the hallux (big toe), select metatarsal heads (1, 3 and 5), the lateral midfoot and the heel using cadaveric specimens from five separate feet. The specimens were compressed and then a cyclic shear load was applied. All specimens showed S-shaped hysteresis in the strain-stress plots. Also, there was large variability in the stresses measured among the specimens taken from different feet. Finally, the linear response seen in the shear stress versus log time plot indicated little frequency-sensitive damping.

The results derived from cadaveric tissue have limited applicability to living tissue and the loads experienced during walking. To address this, Trindade et al., (2014) developed an ultrasonic sensor designed to measure deformation that would be suitable for future embedding into footwear. The sensor was used to record the hysteretic properties of the heel tissues as a participant pressed their heel onto the sensor. The force was recorded using a force platform underneath the sensor. Results showed that the heel tissue had a hysteresis curve that could be fitted with exponential equations. However, applied loads (less than 300 N) that were not comparable to those experienced during walking.

The stress-strain properties of plantar tissue have also been fitted with polynomial equations in order to examine the effects of changing the mechanical properties of the plantar tissue. Gefen (2002) examined the forefoot where the soft tissue was defined using a fifth order stress-strain equation fitted to the data of Nakamura et al. (1981). This model was further used to simulate the stiffening of the tissue up to five times that of normal tissue stiffness (Gefen, 2003). It was found that as tissue stiffness increased, there were increased pressures and stresses under the first and second metatarsal heads. However, this model was used under static loading.

Hysteretic models have shown that there is a difference between the loading and unloading mechanical properties of the plantar tissue. They have also shown that there is variability in the properties between and among participants. None of the experiments discussed using nonlinear plantar tissue models used loads similar to those experienced during walking. This can be viewed as a shortcoming in assessing characteristics of plantar tissue during walking.

1.2.4. Nonlinear plantar tissue material models: Nonlinear spring-damper

Spring-damper systems are used to model the nonlinearity of plantar tissue dynamics, as they are simple to compute. The nonlinear spring-damper models had at least one element represented

as nonlinear. Scott and Winter (1993) developed a model of the plantar soft tissue using seven nonlinear spring and nonlinear damper systems placed at the heel, metatarsals, and hallux. The authors developed the parameters for this model based on the impact tests conducted by Valiant (1984). The parameters were then tested against the walking trials collected for three participants, with an average of 129 trials collected for each participant. The recordings were made of the complete foot, the metatarsals and toes only, and the heel only contacting a force platform. It was found that the model was accurate, although it was time-consuming to perform and analyze the hundreds of trials. Gilchrist and Winter (1996) also used multiple nonlinear spring-damper systems with three placed under the toes and six others distributed across the remainder of the plantar surface. The model was optimized, using the same parameters for all the spring-damper elements, to the walking data collected from a single participant. It was found that the systems were able to model the vertical ground reaction force, but had large errors at heel strike. Gefen et al. (2001) modeled the heel using a Voight-Kelvin model, which used a linear spring and a nonlinear damper in parallel. This model was optimized using the stance phase pressure and fluoroscopic data of two female volunteers that was recorded as they walked across an elevated platform. The results showed that heel strike caused rapid tissue compression that indicated a lower energy absorption than what was reported by earlier researchers, indicating a larger range of acceptable values. The nonlinear spring-damper models assume that the loads are applied to a specific point location, which limit their accuracy.

1.2.5. Nonlinear plantar tissue material models: Quasi-linear, viscoelastic

Previous research has shown that plantar tissue has a dependency on the amount of rest time between loads (Ker, 1996) indicating a possible frequency dependency. A quasi-linear, viscoelastic (QLV) model was developed by Ledoux et al. (2005) to examine the mechanical

properties of plantar tissue while also accounting for frequency-sensitive damping properties. This model uses a linear convolution integral to create a linear relationship between loading and the function of strain. A nonlinear strain model that included viscoelastic parameters of elastic response and reduced relaxation response was proposed. Cadaver specimens from eight separate feet were taken at the following locations: heel, metatarsals, and big toe. These specimens were preconditioned and used in a stress-relaxation experiment where the tissues were loaded until the desired strain measurement was achieved. At this point, the tissue was held at a constant strain and the load was recorded. The parameters of the QLV model were identified based on the results of these experiments. The results showed that the properties of the soft tissue varied across the foot. This research was extended to examine specimens taken from the heel, lateral midfoot, metatarsals and hallux (Ledoux and Blevins, 2007). It was found that the mechanical properties of the tissues were strain rate-sensitive. Grigoriadis et al. (2017) developed both specimen-specific and average QLV models for five different heel specimens to examine the difference in tissue response to quasi-static and dynamic loads. The authors slowly (0.01 mm/s) compressed the tissue for the quasi-static test and then impacted the specimens, with increasing velocity ranging from 0.6 m/s to 3.4 m/s, for the dynamic tests. The initial data from the dynamic tests were used to optimize the model parameters. Both the specimen specific and the average models were able to reproduce the initial dynamic loading but failed to reproduce the peak force or unloading of the tissues. While the quasi-linear viscoelastic models were able to reproduce the relaxation of the plantar tissue accurately in some cases, there were instances where these models failed to reproduce the tissue's response to dynamic loads.

1.2.6. Nonlinear plantar tissue material models: Hyperelastic

Hyperelastic models are used to examine materials that exhibit nonlinearity and elasticity in response to large strains or deformations. Researchers presented several hyperelastic models; all were based on variations of a strain energy density function.

The Ogden model assumes the material is isotropic and incompressible (Ogden, 1972; Ogden et al., 2004). This material model develops a potential function to represent the material with three constants that are calculated from the experimental stress-strain data. Erdemir et al. (2006) analyzed the heel pad of 20 healthy subjects using the geometry and load-deformation data of an indentation test conducted using an ultrasonic probe. The parameters of the Ogden model were optimized based on the load-deformation data. The results showed that the tissue stiffness did not vary significantly between or among subjects; however, when the average material properties were used to model the standing pressure distributions, variations were reported. Budhabhatti et al. (2007) examined the tissue of the first metatarsal and hallux during the push-off phase of gait. The Ogden model parameters were optimized based on recorded loads from a healthy participant using a pressure mat. It was found that the model predicted greater peak pressures than what was found experimentally. When examining the pathological changes in the foot, an increased stiffness and decrease in movement resulted in larger peak pressures. Gu et al. (2010) modeled the heel pad and considered the skin as a separate layer to investigate the effects of skin stiffness. An indentation test on the heel (with and without the skin) was conducted to determine the appropriate coefficients for the Ogden model. Chokhandre et al. (2012) studied the mechanical behavior of heel tissues using an Ogden model that was modified by adding an extra term to describe the nonlinear elastic response. They based the model parameters on the computed tomography scans and indentation tests on the cadaver tissue of a single, male donor. The model

was able to accurately reproduce the results of the indentation tests but reported an elastic modulus, defined as 3μ (Abaqus, 2007), much smaller than the values previously reported in the literature. Isvilanonda et al. (2013) optimized the Ogden model using the load and deformation data collected from cyclic compression tests on subcalcaneal fat. Researchers have also used Ogden models to assess the forefoot plantar tissue. Petre et al. (2013) examined the forefoot using data from magnetic resonance images of a single healthy male participant while the entire foot was progressively loaded from a relaxed state to 50% of the participant's body weight. Chen et al., (2014) chose to focus on the tissue of the second metatarsal head. The model was optimized for six participants using computed tomography scans and the loading data collected while the tissue was indented at a natural position and at a forced dorsiflexion of 30° . The results showed that there was a clear joint-angle dependency in the determination of the model parameters. Behforootan et al., (2017a) developed an automatic method that used an ultrasound indentation device to measure the nonlinear response of heel tissue of five participants. This data was used to develop a finite element model with the tissue defined as a 1st order Ogden material. When validating the model, it was found that the model was able to model the force-deformation accurately, but there were large errors when the same model was used to represent heel strike. The Ogden models presented focused on modeling specific anatomical locations, which allowed for complex models that included analysis of loads associated with walking. However, these location-specific models are not capable of assessing the interactions between the sections of the foot and there were no analyses of the toes (with the exception of the hallux) or the midfoot.

Beside Ogden material model, some researchers used other hyperelastic models to analyze the whole foot plantar tissues, one of the which was the Neo-Hookean model (Treloar, 1943). This model relates the strain energy to the shear modulus and a single constant based on the

uniaxial stress-strain experimental data. The Neo-Hookean model is suited for materials that undergo large deformations but assumes the material is perfectly elastic. Bucki et al. (2016) used a Neo-Hookean model to assess the plantar tissues of the full foot. This model was applied to the soft tissue, where each layer (skin, fat, and muscles) was assigned different material properties collected from published literature (Sopher et al., 2011). It was shown that there was variability in the strains between and among the different participant analyses, indicating that the model parameters needed to be made specific to each participant.

Another model used to examine the full foot is the use of a second-order polynomial strain energy model. This model relates the strain energy to the volume-dependence term and two constants determined from stress-strain experiments. Cheung et al. (2005) used a second-order polynomial strain energy model, to examine the plantar tissues. The model was verified using the data of a single male participant standing and wearing an F-scan insole system. It was found that the model had small errors in simulating the pressures of the insole and that increased tissue stiffness resulted in an increased pressure in select metatarsal heads (1, 2, 3, and 5). Chen et al. (2010) used a hyperelastic second-order polynomial to model the plantar tissues for the full foot. Geometric and loading data taken while a participant was standing were used to optimize the model. It was found that the model was able to accurately measure (less than 15% error) the plantar pressure data. Further analysis showed that the both the peak pressure and internal tissue stresses occur near bony prominences.

The various hyperelastic material models were shown to represent both individual anatomical locations and the full foot. However, none of the models was used to assess dynamic loading that would be similar to gait or consider the viscous characteristics of the foot tissue.

1.2.7. Nonlinear plantar tissue material models: Visco-hyperelastic

Visco-hyperelastic models are capable of considering both the viscous and elastic characteristics of the plantar tissue such as large displacements, incompressibility, nonlinear stress-strain, and time-dependent effects. These models use the Helmholtz free energy equation where the first part of the equations represents the hyperelastic potential while the last part represents the viscous contribution (Johnson et al., 1995; Mohammed, 2014). The constants of these models are determined using mechanical tests such as compression, tension, and stress-relaxation tests. Natali et al. (2010) developed a visco-hyperelastic model based on the stress-strain experiments previously published (Miller-Young et al., 2002). The model was validated against cadaver tissue data and was shown to be in good agreement with the experimental results. Using the same model, Natali et al. (2012) developed the model parameters based on tests conducted on pig tissue, resulting in three separate parameter sets that all showed an acceptable match to the experimental data (Ankersen et al., 1999; Shergold et al., 2006). This model, fitted with each parameter set, was used to reproduce previously published compression experiments conducted on human participants (Miller-Young et al., 2002). The results showed that each parameter set was better suited to different experiments. Fontanella et al. (2014) considered the forefoot plantar tissues, which was modeled as visco-hyperelastic. The skin was modeled as a fiber-reinforced hyperelastic material. The authors used previously published compression and stress-relaxation tests to determine the parameters of the model (Ledoux and Blevins, 2007) and (Klaesner et al., 2002). The model showed small errors in the stress-strain estimations, that led to underestimation of the energy loss. Behforootan et al., (2017) used an ultrasound indenter to perform quasi-static, dynamic, and stress-relaxation tests on the heel of the calcaneus of five participants. These tests were then compared to a visco-hyperelastic model. It was found that

subject-specific models were able to successfully reproduce the forces experienced at maximum deformation, but larger errors occurred when reproducing the plantar pressure.

The visco-hyperelastic models of the plantar tissue show small errors in their assessments, due to the inclusion of the viscous properties of the tissues. The results showed the need for participant specific models as global models lead to increased errors. However, these models did not examine loads similar to walking or examine the full foot.

1.2.8. Nonlinear plantar tissue material models: Varying contact area

A material model that assesses a varying contact area allows for additional complexity in comparison to some of the previously discussed models that assumed that the load is concentrated in a single point. Additionally, these models are still computationally simple, which would be beneficial in full foot assessments and a clinical environment. Researchers have used geometric shapes to create these contact area models.

Many researchers used spheres to examine the soft tissues of the foot. Güler et al. (1998) used a viscoelastic sphere to model the heel where the geometry and the nonlinear stiffness and damping coefficients were determined using previous literature (Valiant, 1984). The optimized model was used to reproduce compression experiments of various loading velocities. The results showed that this model was able to reproduce the force-deformation curves for different loading velocities. Shourijeh and Mcphee, (2013) examined the full foot using different models to describe the plantar tissues: nonlinear spring/linear damper, linear sphere, and a nonlinear sphere. The models were placed at the heel, the metatarsal region, and the toes. Friction was approximated using the dry Coulomb model. These models were optimized and compared to ground reaction results from walking protocols. The results showed that the spring/damper model and the linear sphere model were less accurate in recreating the ground reaction force. The

nonlinear sphere model only showed minimal differences in estimating the ground reaction force. Similarly, Pàmies-Vilà et al. (2014) used viscoelastic spheres, one placed in the rearfoot and three distributed across the rest of the foot, to model the entire foot. Friction was modeled with Coulomb's law, static friction, and viscous friction. The model was optimized using kinematic and kinetic data collected as a single participant walked over two force plates. An extended Kalman filter was used to predict and correct errors in optimization. The optimized model showed excellent kinematic results but had large errors in reproducing kinetic data.

Wojtyra, (2003) used a single truncated cone to model the entire foot. A linear stiffness and nonlinear damper defined the plantar tissues. The model parameters were optimized using multiple test simulations of walking and then used to reproduce the ground reaction force of walking. The results showed that the modeled ground reaction forces were qualitatively similar to the experimental measurements. Quantitatively, there were differences in stance time and the model overestimated the bimodal peaks of walking. These inaccuracies may be attributed to the simple model used.

Another basic model was developed by Millard and Kecskeméthy, (2015) where circular disks were used to model the heel and the forefoot. The mechanical characteristics of the disks were defined using the Hunt-Crossley contact model with nonlinear stiffness. Tangential contact forces were determined using a Coulomb friction model. This model was evaluated using experimental data of a barefoot walking task and a weight-shifting task. The results show that error increased as movement and loading approached the toes in both the walking and weight-shifting tasks. Additionally, reproduction of the weight-shifting tasks resulted in an accumulation of error over time.

The Hertz contact model has the potential of representing internal tissue stresses, which cannot be recorded using living walking experiments. Atlas et al., (2008) developed a foot load monitor based on the Hertz contact model to evaluate deep plantar tissue stresses between the plantar tissue and calcaneus within the heel. This model assumed that the soft tissue was in contact with a spherical, rigid calcaneus. A synthetic phantom foot fitted with internal force sensors was used to create a correction factor for the model. The corrected model was then used to determine the internal tissue stresses of six healthy participants whose foot geometry and tissue thickness were measured using X-rays and the force was measured using force sensors imbedded between the foot and shoe interface. The results showed that internal stress was greater than the stress on the interface. Similar results were found in another experiment comparing healthy and diabetic participants (Atlas et al., 2009).

The research shows that geometric models that have varying contact areas can be used to describe the mechanical characteristics of plantar tissue during gait. Further, they are more accurate as they include the contact area while previous models assumed that load is concentrated in a single point. However, it is difficult to represent the complex shape of the plantar tissue using only a few basic geometric shapes.

1.3. Research hypothesis

The literature has shown that geometric models, while simplified, has the potential to accurately assess the relation between load and deformation of plantar tissues. However, it is apparent that the geometric model needs to be more specific to the plantar tissue in order to be accurate. It is hypothesized that a viscoelastic geometric ellipsoid model used to assess multiple structures of the foot would be accurate and robust. Further, it is hypothesized that this model could be tailored to multiple participants allowing for a participant specific analysis.

1.4. Research Objectives

The objectives were as follows:

- Ellipsoid models were used to model the entire foot. The models were placed on the Heel, Posterior Midfoot, Anterior Midfoot, Metatarsal 1-2, Metatarsal 3-5, Toe 1, Toe 2, and Toes 3-5.
- Plantar tissues were represented using nonlinear viscoelastic material model.
- Experimental data including contact area and loading were collected through gait analysis using pressure-measuring insoles across multiple participants.
- Tissue material properties were determined for each participant and validated through literature comparisons and reproduction of experimental data.

2. Viscoelastic ellipsoidal model of plantar soft tissues

This chapter will focus on the deriving the hypothesized viscoelastic model and the methods used to verify and validate the model. A viscoelastic material model is proposed that has an ellipsoid shape and nonlinear stiffness and damping coefficients. It is hypothesized that the proposed model would be more accurate in describing plantar tissue compression under walking forces. Later, it is planned that the parameters of the model will be optimized and determine the geometric and material properties of the model for each anatomical areas of the plantar tissue. The following sections detail the description and placement of the ellipsoidal model, the kinematic model equations, and the kinetic model equations.

2.1. Ellipsoid model placement and description

The plantar tissues were represented by a sequence of ellipsoids placed at key anatomical areas. In this study, the plantar region was divided as follows (Fig. 2):

- Heel,
- Posterior Midfoot,
- Anterior Midfoot,
- Metatarsals 1-2,
- Metatarsals 3-5,
- Toe 1,
- Toe 2, and
- Toes 3-5.

While a less detailed division is possible, it was decided to pursue this division to identify regions with significant changes in stiffness or damping.

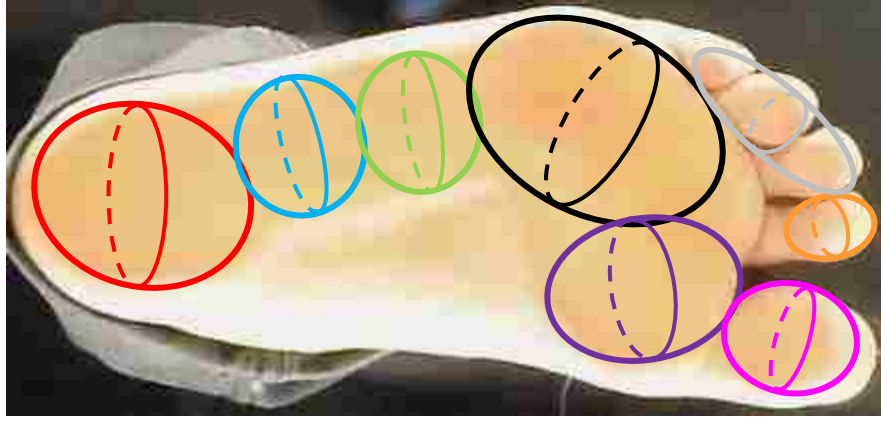


Fig. 2. An example of the placement of the ellipsoid models representing the foot. The ellipsoids are placed at the Heel (red), Posterior Midfoot (blue), Anterior Midfoot (green), Metatarsals 1-2 (black), Metatarsals 3-5 (purple), Toe 1 (pink), Toe 2 (orange), Toes 3-5 (gray).

In the proposed model, the relation between applied force vertical component and deformation within a plantar contact area is represented as:

$$F_z = \int_{A_e} (k\delta + c\dot{\delta})dA_e, \quad (1)$$

where:

- F_z applied force in the z direction,
- k nonlinear stiffness coefficient,
- c nonlinear damping coefficient,
- δ deformation associated with a point (x, y) on the contact plane
- $\dot{\delta}$ rate of δ with respect to time, and
- A_e plantar contact area.

The basic elements of the ellipsoid model are shown in Fig. 3. This ellipsoid is defined using three major radii, A , B , and C along the local X , Y , and Z directions, respectively. When a pressure is applied to the ellipsoid along the Z direction, it is compressed by a distance d , which is measured from the center of the ellipsoid as the difference between the bottom of the ellipsoid

and the current location of the contact plane. The resulting contact area is the ellipse A_e , whose major radii of are r_A and r_B (Fig. 4).

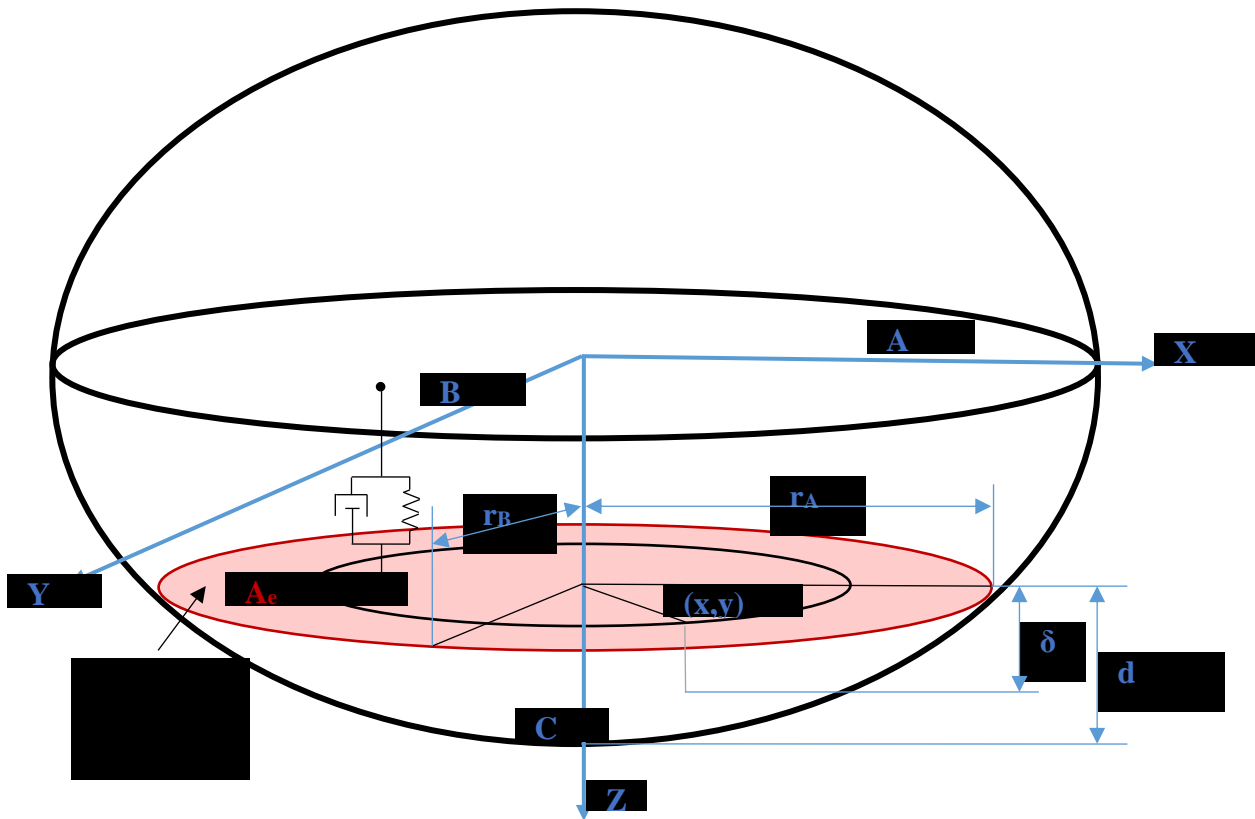


Fig. 3. A dimensional representation of the ellipsoidal model. A , B , and C represented the major radii of the ellipsoid which is centered at the origin of X , Y , and Z . The total deformation is represented by d with δ representing the local deformation at coordinate (x, y) . The measures r_A and r_B are the radii of the contact area A_e .

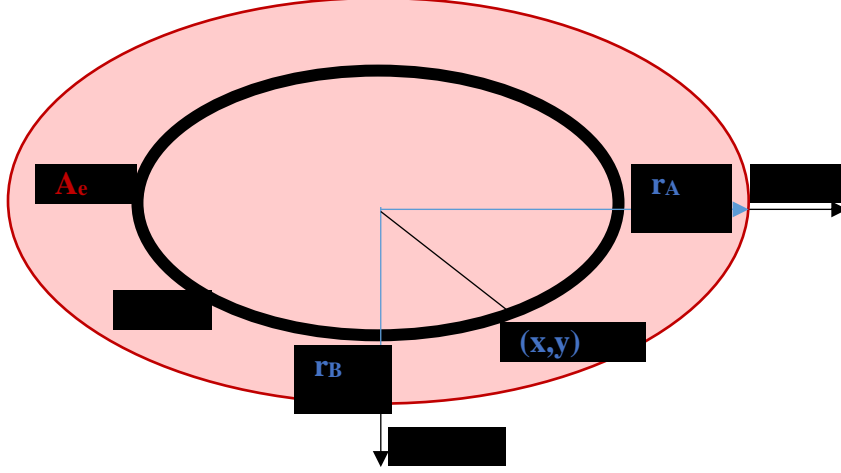


Fig. 4. The elliptical contact area A_e with radii r_A and r_B . The point (x,y) is the location of the local deformation and dA_e is the differential element of the contact area.

2.2. Ellipsoid model kinematics

To solve Equation (1), it is necessary to express the variables of this equation in terms of the ellipsoid geometry and kinematics. The first step in this process is to define the contact area radii. The ellipsoid is defined as,

$$\frac{x^2}{A^2} + \frac{y^2}{B^2} + \frac{z^2}{C^2} = 1 \quad (2)$$

The points $(r_A, 0, C-d)$ or $(0, r_B, C-d)$, which are along the local axes X_e and Y_e of the contact ellipse A_e , are respectively substituted into Equation (2),

$$\frac{r_A^2}{A^2} + \frac{0^2}{B^2} + \frac{(C-d)^2}{C^2} = 1, \quad (3)$$

$$\frac{0^2}{A^2} + \frac{r_B^2}{B^2} + \frac{(C-d)^2}{C^2} = 1, \quad (4)$$

Equations (3) and (4) are used to express the radii, r_A and r_B respectively,

$$r_A = \frac{A\sqrt{2Cd-d^2}}{C}, \quad (5)$$

$$r_B = \frac{B\sqrt{2Cd-d^2}}{C}. \quad (6)$$

Next, it is necessary to define δ . To do this, any point (x, y, z) within the contact ellipse A_e was defined in terms of z and the distorted polar coordinates ρ and θ (Strickland, 2012):

$$x = \rho(r_A \cos(\theta)), \quad (7)$$

$$y = \rho(r_B \sin(\theta)), \quad (8)$$

$$z = \delta + C - d, \quad (9)$$

where:

ρ ratio of the radii ($0 \leq \rho \leq 1$)

θ angle of rotation around the z axis in the contact plane ($0 \leq \theta \leq 2\pi$)

δ ranges between 0 and d .

Equations (7) through (9) are substituted into Equation (2) to create a relationship between δ and the ellipsoid geometry and kinematics,

$$\frac{(\rho(r_A \cos(\theta)))^2}{A^2} + \frac{(\rho(r_B \sin(\theta)))^2}{B^2} + \frac{(\delta+C-d)^2}{C^2} = 1. \quad (10)$$

Equations (5) and (6) are then used to eliminate r_A and r_B ,

$$\frac{(\rho \cos(\theta))^2}{A^2} \left(\frac{A\sqrt{2Cd-d^2}}{C} \right)^2 + \frac{(\rho \sin(\theta))^2}{B^2} \left(\frac{B\sqrt{2Cd-d^2}}{C} \right)^2 + \frac{(\delta+C-d)^2}{C^2} = 1. \quad (11)$$

Rearranging and simplifying Equation (11),

$$(\rho \cos(\theta))^2(2Cd - d^2) + (\rho \sin(\theta))^2(2Cd - d^2) + (\delta + C - d)^2 = C^2. \quad (12)$$

Or,

$$\rho^2(2Cd - d^2) + (\delta + C - d)^2 = C^2. \quad (13)$$

Equation (13) is solved to obtain the local deformation, δ :

$$\delta = d - C + \sqrt{C^2 - \rho^2(2Cd - d^2)}. \quad (14)$$

Differentiating the above equation,

$$\dot{\delta} = \dot{d} \left(1 - \frac{\rho^2(C-d)}{\sqrt{C^2 - 2C\rho^2d + \rho^2d^2}} \right). \quad (15)$$

2.3. Ellipsoid Model Kinetics

As presented in Section 2.1, Equation (1) relates the applied force to the deformation of the plantar tissue ellipsoid. Based on the kinematics of the model, the local deformation and its rate of change, defined in Equation (14) and (15) respectively, can be substituted in Equation (1):

$$F_z = \int_{A_e} \left(k(d - C + \sqrt{C^2 - \rho^2(2Cd - d^2)}) + c\dot{d} \left(1 - \frac{\rho^2(C-d)}{\sqrt{C^2 - 2C\rho^2d + \rho^2d^2}} \right) \right) dA_e, \quad (16)$$

The last step is to express the area integral in terms of the distorted polar coordinates ρ and θ using the approach described by Hass et al., (2016):

$$dA_e = \left| \frac{\partial(x, y)}{\partial(\rho, \theta)} \right| d\rho d\theta. \quad (17)$$

Or,

$$dA_e = \left| \begin{bmatrix} \frac{\partial x}{\partial \rho} & \frac{\partial x}{\partial \theta} \\ \frac{\partial y}{\partial \rho} & \frac{\partial y}{\partial \theta} \end{bmatrix} \right| d\rho d\theta. \quad (18)$$

Substituting Equations (7) and (8) into the above equation,

$$dA_e = \left| \begin{bmatrix} r_A \cos(\theta) & -\rho(r_A \sin(\theta)) \\ r_B \sin(\theta) & \rho(r_B \cos(\theta)) \end{bmatrix} \right| d\rho d\theta. \quad (19)$$

Using Equations (5) and (6) to eliminate r_A and r_B ,

$$dA_e = \left| \begin{bmatrix} \left(\frac{A\sqrt{2Cd - d^2}}{C} \right) \cos(\theta) & -\rho \left(\left(\frac{A\sqrt{2Cd - d^2}}{C} \right) \sin(\theta) \right) \\ \left(\frac{B\sqrt{2Cd - d^2}}{C} \right) \sin(\theta) & \rho \left(\left(\frac{B\sqrt{2Cd - d^2}}{C} \right) \cos(\theta) \right) \end{bmatrix} \right| d\rho d\theta. \quad (20)$$

Expanding the above equation and simplifying,

$$dA_e = \frac{\rho AB(2Cd - d^2)}{C^2} d\rho d\theta. \quad (21)$$

Substituting the above equation into Equation (16) and splitting the equation into two integrals, one for k and c ,

$$F_z = \int_0^1 \int_0^{2\pi} \left(k(d - C + \sqrt{C^2 - \rho^2(2Cd - d^2)}) \left(\rho \frac{ABd(2C-d)}{c^2} d\theta d\rho \right) \right) \quad (22)$$

$$+ \int_0^1 \int_0^{2\pi} \left(c\dot{d} \left(1 - \frac{\rho^2(C-d)}{\sqrt{C^2 - 2C\rho^2d + \rho^2d^2}} \right) \right) \left(\rho \frac{ABd(2C-d)}{c^2} d\theta d\rho \right).$$

Pulling constants outside the integrals,

$$F_z = \frac{ABd(2C-d)}{C^2} \int_0^1 \int_0^{2\pi} \left(k\rho \left(d - C + \sqrt{C^2 - \rho^2(2Cd - d^2)} \right) \right) d\theta d\rho \quad (23)$$

$$+ \frac{ABd(2C-d)}{C^2} \int_0^1 \int_0^{2\pi} \left(c\dot{d}\rho \left(1 - \frac{\rho^2(C-d)}{\sqrt{C^2 - 2C\rho^2d + \rho^2d^2}} \right) \right) d\theta d\rho$$

Integrating the above equation, using Live Editor (MathWorks, Natick, U.S.),

$$F_z = \frac{AB\pi}{C} kd^2 - \frac{AB\pi}{3C^2} kd^3 - \frac{AB\pi}{3C^2(2C-d)} c\dot{d}(6C^2 - 4Cd + d^2) \quad (24)$$

Simplifying the above equation,

$$F_z = \frac{AB\pi d}{c} \left(k \left(d - \frac{d^2}{3C} \right) - c\dot{d} \frac{6C^2 - 4Cd + d^2}{3C(2C-d)} \right). \quad (25)$$

2.4. Relating Ellipsoid deformation to contact area

The force in Equation (25) is expressed in terms of the deformation of the ellipsoid.

However, directly measuring the deformation, d , during walking may be challenging. Instead, we propose to use the contact area associated with the deformation as it can be measured using pressure-measuring insoles.

To achieve this, it may be necessary to go back to kinematics of the ellipsoid model to express the deformation d and \dot{d} in terms of the contact area, A_e , which can be expressed as,

$$A_e = \pi r_A r_B. \quad (26)$$

Using Equations (5) and (6) to eliminate r_A and r_B ,

$$A_e = \pi \left(\frac{A\sqrt{2Cd-d^2}}{c} \right) \left(\frac{B\sqrt{2Cd-d^2}}{c} \right). \quad (27)$$

Or,

$$A_e = \pi \left(\frac{AB(2Cd - d^2)}{C^2} \right). \quad (28)$$

After rearranging, the above equation is quadratic equation in terms of d ,

$$d^2 - 2Cd + \frac{A_e C^2}{\pi AB} = 0. \quad (29)$$

Equation (31) is solved for d ,

$$d = \frac{2C \pm \sqrt{4C^2 - 4 \frac{A_e C^2}{\pi AB}}}{2}. \quad (30)$$

Or,

$$d = \left\{ \begin{array}{l} C + C \sqrt{1 - \frac{A_e}{\pi AB}} \\ C - C \sqrt{1 - \frac{A_e}{\pi AB}} \end{array} \right\}. \quad (31)$$

Since the contact plane is below the X - Y plane and above the bottom of the ellipsoid, the second solution of d is the correct one. The first solution for d has no physical meaning. Rearranging the second solution,

$$d = C \left(1 - \sqrt{1 - \frac{A_e}{\pi AB}} \right). \quad (32)$$

Finally, the deformation rate \dot{d} is defined using the finite differences rule,

$$\dot{d}_i \approx \frac{d_{i+1} - d_i}{t_{i+1} - t_i}. \quad (33)$$

where,

i the current time instance, t_i

Substituting Equation (32) into the above equation,

$$\dot{d}_i \approx \frac{C \left(\left(1 - \sqrt{1 - \frac{A_{e_{i+1}}}{\pi AB}} \right) - \left(1 - \sqrt{1 - \frac{A_{e_i}}{\pi AB}} \right) \right)}{t_{i+1} - t_i}. \quad (34)$$

Or,

$$\dot{d}_i \approx \frac{c \left(\sqrt{1 - \frac{Ae_i}{\pi AB}} - \sqrt{1 - \frac{Ae_{i+1}}{\pi AB}} \right)}{t_{i+1} - t_i}. \quad (35)$$

2.5. Final model

The final model that will be used in the remainder of this research expresses ground reaction force vertical component and contact area for the ellipsoid model based on the derivations presented in Equations (27), (32), and (35). These two relationships are combined to create a relationship between the force applied, ellipsoid kinematics, and the contact area,

$$F_z = \frac{AB\pi d}{c} \left(k \left(C \left(1 - \sqrt{1 - \frac{Ae}{\pi AB}} \right) - \frac{\left(C \left(1 - \sqrt{1 - \frac{Ae}{\pi AB}} \right) \right)^2}{3C} \right) - \right. \\ \left. C \left(\frac{c \left(\sqrt{1 - \frac{Ae_i}{\pi AB}} - \sqrt{1 - \frac{Ae_{i+1}}{\pi AB}} \right)}{t_{i+1} - t_i} \right) \frac{6C^2 - 4C \left(C \left(1 - \sqrt{1 - \frac{Ae}{\pi AB}} \right) \right) + \left(C \left(1 - \sqrt{1 - \frac{Ae}{\pi AB}} \right) \right)^2}{3C \left(2C - \left(C \left(1 - \sqrt{1 - \frac{Ae}{\pi AB}} \right) \right) \right)} \right). \quad (36)$$

The stiffness k and the damping c coefficients were nonlinear and were defined as (Güler et al., 1998):

$$k = \bar{k} \left(\frac{d}{d_0} \right)^n, \quad (37)$$

$$c = \bar{c} \left(\frac{d}{d_0} \right)^m. \quad (38)$$

where:

\bar{k} stiffness coefficient

\bar{c} damping coefficient

d_0 original thickness of the plantar tissue.

These can also be shown as:

$$k = \bar{k} \left(\frac{c \left(1 - \sqrt{1 - \frac{A_e}{\pi AB}} \right)}{d_0} \right)^n, \quad (39)$$

$$c = \bar{c} \left(\frac{c \left(1 - \sqrt{1 - \frac{A_e}{\pi AB}} \right)}{d_0} \right)^m. \quad (40)$$

These equations were substituted into Equation (36), the final equation was derived:

$$F_z = \frac{AB\pi d}{C} \left(\bar{k} \left(\frac{c \left(1 - \sqrt{1 - \frac{A_e}{\pi AB}} \right)}{d_0} \right)^n \left(c \left(1 - \sqrt{1 - \frac{A_e}{\pi AB}} \right) - \frac{\left(c \left(1 - \sqrt{1 - \frac{A_e}{\pi AB}} \right) \right)^2}{3C} \right) \right) \quad (41)$$

$$- \bar{c} \left(\frac{c \left(1 - \sqrt{1 - \frac{A_e}{\pi AB}} \right)}{d_0} \right)^m \left(\frac{c \left(\sqrt{1 - \frac{A_{e_i}}{\pi AB}} - \sqrt{1 - \frac{A_{e_{i+1}}}{\pi AB}} \right)}{t_{i+1} - t_i} \right) \frac{6C^2 - 4C \left(c \left(1 - \sqrt{1 - \frac{A_e}{\pi AB}} \right) \right) + \left(c \left(1 - \sqrt{1 - \frac{A_e}{\pi AB}} \right) \right)^2}{3C \left(2C - \left(c \left(1 - \sqrt{1 - \frac{A_e}{\pi AB}} \right) \right) \right)}$$

3. The use of pressure-measuring insoles to assess ground reaction force and contact area

Development of the ellipsoid model required measurement of force and contact area simultaneously. This was done using pressure-measuring insoles. The following sections will discuss the characteristics of the pressure-measuring insoles, their use with participants to collect walking data, the methods used to pre-process the walking data, and the methods used to determine the force and plantar contact area.

3.1. Pressure-measuring insoles

Medilogic® pressure-measuring insoles (Schönefeld, Germany) were used in this research. The insoles have a grid of sensors (Fig. 5), ranging between 93 and 162 sensors depending on the size of the insole (Table 1). The sensor maps provided by Medilogic® are included in Appendix A. The sensors, which are 0.75 x 1.5 cm rectangles, measure the change in electrical resistance, which is proportional to the pressure applied to these sensors (Medilogic GmbH, 2017). Each sensor outputs the pressure values in the normal direction to the contact surface in the form of a 0-255 digital scale. The manufacturer stated calibration value is 255 bits equals 64 N/cm². The manufacturer recommended using linear interpolation to convert the bit output to pressure based on these values.

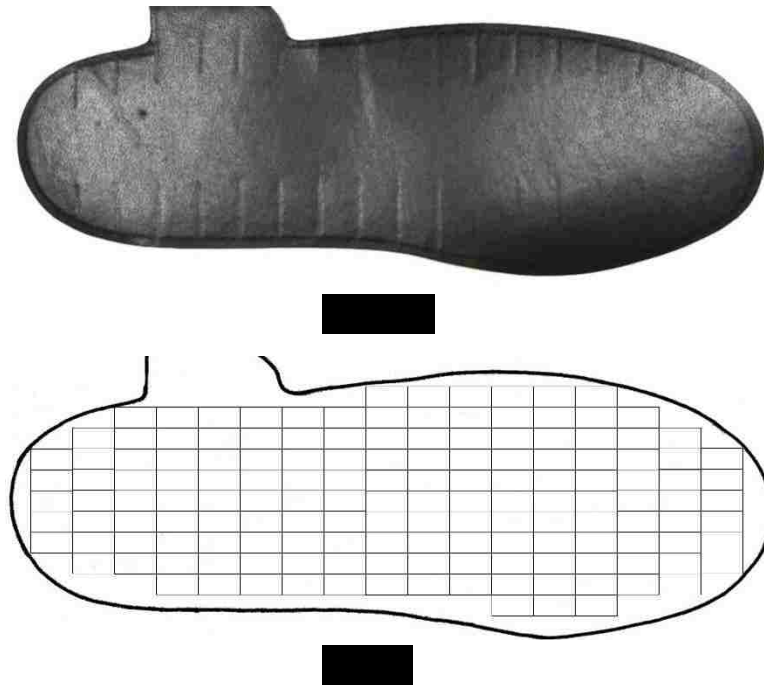


Fig. 5. (A) The Medilogic® left insole, Size 43-44. (B) The corresponding sensor map where each rectangle represents a single sensor. Image taken from DeBerardinis et al. (2018).

Table 1. The number of sensors in each insole size.

Insole Size	Number of Sensors
35-36	93
37-38	107
39-40	116
41-42	130
43-44	151
45-46	162

The sensors of the insole were grouped into anatomical areas (see Section 2.1) by assigning each sensor to the following regions. They have been grouped into sections for clarity.

Heel – approximately posterior third of the insole length.

Midfoot – approximately middle third of the insole length

- Posterior Midfoot– posterior half of the midfoot region.
- Midfoot Anterior – anterior half of the midfoot region.

Metatarsals: approximately anterior third of insole and was the widest section

- Metatarsals 3-5 – lateral two-thirds of the metatarsal region.
- Metatarsals 1-2 – medial third of the metatarsal region.

Toes: approximately the anterior sixth of the insole

- Toes 3-5 – approximately the lateral two thirds of the toe region.
- Toe 2 – a third of the combined Toe 2 and Toe 1 region.
- Toe 1 – two-thirds of the combined Toe 2 and Toe 1 region.

Fig. 6 shows an example of the sensors of the Size 37-38 insole being grouped into the aforementioned anatomical regions. Appendix B presents the sensor groupings for all insole sizes.

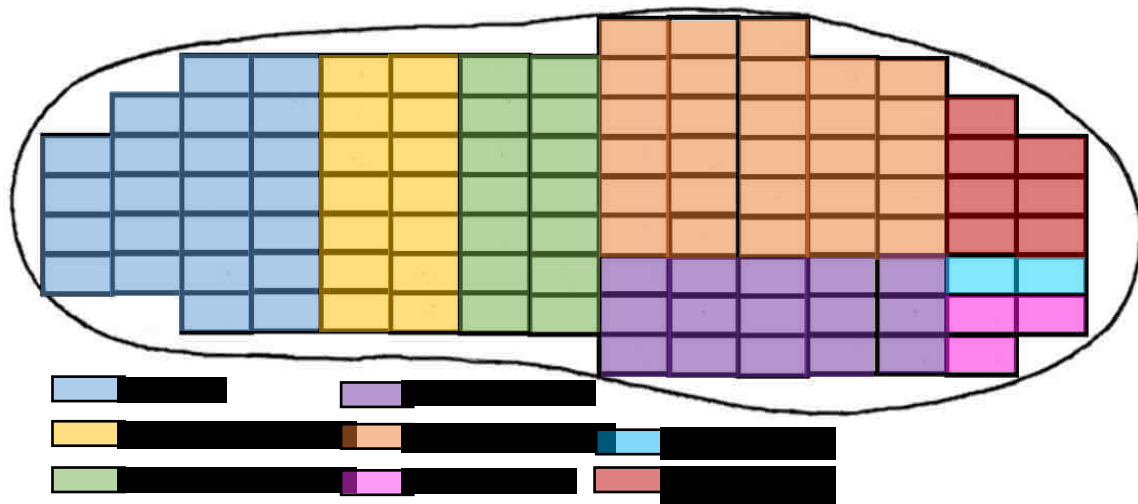


Fig. 6. A depiction of the sensors sorted into the anatomical regions for the size 37-38 insole (left foot).

3.2. Using the insoles to collect walking data

Pressure-measuring insoles were used to obtain walking data from 26 healthy participants (IRB #724468 – Consent form in Appendix C). The demographics with respect to insole size are

shown in Table 2. Each participant was fitted with insoles, which were placed inside socks provided by the researchers. Each participant was then asked to perform the following tasks:

1. Sit and lift both feet off of the floor for 5 seconds;
2. Stand and remain stationary for 10 seconds;
3. Sit again and lift both feet off of the floor for 5 seconds;
4. Stand and walk at a self-selected speed (1.09 ± 0.17 m/s) in a straight path for 5 meters.

The experiment was repeated for three trials. The steps that occurred in the middle of the five-meter walking zone were processed. Figure 7 displays a flowchart describing the methods used to process the data, with details being provided in the sections below.

Table 2

The demographic of the participants, separated by insole size, shown as average (standard deviation).

Insole Size (Eur)	Female/Male	Age (yrs)	Mass (kg)	Height (m)
35-36	5/0	21.6 (0.9)	48.9 (6.0)	1.56 (0.07)
37-38	8/0	22.3 (2.5)	55.1 (5.6)	1.58 (0.06)
39-40	5/0	24.4 (2.6)	75.3 (18.6)	1.64 (0.03)
41-42	3/0	21.6 (1.7)	84.8 (7.2)	1.81 (0.09)
43-44	2/1	33.9 (15.4)	82.8 (34.8)	1.76 (0.05)
45-46	0/2	29.9 (1.5)	86.8 (14.3)	1.84 (0.01)

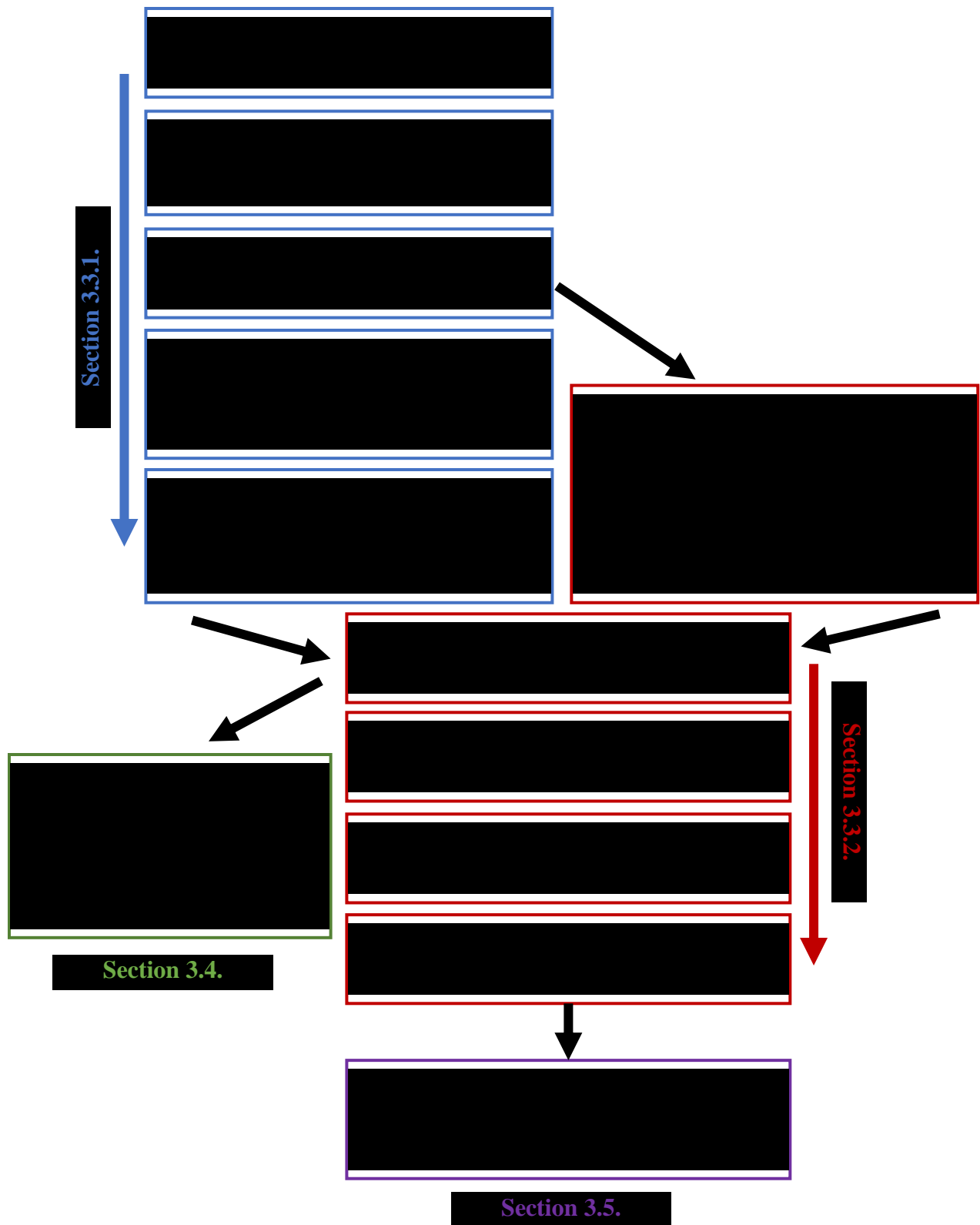


Fig. 7. A flowchart detailing the methods to select the stance time (blue), use an adaptive threshold to identify active sensors (red), determine the ground reaction force (green), and determine the contact area (purple).

3.3.Pre-processing the insole data

To record the ground reaction force and contact area using the Medilogic® insoles, it was necessary to pre-process the data based on earlier experiments (DeBerardinis et al., 2018; Lidstone et al., 2019). First, the pre-processing procedure consisted of isolating the times of the stance phase of walking (when a foot is in contact with the ground) for analysis. Second, the bit data of the isolated stance phase were processed using an adaptive threshold to obtain ground reaction force and contact area. The method used was based on Lidstone et al. (2019).

3.3.1. Determining the times of stance phase

The process was started by summing the insole bit data at each time step. As shown in Fig. 8, the data exhibited low levels of noise associated with the swing phases (when a foot was in the air). This noise was eliminated as follows:

1. Once a stance phase of interest was identified, the midpoints of the pre and post swing phases were identified (Fig. 8).
2. The average of the summed bits at these two instances was calculated and subtracted from the original signal (Fig. 9, red line) to remove direct current (dc) bias (Fig. 9, blue dashed line).
3. The step was isolated from the other steps and the starting time (i.e., heel contact) was set to zero.

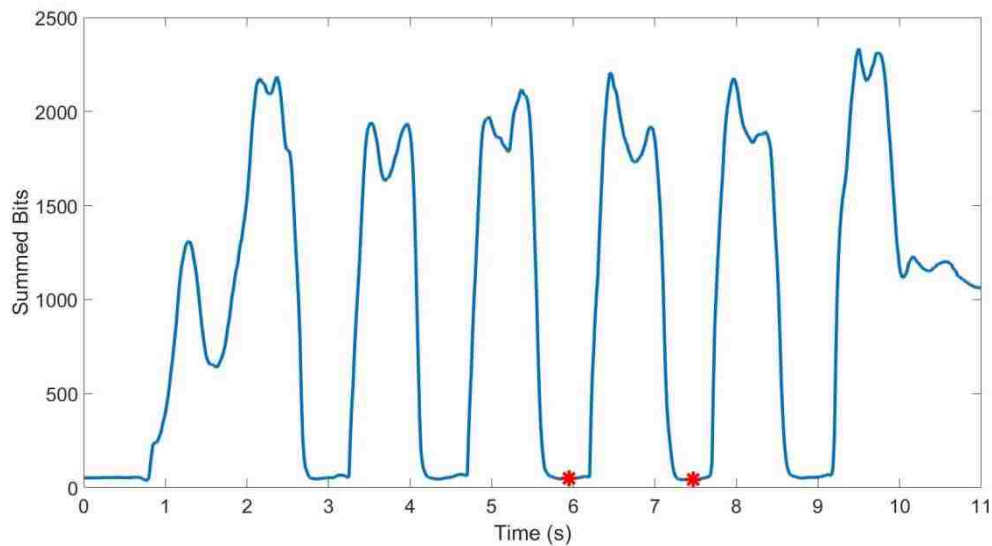


Fig. 8. Shown are several steps recorded by an insole during the walking protocol. The red points are the points selected from the swing phase in order to isolate the step. The time has been adjusted to start at zero.

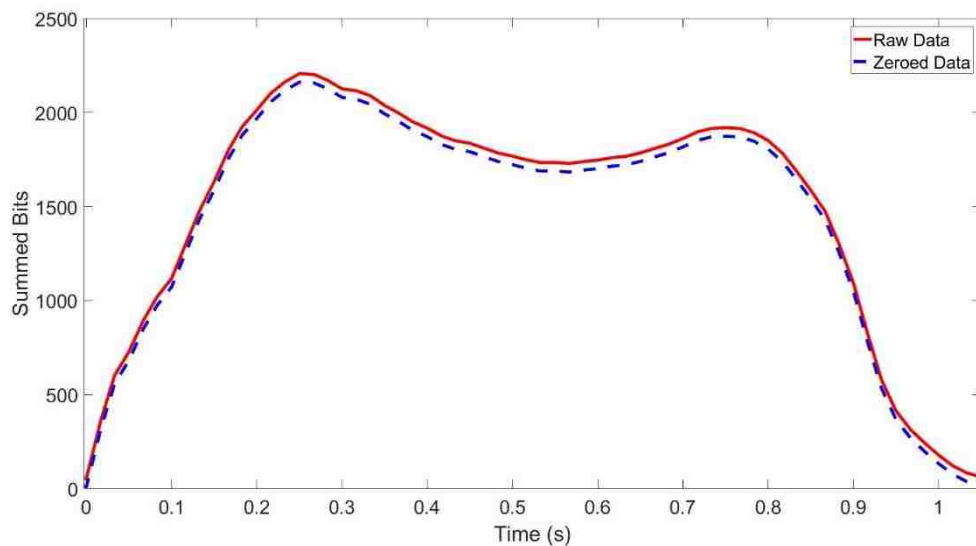


Fig. 9. A step has been isolated from a walking task. Shown in red is the raw, summed bit data collected with the pressure-measuring insole. The blue dashed line shows the step returned to baseline by subtracting the average of the bit values before and after the step. The time has been adjusted to start at zero.

An event detection threshold of 40 N was used to identify the times of heel strike and toe off (Lidstone et al., 2019; Riley et al., 2007). This was equivalent to 142 bits, which was determined

using the linear conversion suggested by the manufacturer. The footstep was adjusted to the times identified by the event detection threshold to identify the stance phase for analysis (Fig. 10).

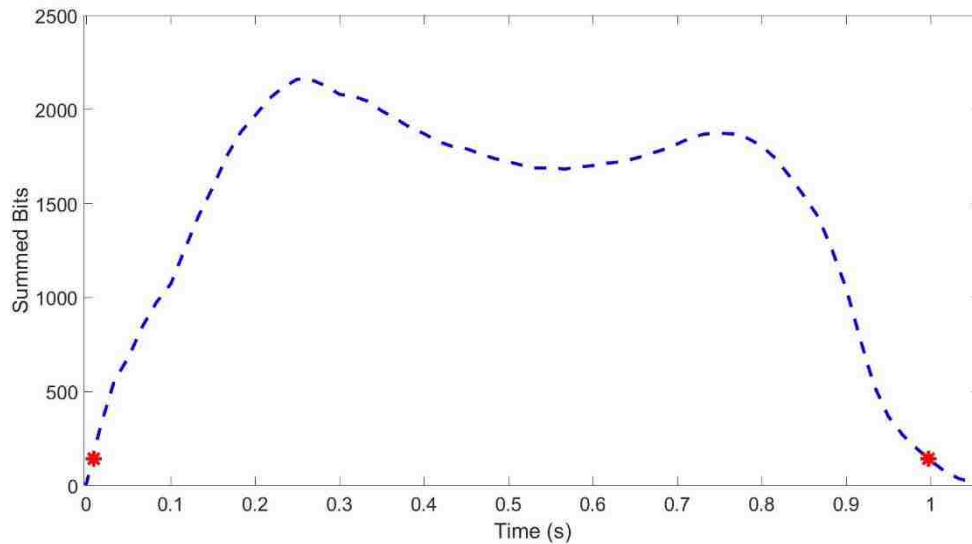


Fig. 10. The stance phase of the step was selected by considering only data between the times where the summed bits were measured to be above 142 bits (equivalent to the 40 N threshold for heel strike and toe off), which is marked with the red points. The support time has been adjusted to start at zero.

3.3.2. Using an adaptive threshold to pre-process the sensor data

The raw sensor data that occurred within the stance phase identified in Section 3.1.1 were zeroed by subtracting the average sensor value determined from the midpoints of swing phase. The resulting sensor data was used to determine the ground reaction force (Section 3.4.). The data were also processed using an adaptive threshold in order to determine the sensors that were active during the stance phase (Lidstone et al., 2019). This threshold was a percentage of the maximum summed bit value during the step and was dependent on the insole size worn by the participant (Table 3). This process was used to identify and exclude sensors that were erroneous and did not correspond to the foot contacting the ground. This approach was shown to be

accurate and has the potential to adapt to participants who have a larger body mass or walk at a greater velocity and thus, apply a higher load to the insoles (Lidstone et al., 2019). Any sensor value less than the threshold was eliminated from analysis while the sum of the remaining sensors was used to represent the corresponding contact area. Figure 11 shows an example of applying the adaptive threshold to determine the active sensors during heel strike. Figure 12 shows how applying the threshold affects the summed total of bits over the entire stance phase. It should be noted in both these figures that the result of excluding noisy sensors with the threshold only causes minimal changes to the overall data results.

Table 2. The threshold (percentage of the maximum summed bits) used for each insole size (Lidstone et al., 2019).

Insole Size	Threshold (% of maximum summed bits)
35-36	0.2
37-38	0.2
39-40	0.1
41-42	0.1
43-44	0.2
45-46	0.2

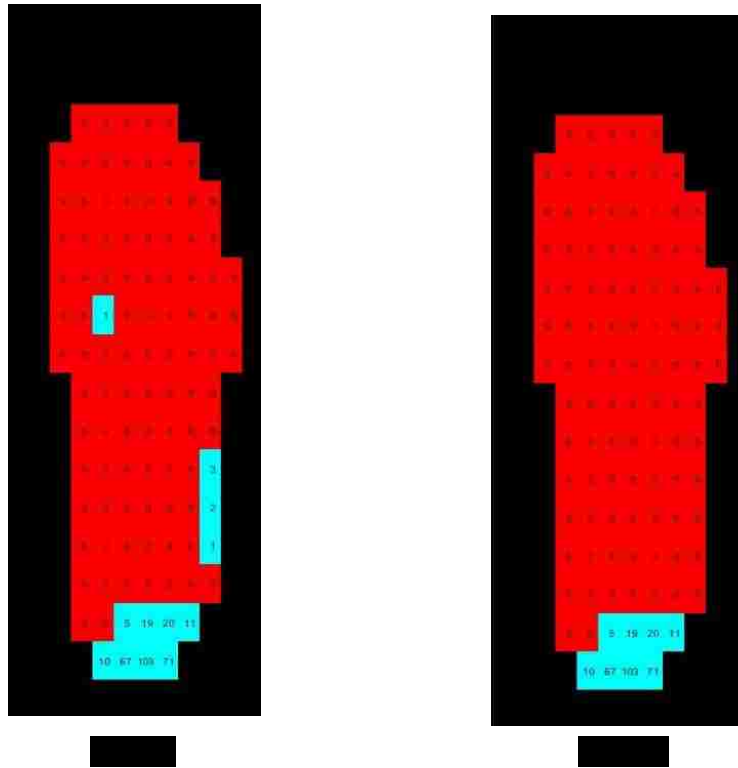


Fig. 11. These two images show the sensors of the insole that were processed using the adaptive threshold. (A) Before the participant-specific threshold was applied. (B) After the participant-specific threshold was applied. In this example, the threshold is 5 bits, which was 0.2% of the maximum summed bits. The blue sensors seen are sensors considered active while the red sensors are considered inactive. It should be noted any sensor reading less than 5 bits was set to zero and thus, excluded from analysis.

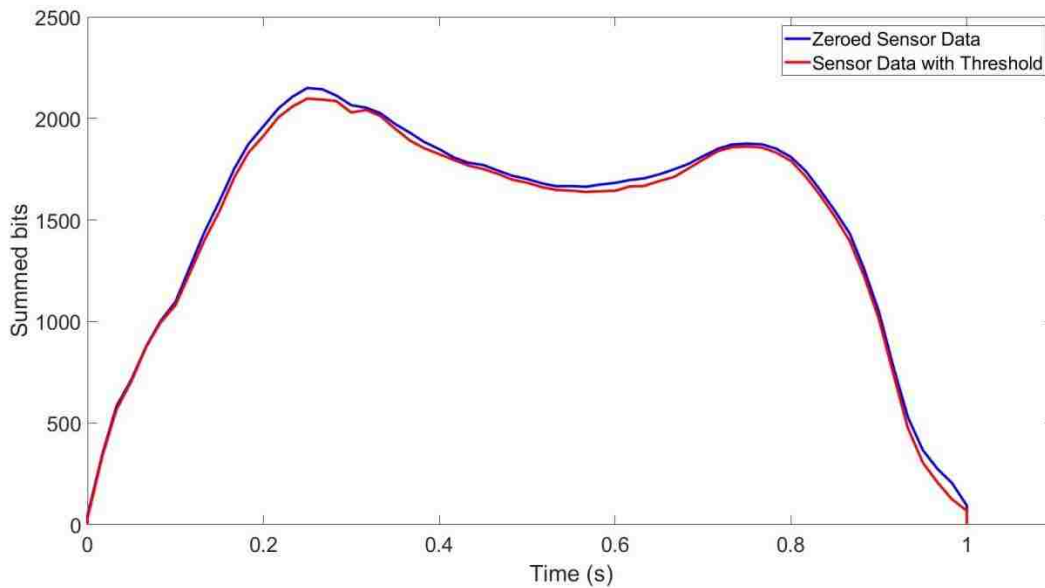


Fig. 12. The results of applying the threshold to the insole data where the red is the zeroed summed bit data and blue is the summed bit data after a threshold was applied. In this example, the threshold is 5 bits, which was 0.2% of the maximum summed bits. This threshold only excludes a few sensors that have small bit values which explains the proximity of the raw data and the data processed with the threshold.

3.4. Determining vertical ground reaction force using pressure-measuring insoles

Several methods have been used to measure the ground reaction force during walking. Research has shown that commercial pressure-measuring insoles are capable of accurate measurements (Chen and Bates, 2000; Fong et al., 2008; Forner Cordero et al., 2004; Koch et al., 2016; Ong and Wong, 2005). Following, we present the method used to calculate ground reaction force for the Medilogic® insoles.

The sensors active during the step that was determined and process using the methods described in Section 3.3 were grouped into each anatomical region. The sensors in each region were calibrated using the following equation and Medilogic’s suggested calibration,

$$F_i = \sum_{n=1}^N B_{i,n} \left(\frac{64 \frac{N}{cm^2}}{255 \text{ bits}} \right) a, \quad (42)$$

where:

F_i force calculated at time instance i ,

n sensor index with N being the total number of sensors in the insole,

$B_{i,n}$ value of sensor n at every time instance i ,

a area of each sensor, 1.125 cm^2 .

An example of the output is shown in Figure 13 where the force of each region has been plotted over time. Figure 14 shows the forces of each region in comparison to the total summed force.

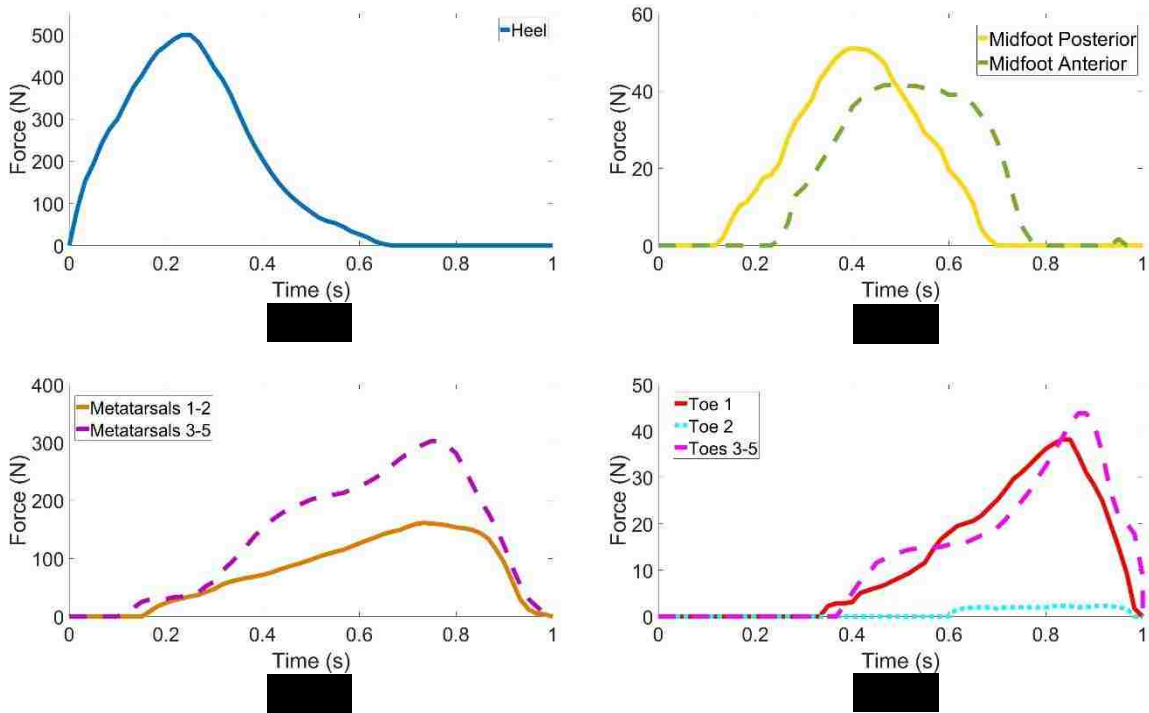


Fig. 13. The ground reaction force for each anatomical area: (A) Heel, (B) Midfoot Posterior and Midfoot Anterior, (C) Metatarsals 1-2 and Metatarsals 3-5, (D) Toe 1, Toe 2, and Toes 3-5.

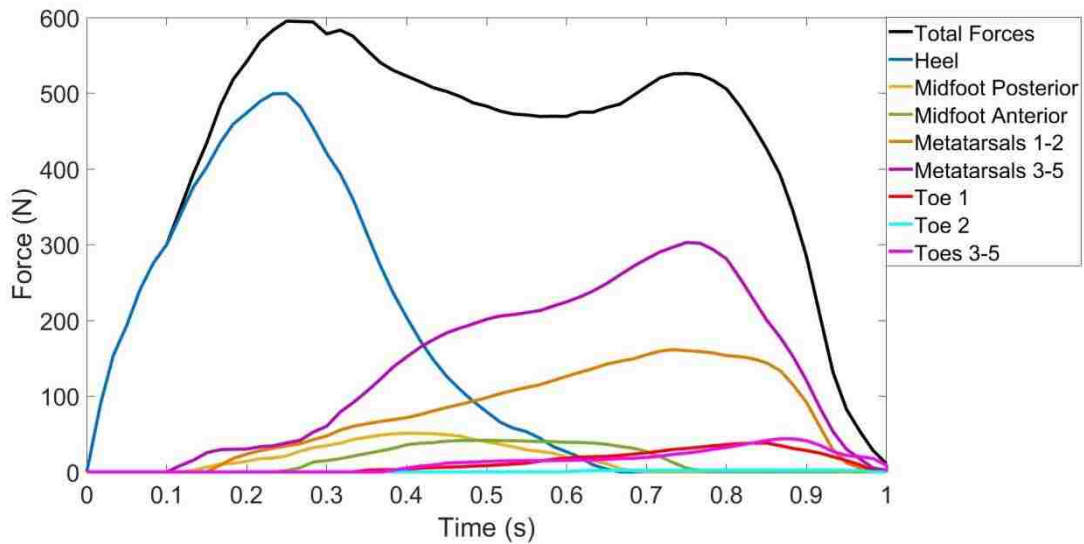


Fig. 14. The total ground reaction force calculated by summing the forces of each anatomical area: Heel, Midfoot Posterior, Midfoot Anterior, Metatarsals 1-2, Metatarsals 3-5, Toe 1, Toe 2, and Toes 3-5.

3.5. Determining plantar contact area using pressure-measuring insoles

Multiple techniques have been proposed in the literature to measure plantar contact area, including ink mats and paper pedography (Fascione et al., 2012; Su et al., 2016), optical pedography (Aruntammanak et al., 2013; Buchelly et al., 2016; Chong et al., 2014; Chu et al., 1995; Lidstone et al., n.d.), and electronic pedography (Lidstone et al., 2019; Urry and Wearing, 2001). Recently, electronic pedography using pressure-measuring insoles has been shown to accurately measure the dynamic plantar contact area and to record multiple steps (Lidstone et al., 2019).

To determine the plantar contact area, the sensors that remained after applying the threshold (Section 3.2.2.) were summed at each anatomical region. Figure 15 shows the contact area for

each region versus against time. The total contact summed for all of the regions has also been provided as a comparison against the individual regions (Fig. 16).

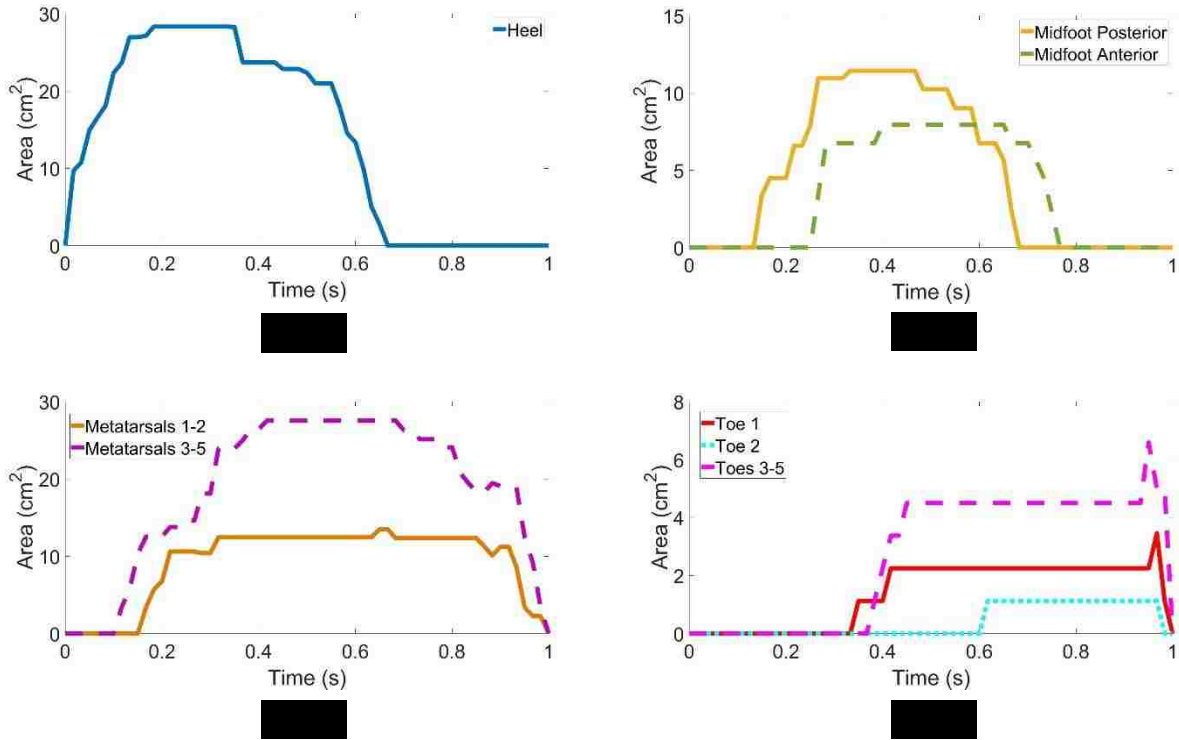


Fig. 15. The contact area for each anatomical area: (A) Heel, (B) Midfoot Posterior and Midfoot Anterior, (C) Metatarsals 1-2 and Metatarsals 3-5, (D) Toe 1, Toe 2, and Toes 3-5.

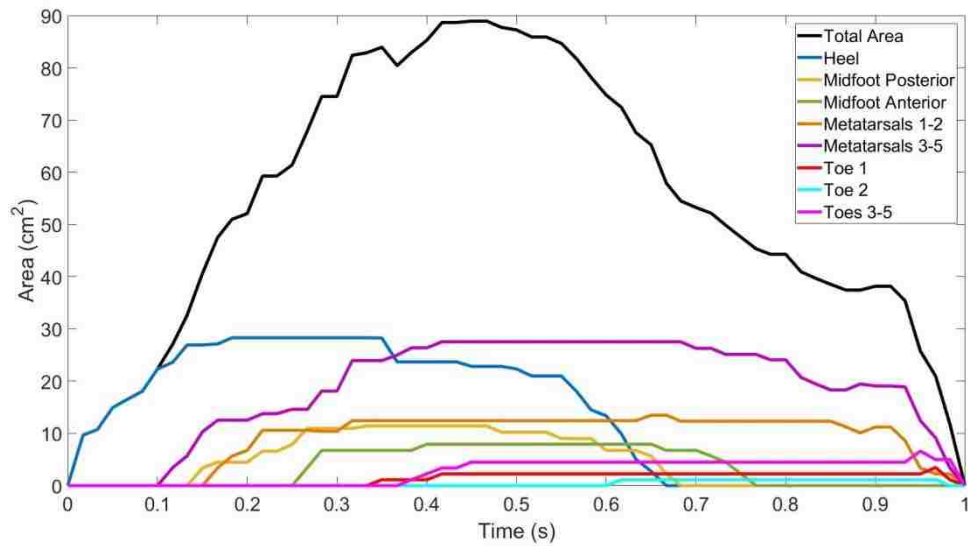


Fig. 16. The total area and for each anatomical area: Heel, Midfoot Posterior , Midfoot Anterior, Metatarsals 1-2, Metatarsals 3-5, Toe 1, Toe 2, and Toes 3-5.

3.6. Summary

This section detailed the methods used to pre-process the insole data by isolating the stance phase and then using an adaptive threshold to identify active sensors at each time point in the stance phase. The preprocessing methods were based on the methods presented by (Lidstone et al., 2019). The active sensors were then used to determine the ground reaction force and contact area. These measures will be used in the ellipsoid model and discussed in the following chapters.

4. Determining the elliptical contact area

The ellipsoidal model requires measurement of the elliptical contact area (Fig. 4). The pressure-measuring insoles separate contact area into groups of rectangles (Section 3.5). In order to use the contact area measured by the insoles, it was necessary to approximate that contact area with ellipses.

The following sections present an approach to convert the sensor readings of the pressure-measuring insoles into a sequence of ellipses within the various regions of the plantar surface during walking. Detailed methods used to fit an ellipse to the contact area measured by the insoles and the testing of the methods on a single participant's data will be discussed. The resulting ellipsoid contact areas will be related to the plantar tissue stiffness ellipsoid model presented in Chapter 5.

4.1. Fitting an ellipse to the contact areas

Each contact area measurement was comprised of active, contributing sensors which were defined as the active area(s). The arrangement of the sensors in the active area was examined and four cases were developed. Each of these cases, discussed in the following subsections, required the development of a specific technique to fit an ellipse to the active area(s).

4.1.1. Case 1 – Isolated active area(s)

An isolated active area(s) was defined as a single sensor that was determined to be active but was surrounded by inactive sensors. If an isolated single sensor became active, it was excluded as it was determined to represent an anomaly due to faulty sensor or signal noise. There were a few exceptions where the isolated active area was not excluded:

- An isolated sensor in the outermost row of the Heel (See section 3.1 for description of this region) during the first recorded time instant of the stance phase. This active sensor indicated initial heel strike (Fig. 16A);
- An isolated sensor in Toe 1, Toe 2, and Toes 3-5 (See section 3.1 for description of these regions). An active sensor indicated contact in any of these three regions as the areas in each of these three regions were of the same order as the area of the sensor (1.5 cm x 0.75 cm) (Fig. 16B).

If either exception was found, the active area was known to be rectangular and the equations of Case 2 (Section 4.1.2., below) were used to fit an ellipse to the active area.

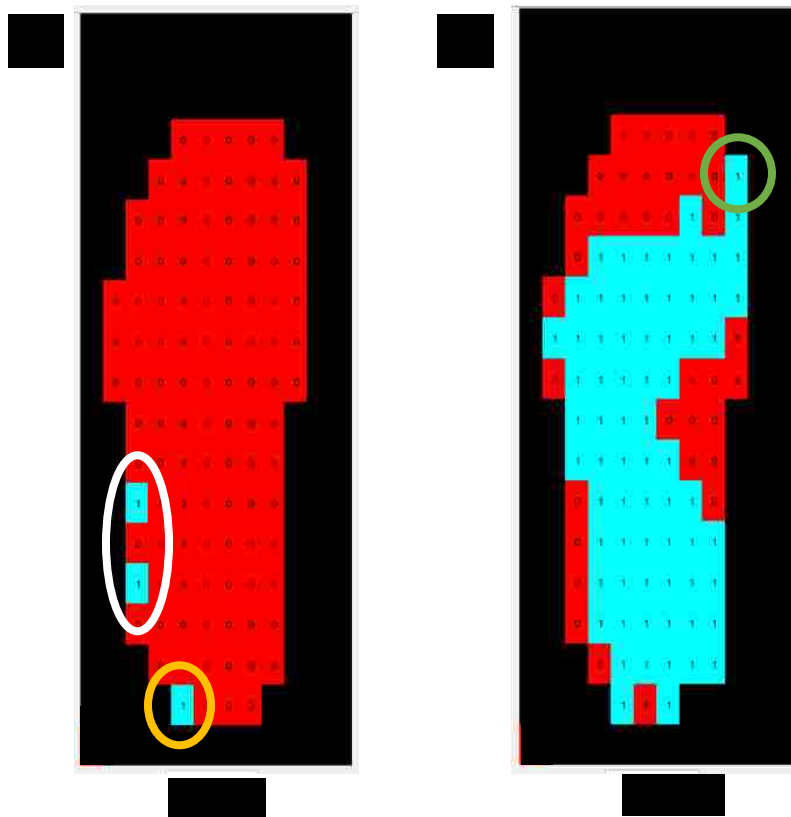


Fig. 17. (A) The isolated sensor in the outermost row of the heel is an exception to Case 1 and would be included for analysis (encircled in yellow). The two other isolated sensors (one in the heel and one in midfoot posterior) would be excluded (encircled in white). (B) The isolated sensor in Toe 1 is an exception to Case 1 and would be included for analysis (encircled in green).

4.1.2. Case 2 – Active area forming a rectangle

If an active area was in the shape of a rectangle, it was approximated to an ellipse of the same area and aspect ratio as the rectangle. Figure 17 shows the ellipse with respect to the rectangular dimensions used in the equations below.

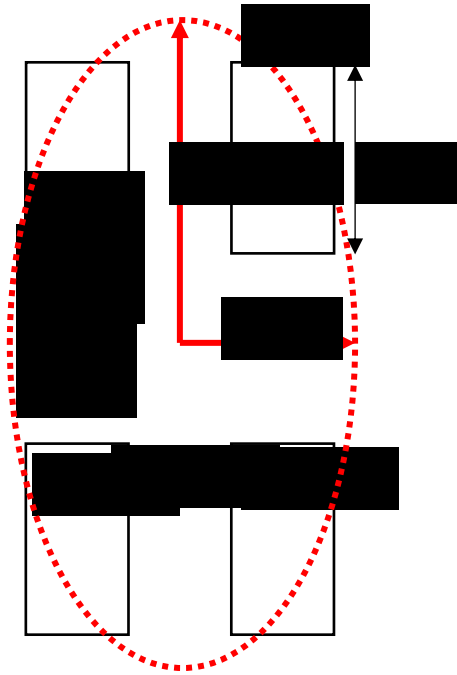


Fig. 18. Example of fitting ellipse to rectangular area so that the ellipse area and the rectangle area are equal. Also shown are the rectangular dimensions and radii used in the equations.

In order to determine the ellipse radii, the rectangular sensor area was defined as,

$$A_s = (N_r W)(N_c H), \quad (43)$$

where:

A_s area of the sensors

N_r number of sensors in a row

W width of the sensor of 0.75 cm,

N_{col} number of sensors in a column,

H height of the sensor of 1.5 cm.

The rectangle was equated to the equivalent ellipse,

$$A_s = (N_r W)(N_c H) = \pi(r_A r_B). \quad (44)$$

The aspect ratio of the sensor area and the radii was defined as,

$$\frac{r_A}{r_B} = \frac{N_r W}{N_c H}. \quad (45)$$

Equation (43) was solved for r_A ,

$$r_A = \frac{N_r W}{N_c H} r_B. \quad (46)$$

The solution was substituted into Equation (45) to derive a relationship between the rectangular area dimensions and r_B ,

$$(N_r W)(N_c H) = \pi \left(\left(\frac{N_r W}{N_c H} r_B \right) r_B \right). \quad (47)$$

Or,

$$r_B = \frac{N_c H}{\sqrt{\pi}}. \quad (48)$$

r_A was obtained from Equation (46) as,

$$r_A = \frac{N_r W}{\sqrt{\pi}}. \quad (49)$$

4.1.3. Case 3 – Active area forming an irregular shape

If the active area did not consist of a single, isolated sensor (Section 4.1.1) or was not rectangular in shape (Section 4.1.2), the active area was considered irregular and the following method was used to determine the ellipse of best fit. In this method, the active area was assessed to determine if each sensor within the active area had inactive neighboring sensors. The surrounding inactive sensors were used to identify corner and points on the sides of the active sensors area (Fig. 18).

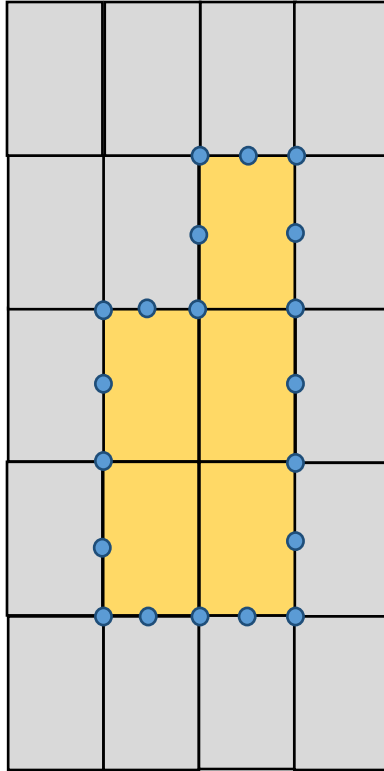


Fig. 19. An example of identifying the boundaries of the active sensors area. In the figure, yellow represented active sensors while gray represented the inactive neighboring sensors. The blue circles represent the points placed to identify the boundaries of the active sensors area.

The method used to select the points around the active area was compared to the *Boundary* method for validation (see Appendix D). *Boundary* is a MATLAB function that can be used to identify the bordering points of the active sensor area. For comparison, an example is provided showing the points chosen for each method (Fig. 19). It can be seen that the proposed method selects all border points while the *Boundary* will not select points in the divots/corners of the sensor area.

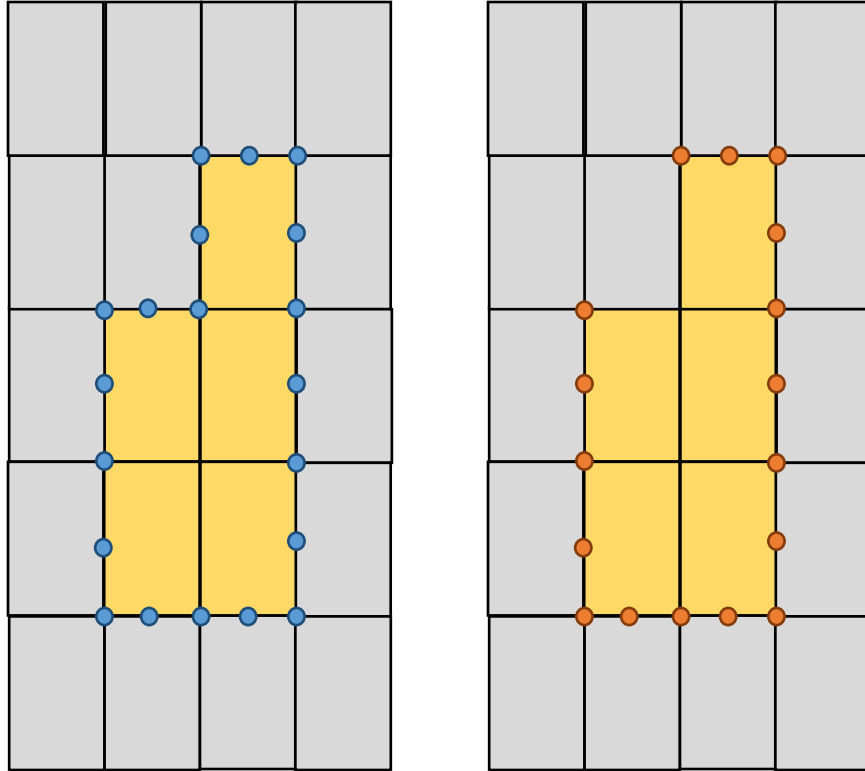


Fig. 20. This is an example shape of how the method of Section 4.1.3. (or Case 3), seen in blue, and the *Boundary*, seen in orange, would choose points for ellipse fitting. It should be noted that the validation method does not consider divots whereas the method for Case 3 does consider the divots.

Once the border points for each method were selected, they were used for ellipse fitting. To fit an ellipse, a program developed by Brown (2007) was used. An overall description of the ellipse fitting method is provided in Appendix E. An example is shown in Fig. 20 where an ellipse has been fitted to the active contact area based on the points selecting using the above described methods and the validation method, *Boundary*. The *Boundary* method was also used as a fail-safe as it was more robust than the neighboring sensor methods. If the neighboring sensor methods resulted in an ellipse that was greater than twice the area of the sensors, then the *Boundary* method was used.

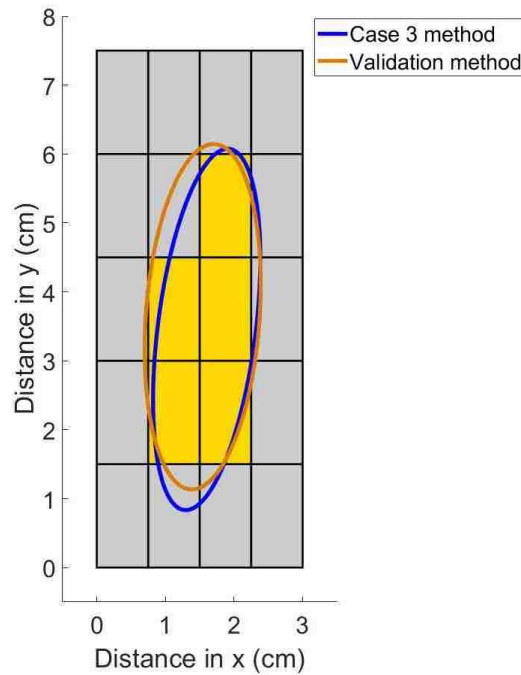


Fig. 21. This is an example of how the ellipses would fit to the sample shape in Fig. 17 using the points chosen with Section 4.1.3. (or Case 3 seen in blue) or the *Boundary* (or the validation method seen in orange) methods. It should be noted the sensor area is 5.625 cm^2 , the ellipse area from Case 3 is 5.9254 cm^2 , and the ellipse area from the validation method is 6.5377 cm^2 .

4.1.4. Case 4 – Active sensor forming an irregular shape with large aspect ratio

If the sensors were not rectangular in shape and were not fitted with an ellipse as in Case 3 (Section 4.1.3), they were assessed for long shapes. Long shapes had a large aspect ratio as shown by the “long” shapes in Fig. 21. When the sensors were arranged in a long shape, the methods in Case 3 resulted in errors in the ellipse fitting (Fig. 22). This occurs as the ellipse fitting method optimized the distance of the data points to the ellipse (Brown, 2007) which resulted in an ellipse that also had a large aspect ratio.

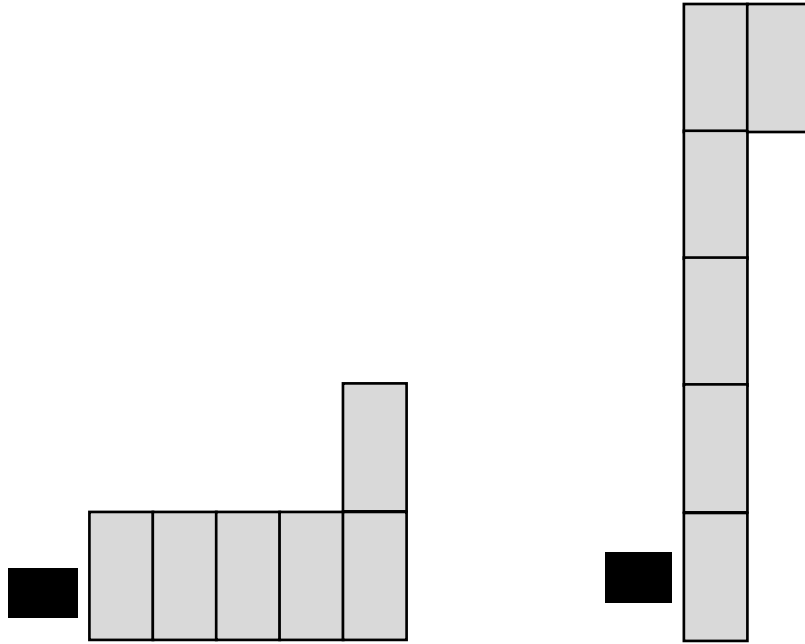


Fig. 22. Two examples of long shapes. (A) This example gives a ratio (Eq. 53) of 2.5 and (B) is an example gives a ratio (Eq. 53) of 0.4. In both cases, utilizing the path under Case 3 would result in errors during curve fitting and the methods of Case 4 would need to be used.

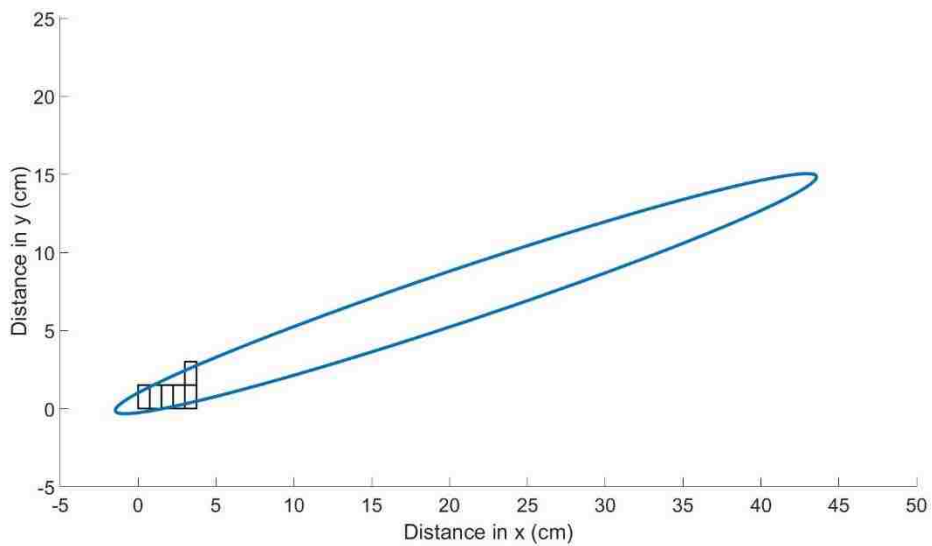


Fig. 23. An example of a long shape being fitted with an ellipse. It can be seen that the ellipse fitting method results in a poor fit, where the ellipse has an area of 126.51 cm^2 while the sensors have an area of 6.75 cm^2 .

To assess if the sensors are in a long shape, the variables N_r and N_c were identified. The ratio R of N_r and N_c was calculated as follows:

$$R = \frac{N_c}{N_r}, \quad (50)$$

Based on this ratio, the rectangular equations (Equation 48 and 49) from Case 2 were adjusted by adding the number of sensors along the shorter aspect to the number of sensors along the larger aspect. This was done to fit an ellipse that had the same area of the sensors and was arranged in the direction of the largest aspect of the sensors. Two cases were determined after multiple simulations of long shapes and were considered:

1. If R was less than or equal to 0.4 , then the sensors had a long shape in the horizontal direction. In this case, Equation (49) was modified as follows:

$$r_A = (N_r + N_c - 1) \frac{W}{\sqrt{\pi}}. \quad (51)$$

2. When R was greater than or equal to 2 , then the sensors had a “long” shape in the vertical direction. In this case, Equation (48) was modified as follows:

$$r_B = \frac{H}{\sqrt{\pi}} (N_r + N_c - 1). \quad (52)$$

4.2. Performance assessment

To verify and validate the methods used to fit the elliptical contact areas, pressure-insole data were collected for multiple participants (See Section 3.2). As a large number of the participants wore size 37-38 insoles, one subject was randomly selected from this group. This resulted in Participant 112 being chosen for analysis. Participant 112 had a mass and height of 61 kg and 1.54 m, respectively.

The area of the sensors for these steps was determined for each anatomical area and each time point during the step using the methods described in Chapter 3. An ellipse was fitted to the area based on the methods previously described for each time point in the step (Section 4.1). The performance assessment was done using the methods described above and on the validation method, *Boundary*, used in Case 3.

To determine the accuracy of the ellipses fitted to the insole sensor areas, a normalized area value was determined to give a performance index:

$$PI = \frac{A_e}{A_s}, \quad (53)$$

where:

PI performance index,

A_e area of the ellipse determined by the four previously mentioned cases,

A_s contact area measured by the insole sensors.

If PI was greater than 1, the ellipse overestimated the area of the sensors. If PI was less than 1, the ellipse underestimated the area of the sensors. Finally, if PI was equal to 1, it precisely represented the area of the sensors.

In addition to the performance index calculation, the ellipses fitted to the sensors were visually examined to determine appropriateness of the fit. The qualitative analysis examined how the shape of the sensor area affects the shape of the ellipse.

4.2.1. Results of performance assessment

Appendix F and G show the ellipse fitting results for the left and right foot, respectively, at each time point. These appendices contain images of the sensors, the ellipses fitted, the area of the sensors, and the PI for the Case 2 results and the Case 3 results, including the validation method for Case 3.

To summarize the data, Table 3 and Table 4 are given. Table 3 shows the number of occurrences that each case was used, separated by anatomical area. There are several instances where Case 1 methods were applied, where an isolated sensor was removed. Further, the left foot had more occurrences of Case 1, which could be due to asymmetry in the participant. It can be seen that Case 2 (sensor area is in rectangular in shape) and Case 3 (ellipse fitted to an irregular sensor shape) were used the most. There was only one occurrence of Case 4 for the right foot.

Table 3. The number of occurrences that each of the Case methods was used for each anatomical area for each case. The Cases are as follows: Case 1 – there were only individual sensors; Case 2 – the sensor area was rectangular; Case 3 – the sensor area was irregularly shaped; and Case 4 – the sensor area formed a long shape.

Anatomical Location	Total number of time instances recorded.		Case 1 occurrences		Case 2 occurrences		Case 3 occurrences		Case 4 occurrences	
	Left foot	Right foot	Left foot	Right foot	Left foot	Right foot	Left foot	Right foot	Left foot	Right foot
Heel	39	39	10	0	1	0	38	39	0	0
Midfoot Posterior	32	32	18	4	2	8	30	23	0	1
Midfoot Anterior	34	30	1	1	15	11	19	19	0	0
Metatarsals 1-2	42	50	0	2	21	5	21	45	0	0
Metatarsals 3-5	45	53	0	0	1	1	44	52	0	0
Toe 1	22	39	0	0	12	38	10	1	0	0
Toe 2	23	22	0	0	23	22	0	0	0	0
Toes 3-5	23	37	0	0	6	34	17	3	0	0

The rectangular shapes and long shapes were fitted perfectly with an ellipse (Case 2 and Case 4). In contrast, Case 3 was further assessed by calculating the PI. The averages and standard deviations of the PI are shown in Table 4. It was found that the Case 3 method was more accurate than the validation method (*Boundary*). The only exception was a single instance in Toe 1 where over 20% of error was found for both the Case 3 and validation methods. However, in this instance, the active sensors were only bordering by a corner, which led to a relatively poor ellipse fit.

Table 4. The normalized area results of Case 3. The ellipses fitted to the Neighbors method were compared to the validation method (*Boundary*).

Anatomical Location	Average sensor area over all occurrences of Case 3 (cm ²)		Case 3 PI		Validation PI	
	Left	Right	Left	Right	Left	Right
Heel	19.75 (2.74)	20.08 (6.70)	1.02 (0.07)	1.02 (0.04)	1.77 (0.07)	1.09 (0.05)
Midfoot Posterior	11.44 (1.40)	9.54 (2.07)	1.02 (0.02)	1.04 (0.05)	1.09 (0.05)	1.13 (0.06)
Midfoot Anterior	8.94 (2.01)	7.34 (1.28)	1.01 (0.01)	1.01 (0.01)	1.08 (0.02)	1.09 (0.03)
Metatarsals 1-2	10.34 (2.68)	11.65 (1.56)	1.02 (0.06)	1.02 (0.05)	1.11 (0.04)	1.16 (0.13)
Metatarsals 3-5	21.94 (5.7)	21.09 (6.47)	1.02 (0.02)	1.02 (0.02)	1.11 (0.06)	1.18 (0.06)
Toe 1	2.25	3.375	1.25	1.02	1.22	1.15
Toe 2	N/A	N/A	--	--	--	--
Toes 3-5	3.71 (1.00)	4.88 (0.53)	1.07 (0.11)	1.13 (0.03)	1.15 (0.04)	1.26 (0.01)

4.2.2. Discussion of the performance assessment.

The results of the ellipse fitting showed that the elliptical contact area was accurately fitted to the contact area measured by the insoles. Further, the methods used for the irregular shapes were shown to be more accurate than the validation method. Visual analysis of the results in the Appendix F and G show that the ellipses were well placed and represent the general shape of the sensor area.

5. Application of ellipsoid model on each region of the foot

The ellipsoid model was applied to each region of the foot as mentioned in Chapter 2. The accuracy was assessed by comparing the model results to the ground reaction forces recorded by the insoles. In order to accomplish these tasks, the data from the insoles had to be preprocessed. Then the model variables were determined using Matlab curve fitting.

5.1. *Insole data preprocessing*

Plantar contact area and ground reaction force data needed to be expressed mathematically to be used in the proposed model. This allowed for smooth curves to be used in the plantar tissue model and prevented large spikes in the resulting model output. The preprocessing methods used for the area and force data are discussed in the following sections.

5.1.1. *Preprocessing the area-time curve*

The areas calculate for each region as described in Chapter 4, were step-like in nature due to the resolution of the sensors (Figure 24). Using this type curve with the ellipsoid and spherical models would result in a step-like force curve. Also, there were cases where sudden spikes in the data were seen due to the resolution the sensor area. To address this problem, the area-time curves for each region were first smoothed with a three-point moving average (Eq. 54) and then were fitted with a 5th order polynomial curve (Figure 23). A 5th order polynomial was chosen as the best fit for all participants and trials after multiple tests with polynomials of different orders.

$$A(i) = \frac{A(i+1)+A(i)+A(i-1)}{3}, \quad (54)$$

where:

A the measured elliptical contact area

i the time instance

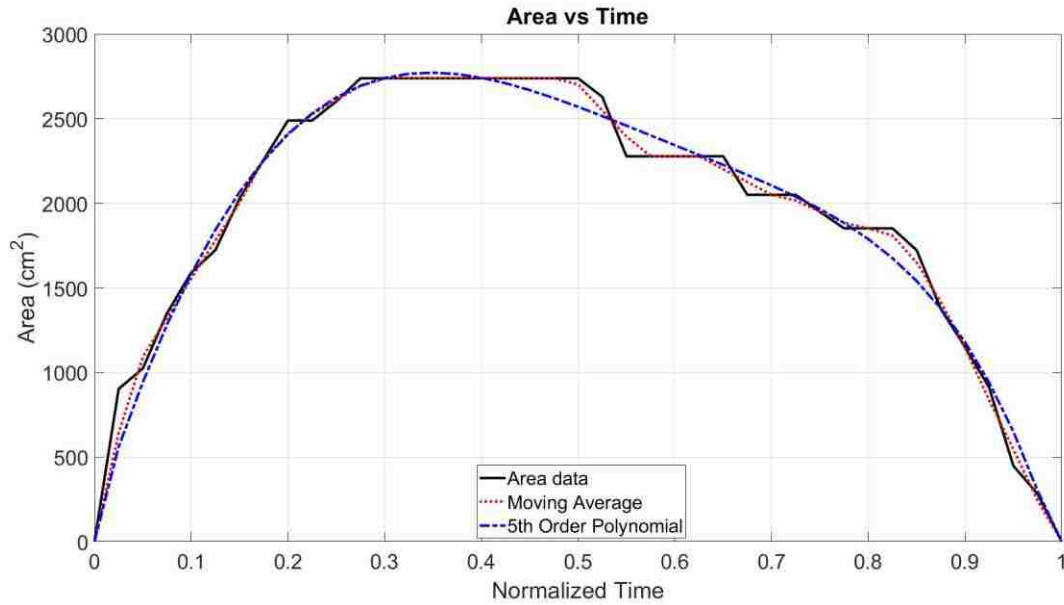


Fig. 24. An exemplar area-time curve for the showing the step-like raw (black line), the moving average smoothing the sharpness of the steps (red dotted line), and the 5th order polynomial fitted to the area (blue dashed line).

It can be seen in Figure 24 that the combination of the moving average and the 5th order polynomial is able to capture the general shape of the exemplar curve while simultaneously smoothing it. The correlation of the polynomial curve compared to the original data shown in Figure 24 is 0.9923, showing an excellent match between the curves.

5.1.2. Preprocessing the force-time curve

Similar to the area curve, the force vs. time curves for the heel were also smoothed. However, the force curves had a better resolution and thus, did not need to be smoothed by a moving average. Therefore, the data were fitted with a 5th order polynomial (Figure 25). A 5th order polynomial was chosen as the best fit for all participants and trials after multiple tests of different ordered polynomials.

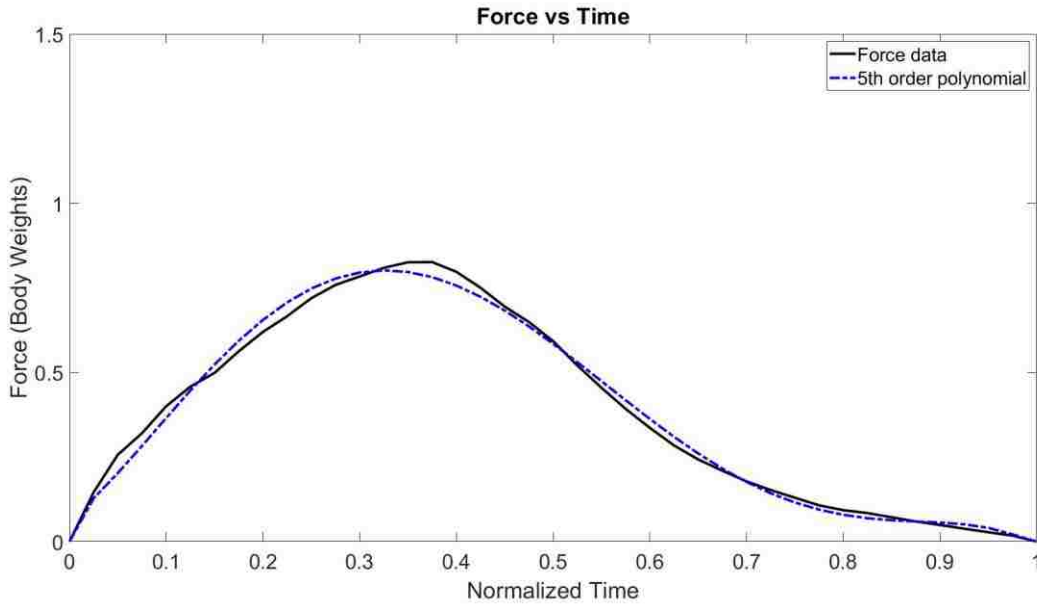


Fig. 25. An exemplar force-time curve for the heel showing the raw data (black line), and the 5th order polynomial fitted to the force (blue dashed line).

It can be seen in Figure 25 that the 5th order polynomial is able to capture the general shape of the exemplar curve while simultaneously smoothing it. The root-mean-square error of the exemplar curve shown in Figure 25 is 0.9967, showing an excellent match between the curves.

5.2. Identification of the plantar tissue model of each participant

In order to assess the models, the experimental area was used as an input and the geometric and material variables ($A, B, C, d_0, \bar{k}, n, \bar{c},$ and m) were optimized by fitting the models to the experimental force. The following sections detail the variable boundaries and coding to optimize the model variables.

5.2.1. Objective function and model penalty

The goal of the optimization process was to have the model forces match the experimental forces as closely as possible. It was expected that the plantar tissues of participants would vary

and thus, the variables for each region had to be identified for each participant separately. The variables that were identified for each region were:

$$x \in (A, B, C, d_0, \bar{k}, n, \bar{c}, m), \quad (55)$$

These variables were identified by tuning these variables so that the tissue model force matched the experimental ground reaction force measured in each region. To accomplish this, the sum of the squared difference between the experimental force and the model force of each plantar region was minimized (Eq. 56).

$$\text{Minimize: } O_{i,j,k}(x) = \sum_{t=1}^n \left(FE_{i,j,k}(t) - FM_{i,j,k}(x, t) \right)^2, \quad (56)$$

where:

$O_{i,j,k}$ objective function of plantar region j of limb k for participant i

$FE_{i,j,k}(t)$ measured ground reaction force of plantar region j of limb k for participant i at time instant t ,

$FM_{i,j,k}(x, t)$ ground reaction force output of the model of plantar region j of limb k for participant i at time instant t ,

n number of total time instants when plantar region j of limb k for participant i was active

In normal walking gait, it is physically impossible to apply a negative value, of vertical ground reaction force. To prevent the choice of variable values that would cause the tissue model to yield a negative force output, a penalty term, P , was added to the force output of the model.

The penalty was severe and equal to 10^8 .

$$FM_{i,j,k}(x, t) = \begin{cases} FM_{i,j,k}(x, t) & \text{if } FM_{i,j,k}(x, t) \geq 0 \\ FM_{i,j,k}(x, t) + P \left(FM_{i,j,k}(x, t) \right)^2 & \text{if } FM_{i,j,k}(x, t) < 0 \end{cases} \quad (57)$$

5.2.2. *Determining boundaries for each anatomical region*

As previously discussed, each region of the foot has different properties and it is apparent that each region is also a different size. Further, the geometric size will differ between the insole sizes. The optimization process using *fmincon* allowed for the variables to be constrained using a set of boundaries. Appendix H details the upper and lower boundaries for each variable and the initial guess used for optimization was set to be in the middle of the two limits. The constraints were specific to the insole sizes and were based on previous measurements. The plantar tissue thickness constraints were based on measurements made using many different methods (Thomas et al., 2004; Uzel et al., 2006; Valiant, 1984; Zheng et al., 2000). The material variables of the plantar tissue material models were constrained based on previous modeling work (Güler et al., 1998; Shourijeh and McPhee, 2015). Thus, the boundaries were set to be specific to all of the participants in each insole size. These boundaries were then corrected through iterative processes in which the boundaries were adjusted to achieve the smallest amount of error for all subjects within a specific insole size.

5.2.3. *Nonlinear multivariate identification*

The Matlab function *fmincon* was used to assess the models. This function, described in the MathWorks documentation (MathWorks, 2018a), is a nonlinear program solver that finds the minimum of a constrained nonlinear multivariable function. Within this function, options can be specified to determine how the solver optimizes the function. These options, found in the documentation provided by Matlab (MathWorks, 2018a), are:

- Algorithm – the type of algorithm used to find the minimum of the function. The algorithm used for the ellipsoid and spherical models was the ‘interior-point’ algorithm. This algorithm “handles large, sparse problems, as well as small dense problems. This

algorithm satisfies bounds at all iterations, and can recover from NaN or Inf results. It is a large-scale algorithm” (MathWorks, 2018b). This method tends to be robust when the function has unknown results or effects.

- `FinDiffType` – the calculation of the finite differences can be either forward or central. Central finite differences were chosen as they perform twice as many evaluations and were more accurate.
- `TolFun` – the termination tolerance of the first-order optimality. In order to continue the evaluations until there was a good fit, the tolerance was set to 10^{-15} .
- `MaxFunEvals` – the number of maximum evaluations that could be performed. It was found that 3000 evaluations.
- `Tolx` – the termination tolerance for the change in the variable results. In order to achieve a good fit, the tolerance was set to 10^{-9} .
- `Display` – the method in which the results were displayed. In order to examine the individual evaluations and track the progress of the function in fitting the models, iteration-detailed or iter-detailed was chosen.

5.3. Results of model application

The viscoelastic ellipsoid model was assessed in two different ways. First, the model output was compared to the experimental ground reaction force. Second, the model variables that were determined were assessed. The following sections detail these results.

5.3.1. Comparing the model output to experimental ground reaction forces.

The typical model output can be seen in Figure 26, with the results separated by the plantar regions. As the figure shows, the model was able to qualitatively match the experimental data for most areas. The largest deviations were seen in the Heel and Toe areas. The effect of the models combined together in comparison to the original total experimental force is shown in Figure 27.

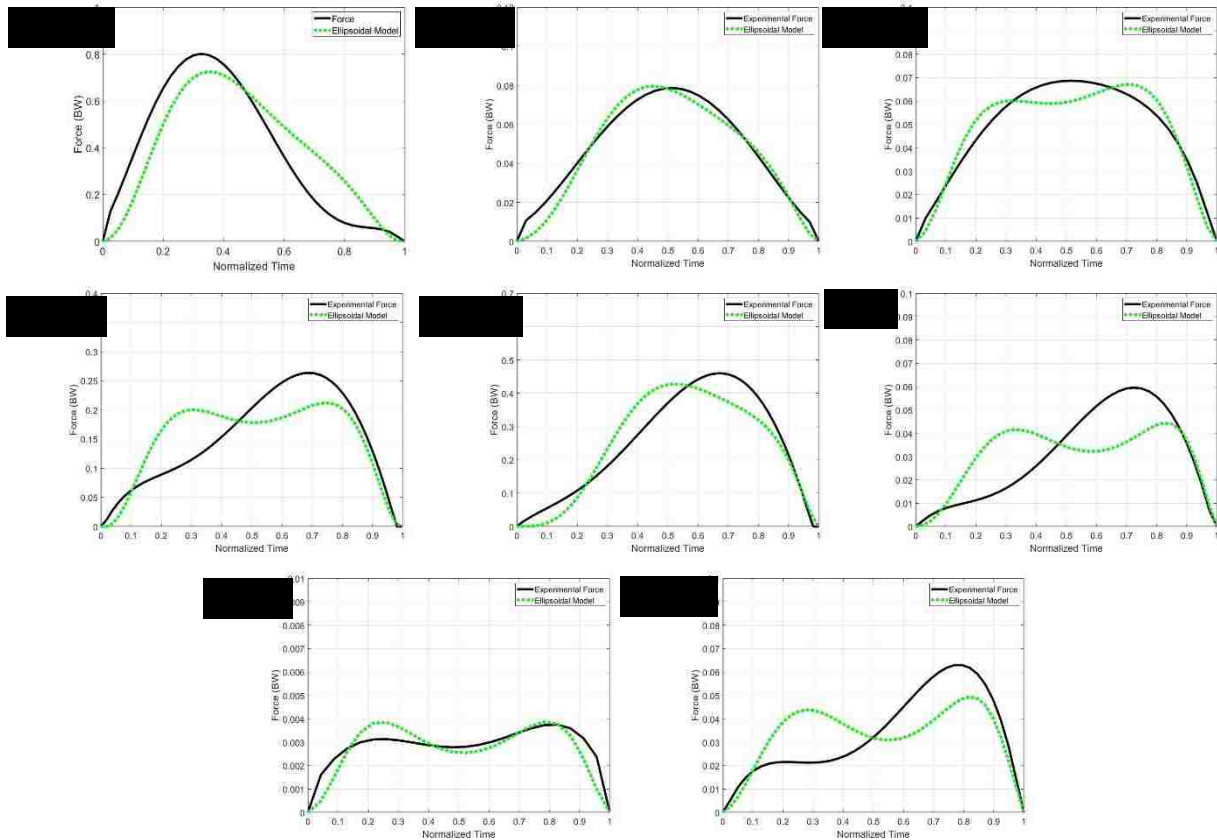


Fig. 26. An exemplar of curves showing the typical model output and experimental ground reaction force for each plantar region. These data were from the right foot of a participant wearing insole size 37-38. The graphs correspond to the following plantar regions: (a) Heel, (b) Posterior Midfoot, (c) Anterior Midfoot, (d) Metatarsals 1-2, (e) Metatarsals 3-5, (f) Hallux, (g) Toe 2, (h) Toes 3-5.

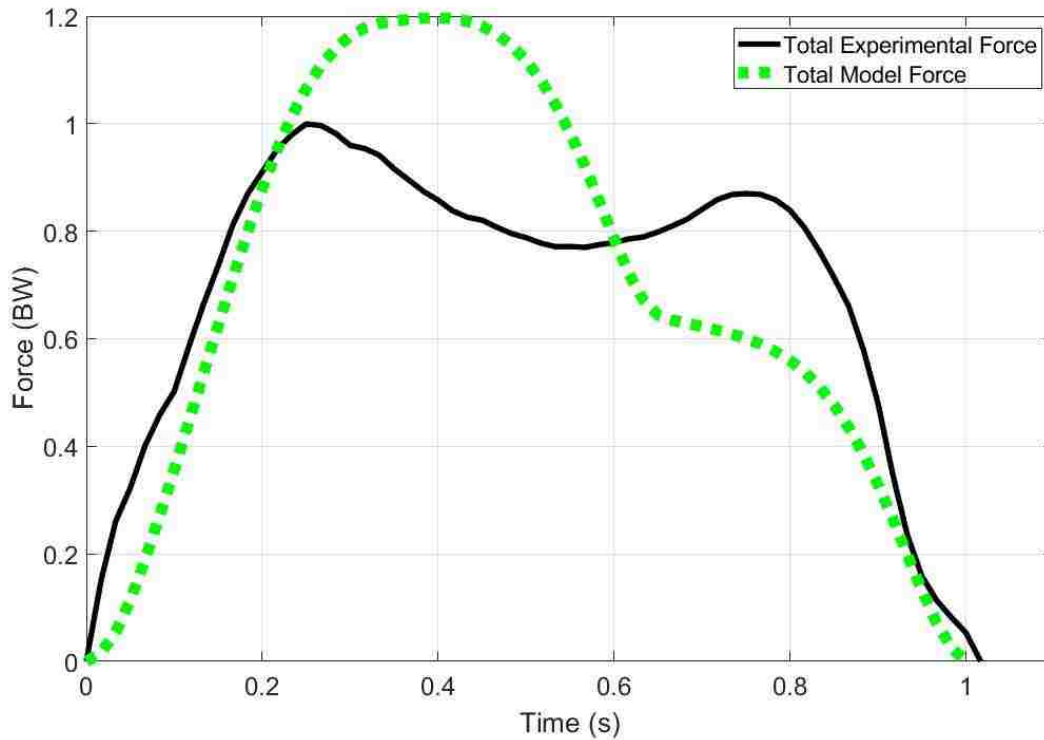


Fig. 27. An exemplar of curves showing the combined model output, resulting from all of the individual anatomical areas summed together. This is compared to the total experimental ground reaction force.

To further assess the accuracy of the model in comparison to the experimental ground reaction force, the root square error normalized to the maximum experimental force (NRMSE) was calculated for each plantar region (Eq. 58). Table 5 shows the NRMSE results of the exemplar data shown in Figure 26. As seen in the figures, the Heel and Toe areas had the biggest errors while the other areas had reasonable error. To examine the complete data set, the NRMSE results for the three trials and two limbs of each participant were averaged. The NRMSE results of the participants were averaged for each region, separated by insole sizes. Standard deviations were also calculated to determine the consistency of the results and the robustness of the model. The NRMSE results are shown in Figure 27, and tabulated in Appendix I.

$$NRMSE = \sqrt{\frac{\sum_{i=1}^n (F_{exp}(i) - F_{model}(i))^2}{n_{i,j,k} \max(F_{exp})}} * 100\%, \quad (58)$$

Table 5. The NRMSE results of exemplar data from the right foot of a participant who wore size 37-38 insole.

Plantar Region	NRMSE
Heel	22.1%
Midfoot Posterior	6.1%
Midfoot Anterior	8.2%
Metatarsals 1-2	18.1%
Metatarsals 3-5	11.7%
Toe 1	24.5%
Toe 2	13.9%
Toes 3-5	20.9%

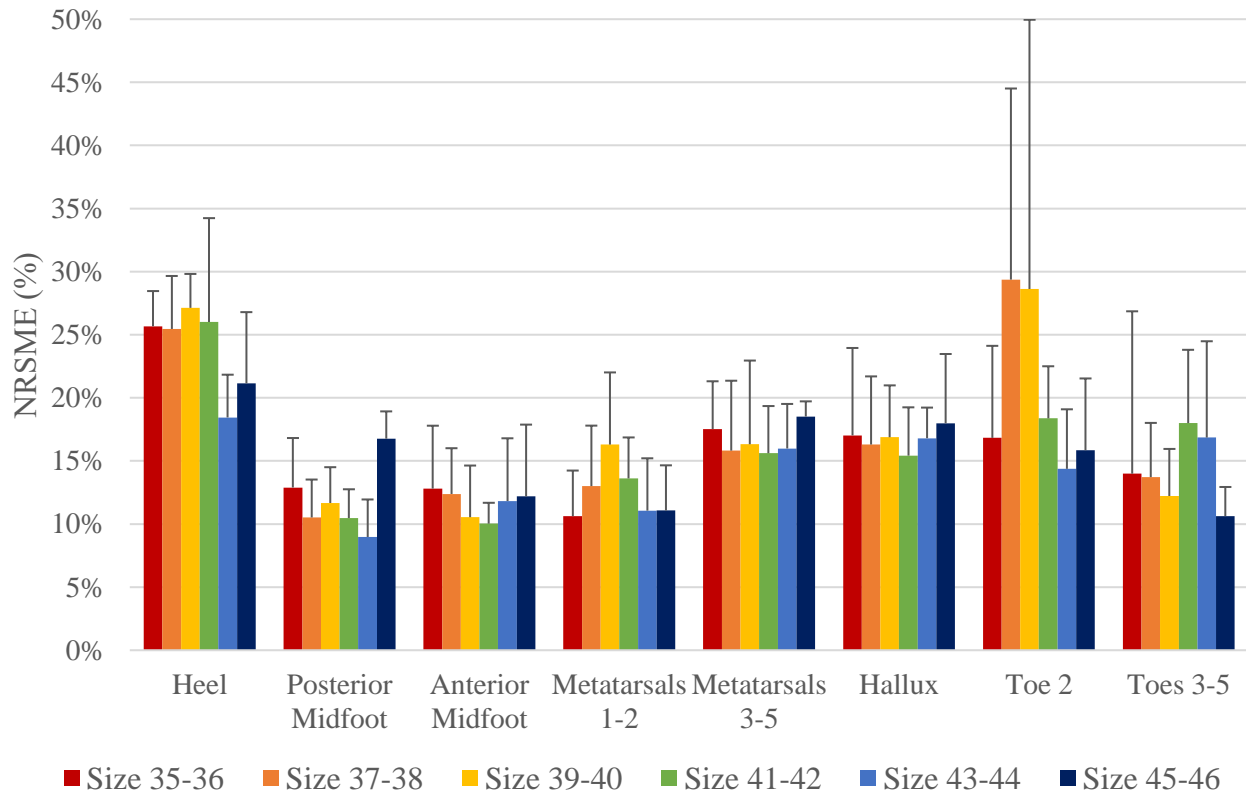


Fig. 28. The NRMSE results for all anatomical regions and insole sizes.

5.3.2. *Plantar tissue model variable results*

The variable results from the model application of each participant were averaged to create a set of variables ($d_0, A, B, C, \bar{k}, n, \bar{c}, m$) for each plantar region for that participant. This was done by combining the data from the three trials and two limbs (six data sets per participant). The participant results were then averaged to determine the variable results for each region, separated by insole size. These results are displayed in Figure 28 and tabulated in Appendix I.

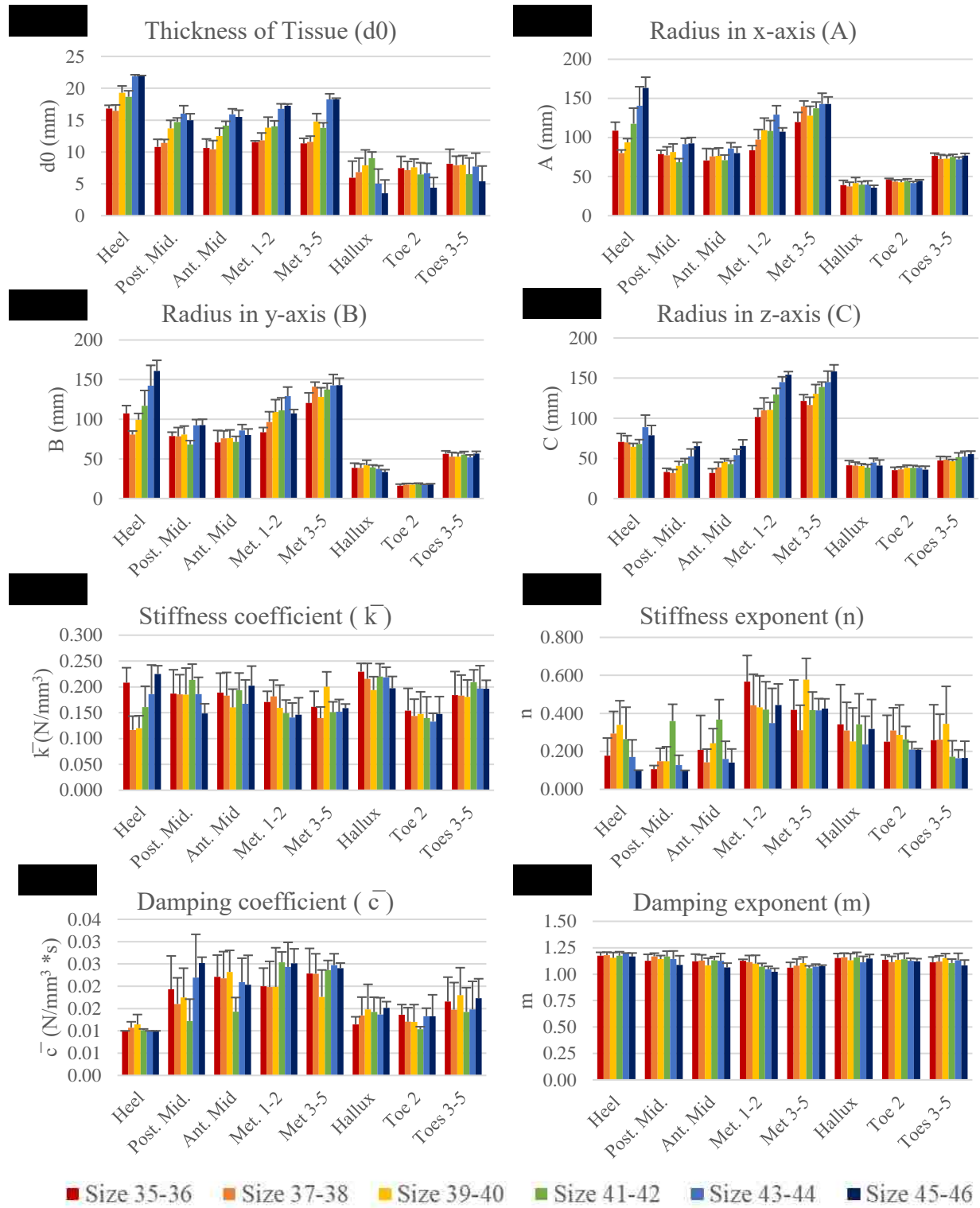


Fig. 29. Averages and standard deviations for the plantar tissue model variables: (a) tissue thickness, (b) radius in x axis, (c) radius in y-axis, (d) radius in z-axis, (e) stiffness, (f) stiffness coefficient, (g) damping, and (h) damping coefficient. Values are displayed for each insole size and plantar region.

5.4. Discussion of plantar tissue model application results

The ellipsoid model was able to reproduce the vertical ground reaction force with varying degrees accuracy, as shown by Figures 26-28 and Table 5. Overall, there was small variations in errors between insole sizes, with respect to plantar region, despite there being several different participants for each insole size. This indicates that the ellipsoid model was robust. These figures and table display that the largest errors were in the heel and toe regions, in particular Toe 2. The toe regions also had larger standard deviations than the other plantar regions. The errors and large standard deviations might have been due to the limited number of sensors available (smaller comparative area) to record the kinetic data. The heel, in contrast, may have had larger errors due to the comparatively high forces seen at heel strike which may not be able to be modeled accurately.

The geometric variables (d_0 , A , B , and C) would increase with insole size, as seen in Figure 28. The ellipsoid radii were the largest for the metatarsals, followed by the heel, which are the largest plantar regions of the foot and have the largest number of insole sensors attributed to them. The results seen in Figure 28 and in Appendix I also indicate that the plantar regions have an approximately circular cross-section, where A and B were close in value, while the radius in the z-axis (C) often was smaller. This would indicate that the spherical models that were proposed earlier had a limited ability to describe the various plantar regions (Güler et al., 1998; Pàmies-Vilà et al., 2014; Shourijeh and McPhee, 2015). The model results show that the plantar tissues were thickest at the heel, followed by the metatarsals and midfoot for all insole sizes. These results are consistent with values previously measured (Thomas et al., 2004; Uzel et al., 2006; Valiant, 1984; Zheng et al., 2000).

The material variables (\bar{k} , n , \bar{c} , m), as shown in Fig. 8, show that each plantar region had a different stiffness and damping characteristics. This means that general foot models or models that combine multiple plantar regions may lead to inaccuracies. The results show that the stiffness \bar{k} was relatively uniform for all plantar regions and insole sizes, but n was the largest at the metatarsal regions. This indicates that these regions had the highest tissue stiffness. These results were comparable to those found in previous research that used load-unload or ultrasound elastography (Thomas et al., 2004; Zheng et al., 2000). In contrast, m was uniform for all plantar regions and insole sizes while \bar{c} was the highest at the midfoot and metatarsal regions, indicating that these regions had the highest energy absorption. The damping values were smaller than that reported by Güler et al., (1998), which highlights the importance of using gait data instead of mechanical experiments where the participant is standing or with their feet in the air.

6. Conclusion and future work

The mechanical characteristics of the plantar tissues during walking is not well understood as most of the current research focuses on testing specific plantar regions in cadavers or while the feet of the participants are raised. Thus, it is necessary to develop a model and conduct experiments that can allow for studying mechanical characteristics of plantar tissues during walking. Researchers have developed various types of models to represent the mechanical behavior of plantar tissues, which include linear material models, load-deformation models, hysteresis models, nonlinear spring-damper models, quasilinear and viscoelastic models, hyperelastic models, and visco-hyperelastic models. These models were often focused on specific regions of the plantar tissues, were not suited for loads experienced during walking, or were not participant specific. Models with varying contact area have been shown to accurately assess the relation between load and deformation of plantar tissues but they need to be more specific to the plantar tissue to be accurate.

In this work, it is hypothesized that a viscoelastic geometric ellipsoid model used to assess multiple structures of the foot would be accurate and robust. This model would be participant-specific and applicable to the entire stance phase of gait.

The proposed viscoelastic ellipsoid model would represent several key anatomical areas: Heel, Posterior Midfoot, Anterior Midfoot, Metatarsals 1-2, Metatarsals 3-5, Toe 1, Toe 2, and Toes 3-5. In this model, the relationship between the applied vertical component of ground reaction force and the deformation within a plantar contact area was represented using a nonlinear spring and damper that were applied to multiple ellipsoids. The equations for the ellipsoid model were developed.

The ellipsoid model required measurement of force and contact area simultaneously. This was done using pressure-measuring insoles (Medilogic ®, Schönefeld, Germany), which are comprised of an arrays of sensors. In this work, these sensors were grouped into each anatomical region. To develop a participant-specific model, multiple participants will wear the insoles while walking, and the resulting data will be processed to calculate ground reaction forces and the corresponding contact areas. The contact areas are approximated into ellipses using an algorithm developed for this purpose. The accuracy of this algorithm was verified through extensive testing.

The insole force and area data were used to optimize the model for each participant as the material properties and geometry of each participant's foot will differ. In particular, the geometry of the ellipse, plantar tissue thickness, and nonlinear spring and damper parameters will be optimized for each participant. The summed square difference between the experimental ground reaction force measured by the insoles and the force produced by the model was the objective function and minimized. Additionally, the root mean square was calculated and normalized to the maximum experimental force in order to determine the error between the model and experimental force. This process was repeated for three trials and the two limbs. The results were averaged to create specific values for each participant and then the averages and standard deviations were calculated for each insole size and plantar region.

The results of the model application was able to show that the ellipsoid model was fairly successful in producing the ground reaction force during walking. It was also able to characterize the footpad thickness that was similar to previous measurements and ellipsoid radii that were able to show the that previous spherical models may be inaccurate. Further, the ellipsoid model was able to characterize stiffness and damping results, that were different for all the plantar

regions. These results were also different from previous research that used data from mechanical tests and experiments where the participant's foot was static. Further, it highlights the importance of considering individual plantar regions as combining these regions could lead to error.

There are limitations to this work. The accuracy of the input data was reliant on the accuracy of the pressure-measuring insoles in measuring ground reaction force and contact area. These measurements have been shown to be accurate by many researchers (Chen and Bates, 2000; Fong et al., 2008; Koch et al., 2016; Lidstone et al., 2019), but the size of the sensing elements can create errors when only a few sensing elements are available for measurement. This would explain the larger errors seen in the toe areas in comparison to other areas of the foot. Future work should consider using insoles with a larger number of sensors and identification techniques to reduce the errors and enhance measurement accuracy. Further, this work had a limited comparison to other literature and physical measurements. Only one researcher examined three-dimensional measurements of stiffness and damping and there has been no research on regions as small as the ones used in this study. However, a large number of participants was used, in comparison to previous plantar tissue model research. Also, the results show relatively small standard deviations in the results. This indicates that the plantar tissue model is robust. Further, the ellipsoid model was able to reproduce ground reaction force data with reasonable accuracy. However, additional research assessing smaller plantar regions of the foot would provide more comparable research to the presented ellipsoid model.

Future uses of the model will be with clinical data collected from persons with plantar diseases, such as diabetes, plantar fasciitis, chronic pain, etc. The results from the application of the viscoelastic ellipsoid model with clinical data will be compared to previous results

determined from healthy data. This comparison would show if there are material differences between the two groups and could lead to predictions and preventions of plantar disease.

Appendix A. Sensor Maps of Medilogic Pressure-Measuring Insoles

The below figures are sensor maps provided by the Medilogic company. These maps show the left insole with the position of the center of each sensor marked with a cross and a number. The total number of sensors is listed in the figure caption of each image. The sizes shown are size 35-36, 37-38, 39-40, 41-42, 43-44, and 45-46.

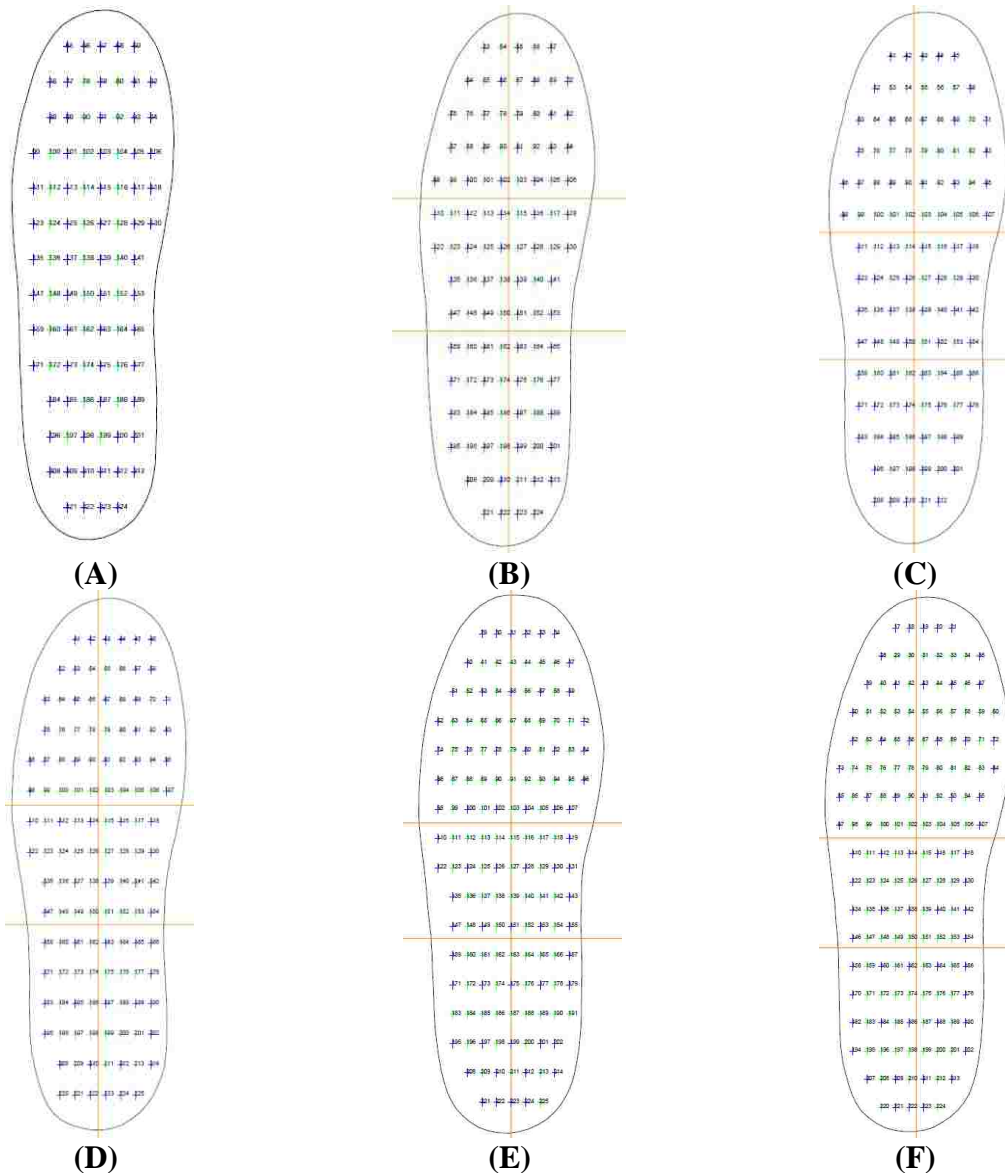


Fig. A.1. (A) Size 35-36 insole with 93 sensors. (B) Size 37-38 insole with 107 sensors. (C) Size 39-40 insole with 116 sensors. (D) Size 41-42 insole with 130 sensors. (E) Size 43-44 insole with 151 sensors. (F) Size 45-46 insole with 162 sensors

Appendix B - Sensor Maps of Medilogic Pressure-Measuring Insoles

Each table presents the sensors of each insole size grouped into the anatomical region. The location of the sensors was determined by the row the sensor resided, with the row that was most anterior being labeled as the first row (first toe row), and the number of sensor in that row progressing from the lateral portion of the foot to the medial portion.

Table B. 1. The sensors for the insole size 35-36 grouped into anatomical regions.

Anatomical Position	Row	Sensor Number
Toe 1	1	5
	2	6 – 7
Toe 2	1	4
	2	5
Toe 3 – 5	1	1 – 3
	2	1 – 4
	3	5 – 7
Metatarsals 1 – 2	4	6 – 8
	5	6 – 8
	6	6 – 8
	3	1 – 4
Metatarsals 3 – 5	4	1 – 5
	5	1 – 5
	6	1 – 5
Midfoot Anterior	7	1 – 7
	8	1 – 7
Midfoot Posterior	9	1 – 7
	10	1 – 7
Heel	11	1 – 6
	12	1 – 6
	13	1 – 6
	14	1 – 4

Table B. 2. The sensors for the insole size 37-38 grouped into anatomical regions.

Anatomical Position	Row	Sensor Number
Toe 1	1	5
	2	6 – 7
Toe 2	1	4
	2	5
Toe 3 – 5	1	1 – 3
	2	1 – 4
	3	6 – 8
Metatarsals 1 – 2	4	6 – 8
	5	7 – 9
	6	7 – 9
	7	7 – 9
Metatarsals 3 – 5	3	1 – 5
	4	1 – 5
	5	1 – 6
	6	1 – 6
Midfoot Anterior	7	1 – 6
	8	1 – 7
Midfoot Posterior	9	1 – 7
	10	1 – 7
Heel	11	1 – 7
	12	1 – 7
	13	1 – 7
	14	1 – 6
	15	1 – 4

Table B. 3. The sensors for the insole size 39-40 grouped into anatomical regions.

Anatomical Position	Row	Sensor Number
Toe 1	1	5
	2	6 – 7
Toe 2	1	4
	2	5
Toe 3 – 5	1	1 – 3
	2	1 – 4
Metatarsals 1 – 2	3	6 – 9
	4	6 – 9
	5	7 – 10
	6	7 – 10
Metatarsals 3 – 5	3	1 – 5
	4	1 – 5
	5	1 – 6
	6	1 – 6
Midfoot Anterior	7	1 – 8
	8	1 – 8
Midfoot Posterior	9	1 – 8
	10	1 – 8
Heel	11	1 – 8
	12	1 – 8
	13	1 – 7
	14	1 – 6
	15	1 – 5

Table B. 4. The sensors for the insole size 41-42 grouped into anatomical regions.

Anatomical Position	Row	Sensor Number
Toe 1	1	5 – 6
	2	6 – 7
Toe 2	1	4
	2	5
Toe 3 – 5	1	1 – 3
	2	1 – 4
Metatarsals 1 – 2	3	6 – 9
	4	6 – 9
	5	7 – 10
	6	7 – 10
	7	7 – 9
Metatarsals 3 – 5	3	1 – 5
	4	1 – 5
	5	1 – 6
	6	1 – 6
Midfoot Anterior	7	1 – 6
	8	1 – 8
Midfoot Posterior	9	1 – 8
	10	1 – 8
Heel	11	1 – 8
	12	1 – 8
	13	1 – 8
	14	1 – 8
	15	1 – 7
	16	1 – 6

Table B. 5. The sensors for the insole size 43-44 grouped into anatomical regions.

Anatomical Position	Row	Sensor Number
Toe 1	1	6
	2	7 – 8
Toe 2	1	5
	2	6
Toe 3 – 5	1	1 – 4
	2	1 – 5
Metatarsals 1 – 2	3	7 – 9
	4	8 – 11
	5	8 – 11
	6	8 – 11
	7	8 – 10
	8	8 – 10
Metatarsals 3 – 5	3	1 – 6
	4	1 – 7
	5	1 – 7
	6	1 – 7
	7	1 – 7
Midfoot Anterior	8	1 – 7
	9	1 – 10
Midfoot Posterior	10	1 – 9
	11	1 – 9
Heel	12	1 – 9
	13	1 – 9
	14	1 – 9
	15	1 – 8
	16	1 – 7
	17	1 – 5

Table B. 6. The sensors for the insole size 45-46 grouped into anatomical regions.

Anatomical Position	Row	Sensor Number
Toe 1	1	5
	2	6 – 8
Toe 2	1	4
	2	5
Toe 3 – 5	1	1 – 3
	2	1 – 4
Metatarsals 1 – 2	3	8 – 11
	4	8 – 11
	5	8 – 11
	6	8 – 11
	7	8 – 10
	8	8 – 10
Metatarsals 3 – 5	3	1 – 7
	4	1 – 7
	5	1 – 7
	6	1 – 7
	7	1 – 7
Midfoot Anterior	8	1 – 7
	9	1 – 9
Midfoot Posterior	10	1 – 9
	11	1 – 9
Heel	12	1 – 9
	13	1 – 9
	14	1 – 9
	15	1 – 9
	16	1 – 9
	17	1 – 7
	18	1 – 5

Appendix C – IRB Approval of Protocol #724468-5



INFORMED CONSENT

Department of Kinesiology and Nutrition Sciences

TITLE OF STUDY: Reliability of pressuring measuring insoles

INVESTIGATOR(S): J.S. Dufek, Ph.D., M.B. Trabia, Ph.D., J. DeBerardinis, B.S., David Samson

For questions or concerns about the study, you may contact Dr. J.S. Dufek at 702.895.0702.

For questions regarding the rights of research subjects, any complaints or comments regarding the manner in which the study is being conducted, contact the UNLV Office of Research Integrity – Human Subjects at 702-895-2794, toll free at 877-895-2794 or via email at IRB@unlv.edu.

Purpose of the Study

You are invited to participate in a research study. The purpose of this study is to assess the reliability of a pressure-measuring insole system.

Participants

You are being asked to participate in the study because you fit these criteria:

- Healthy individual between the ages of 18-55 years;
- Able to walk a distance of for 20 m, unassisted, 3-15 times at each of three speeds; with breaks as desired;
- You are not a pregnant female beyond your first trimester.

Procedures

If you volunteer to participate in this study, you will be asked to do the following:

- Measure and/or record your weight, height, gender, birthdate, and insole size;
- Take off your shoes and place insoles inside a pair of socks;
- Practice walking in the experimental environment;
- Sit with your feet up approximately 1-2 inches in the air, not touching the floor, for two 5-second sessions;
- Stand quietly (as motionless as possible) on both feet with weight equally distributed, for 15 seconds;
- Walk at a normal speed, a fast speed, and a slow speed for up to 20-m, contacting your each foot on each of two force platforms, mounted flush on the floor;
- This procedure will be repeated until the total number of acceptable trials (n=3) have been completed or until the maximum number of attempts (n=15) have been performed at each speed.

Benefits of Participation

There may not be direct benefits to you as a participant in this study. However, we hope to learn about the reliability of the pressure-measuring insole system.

TITLE OF STUDY: *Reliability of pressure measuring insoles*

Risks of Participation

There are risks involved in all research studies. This study may include only minimal risks. It is possible that you might experience delayed muscle soreness or discomfort as a result of your physical performance. This is a reversible outcome after rest. Every effort will be made to avoid soreness by asking you to walk at a comfortable speed, at a self-determined slow speed, and at a self-determined fast speed. In addition, you might slip or trip while walking without shoes, wearing only socks. We will keep the walkway clean, dry and free of any obstacles or hazards to minimize this risk.

Cost/Compensation

There may not be financial cost to you to participate in this study. The study will take 20 to 60 minutes of your time. You will not be compensated for your time.

Confidentiality

All information gathered in this study will be kept as confidential as possible. No reference will be made in written or oral materials that could link you to this study. Your data will be referred to only by subject number. Your name will not be associated with the data. All records will be stored in a locked facility at UNLV for 3 years after completion of the study. After the storage time the information gathered will be destroyed.

Voluntary Participation

Your participation in this study is voluntary. You may refuse to participate in this study or in any part of this study. You may withdraw at any time without prejudice to your relations with UNLV. You are encouraged to ask questions about this study at the beginning or any time during the research study.

Participant Consent:

I have read the above information and agree to participate in this study. I have been able to ask questions about the research study. I am at least 18 years of age. A copy of this form has been given to me.

Signature of Participant

Date

Participant Name (Please Print)

Appendix D - Boundary Method used for Verification of Neighbors

The methods used in Case 3 to select the points bordering an active sensor were validated against the Matlab function *Boundary*. This function uses a matrix of points to create a single, conforming 2-D boundary from the given points. The output is a coordinate vector of the boundary points chosen.

The *Boundary* method utilizes circular alpha shapes to “scoop out” the shape created by the points (Amenta, 2011). This can be seen in Fig. D.1 (A). Then, the Delaunay triangulation is used to determine the outside boundary of the shape by connecting intersecting circles. These can be seen in Fig. D.1 (B).

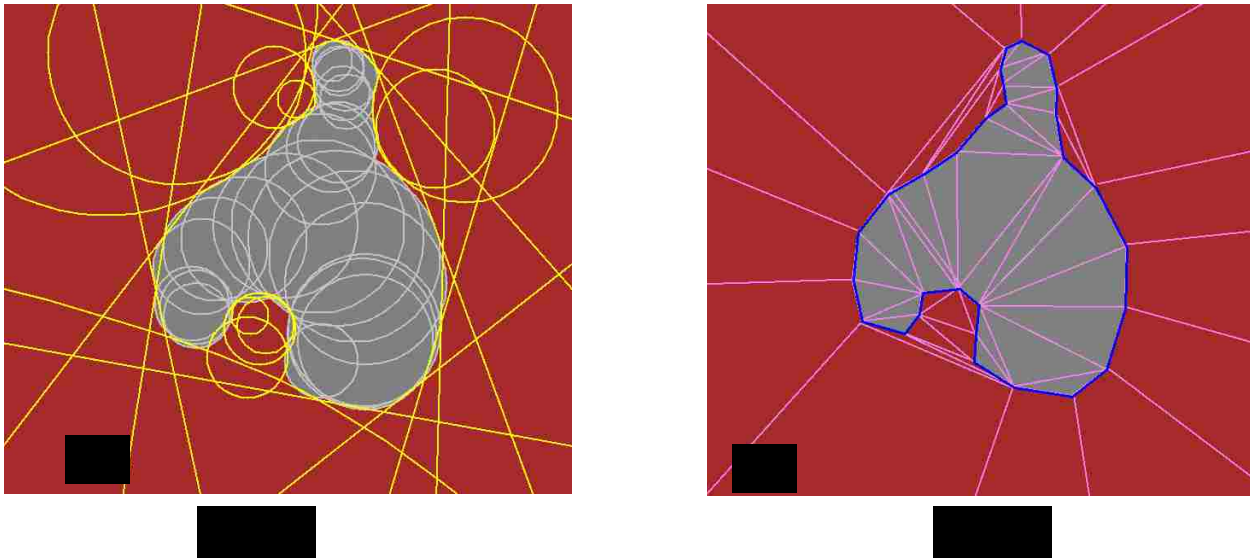


Fig. D. 1. This figure shows the steps used by the boundary function. (A) Alpha shapes in the form of circles are used to “scoop out” the 2D shape. (B) The Delaunay triangulation is used to determine the border (in blue). These images are taken, with permission, from Amenta (2011).

Appendix E - Ellipse fitting method

This ellipse fitting method designed by Brown (2007) utilizes the points given has an ellipse fitted using a nonlinear least-squares method. The initial guess for the fitting method uses a linear least squares routine which, by default, uses a Bookstein constraint. The Bookstein constraint is an Euclidean-invariant constraint comprised of eigen values.

It utilizes the following equation to describe an ellipse and outputs the variables z , a , b , and α .

$$X = z + Q(\alpha) \begin{bmatrix} a \cos(\theta) \\ b \sin(\theta) \end{bmatrix}, \quad (\text{F. 1})$$

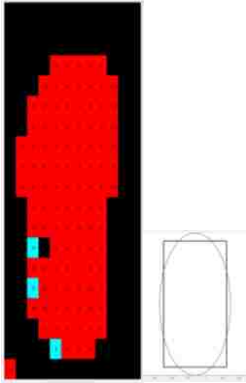
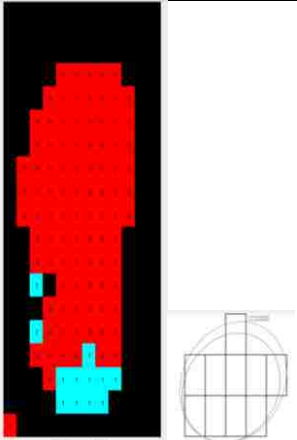
where:

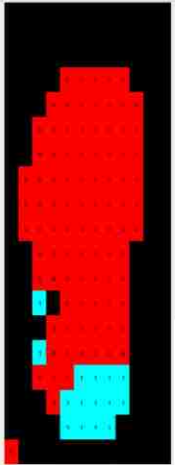
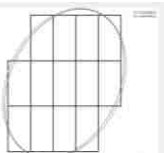
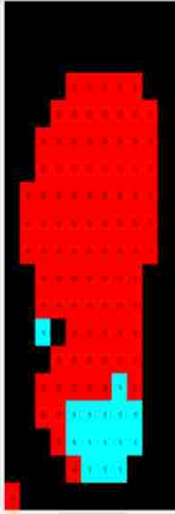
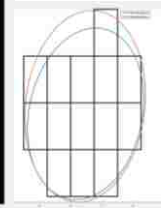
- X vector of the point coordinates
- z coordinate center of the ellipse
- a radii in the x direction
- b radii in the y direction
- θ parameter that ranges from 0 to 2π

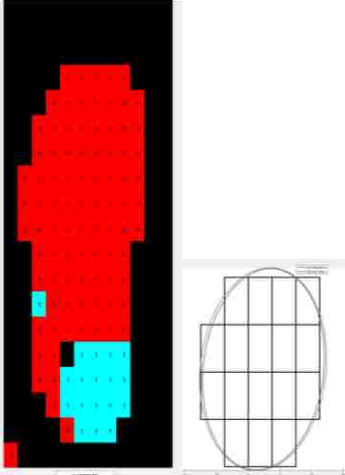
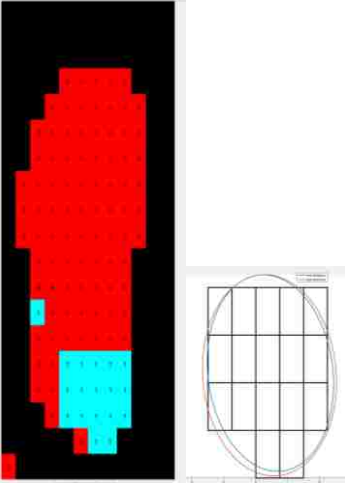
$Q(\alpha)$ rotation matrix, defined in as:

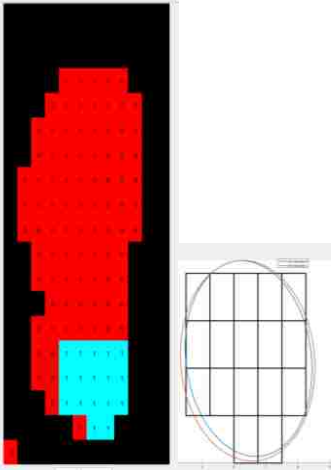
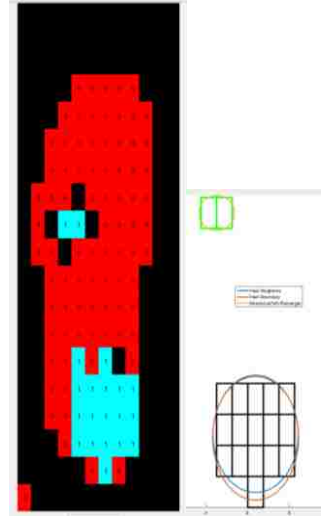
$$Q(\alpha) = \begin{bmatrix} \cos(\alpha) & -\sin(\alpha) \\ \sin(\alpha) & \cos(\alpha) \end{bmatrix}. \quad (\text{F. 2})$$

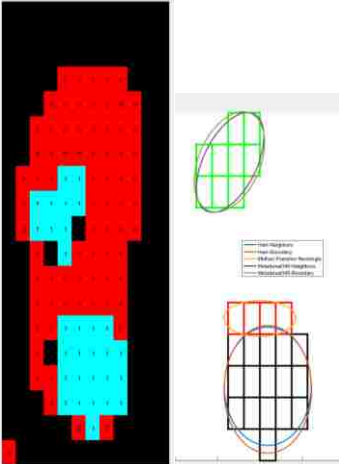
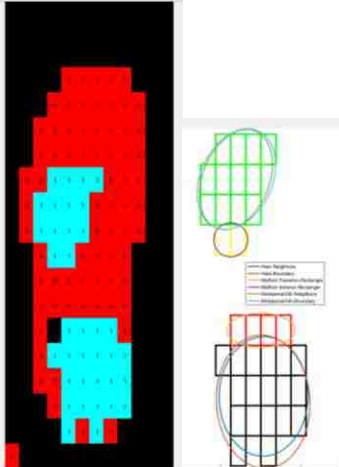
Appendix F – Results of Ellipse Fitting for Participant 112, Trial 1 – Left Foot

Time instant	Images: • Threshold insole – 1 is active sensor, 0 is inactive. • Ellipses fitted to the active sensors	Anatomical Location	Sensor Area (cm)	Normalized Area					
				Rectangle		Boundaries		Neighbors	
				Norm. Area	Area (cm ²)	Norm. Area	Area (cm ²)	Norm. Area	Area (cm ²)
1		Heel	1.1250	1.0000	1.1250	--	--	--	--
		Midfoot Posterior	--	--	--	--	--	--	--
		Midfoot Anterior	--	--	--	--	--	--	--
		Metatarsals 1-2	--	--	--	--	--	--	--
		Metatarsals 3-5	--	--	--	--	--	--	--
		Toe 1	--	--	--	--	--	--	--
		Toe 2	--	--	--	--	--	--	--
		Toes 3-5	--	--	--	--	--	--	--
		2		Heel	11.2500	--	--	1.2066	13.5740
Midfoot Posterior	--			--	--	--	--	--	--
Midfoot Anterior	--			--	--	--	--	--	--
Metatarsals 1-2	--			--	--	--	--	--	--
Metatarsals 3-5	--			--	--	--	--	--	--
Toe 1	--			--	--	--	--	--	--
Toe 2	--			--	--	--	--	--	--
Toes 3-5	--			--	--	--	--	--	--

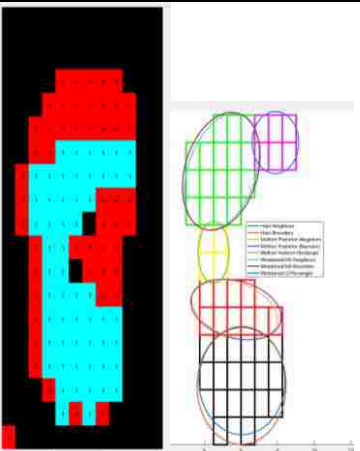
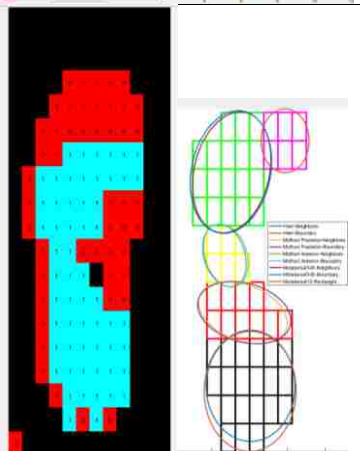
Time instant	Images: • Threshold insole – 1 is active sensor, 0 is inactive. • Ellipses fitted to the active sensors		Anatomical Location	Sensor Area (cm)	Normalized Area					
					Rectangle		Boundaries		Neighbors	
					Norm. Area	Area (cm ²)	Norm. Area	Area (cm ²)	Norm. Area	Area (cm ²)
3			Heel	14.6250	--	--	1.0550	15.4296	1.0019	14.6523
			Midfoot Posterior	--	--	--	--	--	--	--
			Midfoot Anterior	--	--	--	--	--	--	--
			Metatarsals 1-2	--	--	--	--	--	--	--
			Metatarsals 3-5	--	--	--	--	--	--	--
			Toe 1	--	--	--	--	--	--	--
			Toe 2	--	--	--	--	--	--	--
			Toes 3-5	--	--	--	--	--	--	--
4			Heel	15.7500	--	--	1.1740	18.4909	1.0049	15.8279
			Midfoot Posterior	--	--	--	--	--	--	--
			Midfoot Anterior	--	--	--	--	--	--	--
			Metatarsals 1-2	--	--	--	--	--	--	--
			Metatarsals 3-5	--	--	--	--	--	--	--
			Toe 1	--	--	--	--	--	--	--
			Toe 2	--	--	--	--	--	--	--
			Toes 3-5	--	--	--	--	--	--	--

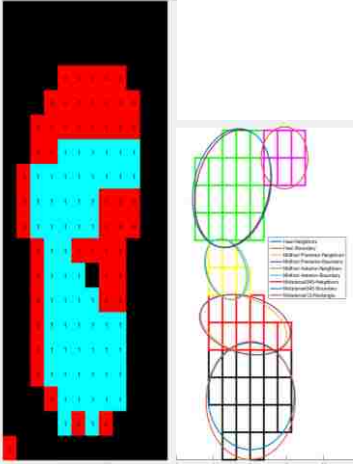
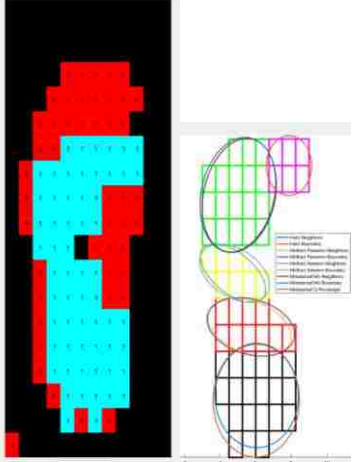
Time instant	Images: <ul style="list-style-type: none"> • Threshold insole – 1 is active sensor, 0 is inactive. • Ellipses fitted to the active sensors 	Anatomical Location	Sensor Area (cm)	Normalized Area					
				Rectangle		Boundaries		Neighbors	
				Norm. Area	Area (cm ²)	Norm. Area	Area (cm ²)	Norm. Area	Area (cm ²)
5		Heel	19.1250	--	--	1.0520	20.1203	1.0008	19.1395
		Midfoot Posterior	--	--	--	--	--	--	--
		Midfoot Anterior	--	--	--	--	--	--	--
		Metatarsals 1-2	--	--	--	--	--	--	--
		Metatarsals 3-5	--	--	--	--	--	--	--
		Toe 1	--	--	--	--	--	--	--
		Toe 2	--	--	--	--	--	--	--
		Toes 3-5	--	--	--	--	--	--	--
6		Heel	19.1250	--	--	1.0940	20.9229	1.0024	19.1716
		Midfoot Posterior	--	--	--	--	--	--	--
		Midfoot Anterior	--	--	--	--	--	--	--
		Metatarsals 1-2	--	--	--	--	--	--	--
		Metatarsals 3-5	--	--	--	--	--	--	--
		Toe 1	--	--	--	--	--	--	--
		Toe 2	--	--	--	--	--	--	--
		Toes 3-5	--	--	--	--	--	--	--

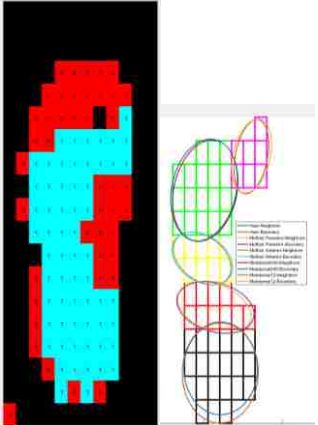
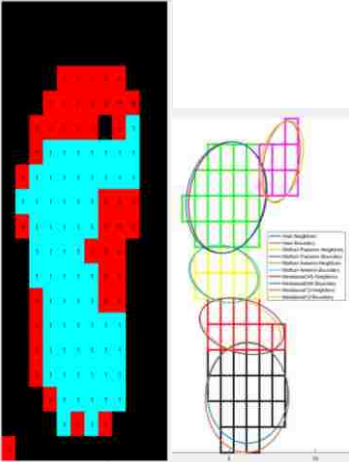
Time instant	Images: <ul style="list-style-type: none"> • Threshold insole – 1 is active sensor, 0 is inactive. • Ellipses fitted to the active sensors 	Anatomical Location	Sensor Area (cm)	Normalized Area					
				Rectangle		Boundaries		Neighbors	
				Norm. Area	Area (cm ²)	Norm. Area	Area (cm ²)	Norm. Area	Area (cm ²)
7		Heel	19.1250	--	--	1.0940	20.9229	1.0024	19.1716
		Midfoot Posterior	--	--	--	--	--	--	--
		Midfoot Anterior	--	--	--	--	--	--	--
		Metatarsals 1-2	--	--	--	--	--	--	--
		Metatarsals 3-5	--	--	--	--	--	--	--
		Toe 1	--	--	--	--	--	--	--
		Toe 2	--	--	--	--	--	--	--
		Toes 3-5	--	--	--	--	--	--	--
8		Heel	18.0000	--	--	1.0940	19.6299	1.0024	18.0834
		Midfoot Posterior	--	--	--	--	--	--	--
		Midfoot Anterior	--	--	--	--	--	--	--
		Metatarsals 1-2	--	--	--	--	--	--	--
		Metatarsals 3-5	2.2500	1.0000	2.2500	--	--	--	--
		Toe 1	--	--	--	--	--	--	--
		Toe 2	--	--	--	--	--	--	--
		Toes 3-5	--	--	--	--	--	--	--

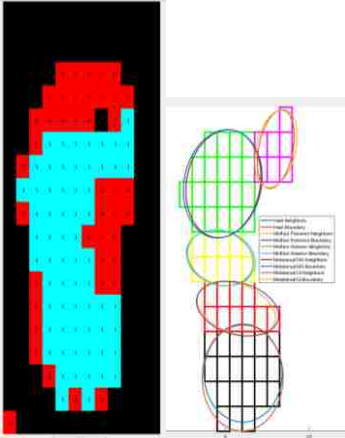
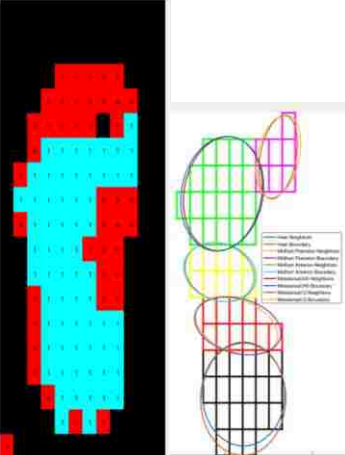
Time instant	Images: <ul style="list-style-type: none"> • Threshold insole – 1 is active sensor, 0 is inactive. • Ellipses fitted to the active sensors 	Anatomical Location	Sensor Area (cm)	Normalized Area					
				Rectangle		Boundaries		Neighbors	
				Norm. Area	Area (cm ²)	Norm. Area	Area (cm ²)	Norm. Area	Area (cm ²)
9		Heel	18.0000	--	--	1.0940	19.6299	1.0024	18.0834
		Midfoot Posterior	4.5000	1.0000	4.5000	--	--	--	--
		Midfoot Anterior	--	--	--	--	--	--	--
		Metatarsals 1-2	--	--	--	--	--	--	--
		Metatarsals 3-5	10.1250	--	--	1.1322	11.4635	1.0013	10.1385
		Toe 1	--	--	--	--	--	--	--
		Toe 2	--	--	--	--	--	--	--
		Toes 3-5	--	--	--	--	--	--	--
10		Heel	20.2500	--	--	1.1978	24.2550	1.0197	20.6490
		Midfoot Posterior	4.5000	1.0000	4.5000	--	--	--	--
		Midfoot Anterior	2.2500	1.0000	2.2500	--	--	--	--
		Metatarsals 1-2	--	--	--	--	--	--	--
		Metatarsals 3-5	13.5000	--	--	1.0895	14.7077	1.0032	13.5432
		Toe 1	--	--	--	--	--	--	--
		Toe 2	--	--	--	--	--	--	--
		Toes 3-5	--	--	--	--	--	--	--

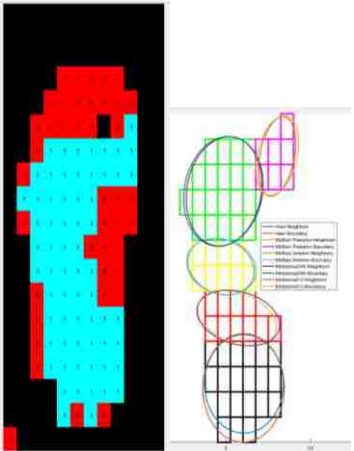
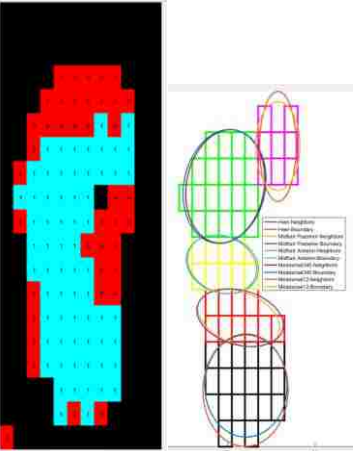
Time instant	Images: <ul style="list-style-type: none"> • Threshold insole – 1 is active sensor, 0 is inactive. • Ellipses fitted to the active sensors 	Anatomical Location	Sensor Area (cm)	Normalized Area					
				Rectangle		Boundaries		Neighbors	
				Norm. Area	Area (cm ²)	Norm. Area	Area (cm ²)	Norm. Area	Area (cm ²)
11		Heel	20.2500	--	--	1.1978	24.2550	1.0197	20.6490
		Midfoot Posterior	7.8750	--	--	1.1955	9.4149	1.1378	8.9598
		Midfoot Anterior	3.3750	--	--	1.1090	3.7429	1.0248	3.4588
		Metatarsals 1-2	2.2500	1.0000	2.2500	--	--	--	--
		Metatarsals 3-5	13.500	--	--	1.0895	14.7077	1.0032	13.5432
		Toe 1	--	--	--	--	--	--	--
		Toe 2	--	--	--	--	--	--	--
		Toes 3-5	--	--	--	--	--	--	--
12		Heel	21.3750	--	--	1.1481	24.5404	1.0081	21.5486
		Midfoot Posterior	11.2500	--	--	1.0987	12.3602	1.0152	11.4211
		Midfoot Anterior	4.5000	1.0000	4.5000	--	--	--	--
		Metatarsals 1-2	5.6250	--	--	1.0940	6.1538	1.0050	5.6530
		Metatarsals 3-5	16.8750	--	--	1.1649	19.6579	1.0064	16.9826
		Toe 1	--	--	--	--	--	--	--
		Toe 2	--	--	--	--	--	--	--
		Toes 3-5	--	--	--	--	--	--	--

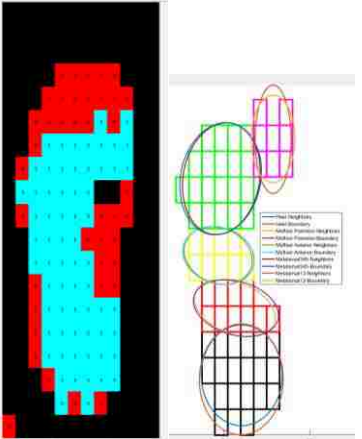
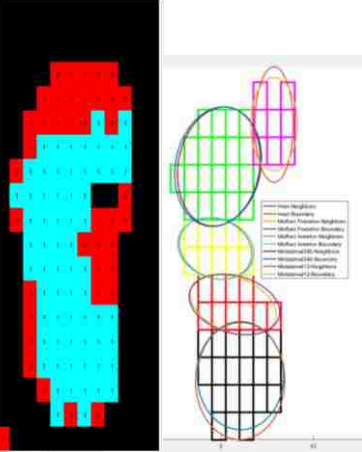
Time instant	Images: <ul style="list-style-type: none"> • Threshold insole – 1 is active sensor, 0 is inactive. • Ellipses fitted to the active sensors 	Anatomical Location	Sensor Area (cm)	Normalized Area					
				Rectangle		Boundaries		Neighbors	
				Norm. Area	Area (cm ²)	Norm. Area	Area (cm ²)	Norm. Area	Area (cm ²)
13		Heel	21.3750	--	--	1.1481	24.5404	1.0081	21.5486
		Midfoot Posterior	11.2500	--	--	1.0987	12.3602	1.0152	11.4211
		Midfoot Anterior	4.5000	1.0000	4.5000	--	--	--	--
		Metatarsals 1-2	6.7500	1.0000	6.7500	--	--	--	--
		Metatarsals 3-5	19.1250	--	--	1.0772	20.6006	1.0010	19.1436
		Toe 1	--	--	--	--	--	--	--
		Toe 2	--	--	--	--	--	--	--
		Toes 3-5	--	--	--	--	--	--	--
14		Heel	21.3750	--	--	1.1481	24.5404	1.0081	21.5486
		Midfoot Posterior	11.2500	--	--	1.0987	12.3602	1.0152	11.4211
		Midfoot Anterior	5.6250	--	--	1.0940	6.1538	1.0050	5.6530
		Metatarsals 1-2	6.7500	1.0000	6.7500	--	--	--	--
		Metatarsals 3-5	20.2500	--	--	1.0677	21.6214	1.0063	20.3767
		Toe 1	--	--	--	--	--	--	--
		Toe 2	--	--	--	--	--	--	--
		Toes 3-5	--	--	--	--	--	--	--

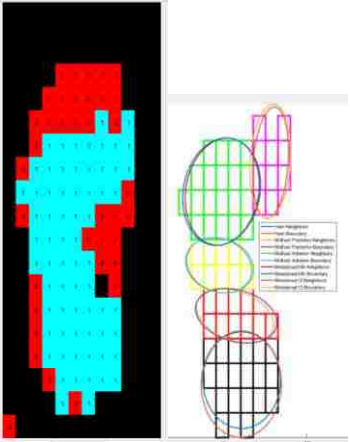
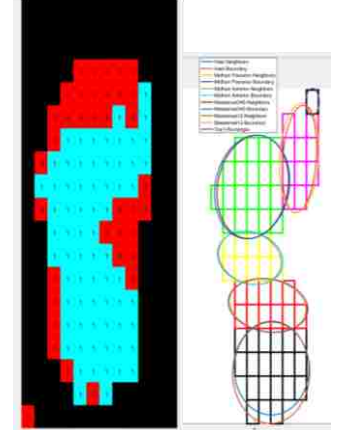
Time instant	Images: • Threshold insole – 1 is active sensor, 0 is inactive. • Ellipses fitted to the active sensors	Anatomical Location	Sensor Area (cm)	Normalized Area					
				Rectangle		Boundaries		Neighbors	
				Norm. Area	Area (cm ²)	Norm. Area	Area (cm ²)	Norm. Area	Area (cm ²)
15		Heel	21.3750	--	--	1.1481	24.5404	1.0081	21.5486
		Midfoot Posterior	11.2500	--	--	1.0987	12.3602	1.0152	11.4211
		Midfoot Anterior	5.6250	--	--	1.0940	6.1538	1.0050	5.6530
		Metatarsals 1-2	6.7500	1.0000	6.7500	--	--	--	--
		Metatarsals 3-5	20.2500	--	--	1.0677	21.6214	1.0063	20.3767
		Toe 1	--	--	--	--	--	--	--
		Toe 2	--	--	--	--	--	--	--
		Toes 3-5	--	--	--	--	--	--	--
16		Heel	21.3750	--	--	1.1481	24.5404	1.0081	21.5486
		Midfoot Posterior	11.2500	--	--	1.0987	12.3602	1.0152	11.4211
		Midfoot Anterior	7.8750	--	--	1.1679	9.1974	1.0018	7.8889
		Metatarsals 1-2	6.7500	1.0000	6.7500	--	--	--	--
		Metatarsals 3-5	20.2500	--	--	1.0677	21.6214	1.0063	20.3767
		Toe 1	--	--	--	--	--	--	--
		Toe 2	--	--	--	--	--	--	--
		Toes 3-5	--	--	--	--	--	--	--

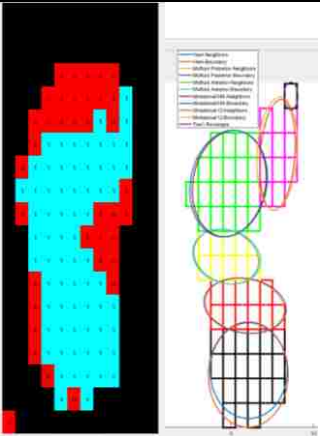
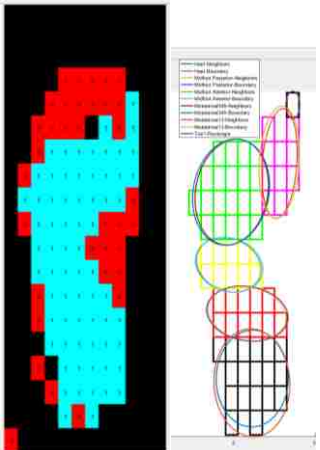
Time instant	Images: • Threshold insole – 1 is active sensor, 0 is inactive. • Ellipses fitted to the active sensors	Anatomical Location	Sensor Area (cm)	Normalized Area					
				Rectangle		Boundaries		Neighbors	
				Norm. Area	Area (cm ²)	Norm. Area	Area (cm ²)	Norm. Area	Area (cm ²)
17		Heel	21.3750	--	--	1.1481	24.5404	1.0081	21.5486
		Midfoot Posterior	11.2500	--	--	1.0987	12.3602	1.0152	11.4211
		Midfoot Anterior	9.0000	--	--	1.0748	9.6731	1.0025	9.0221
		Metatarsals 1-2	7.8750	--	--	1.1315	8.9107	0.9855	7.7612
		Metatarsals 3-5	20.2500	--	--	1.0677	21.6214	1.0063	20.3767
		Toe 1	--	--	--	--	--	--	--
		Toe 2	--	--	--	--	--	--	--
		Toes 3-5	--	--	--	--	--	--	--
18		Heel	21.3750	--	--	1.1481	24.5404	1.0081	21.5486
		Midfoot Posterior	11.2500	--	--	1.0987	12.3602	1.0152	11.4211
		Midfoot Anterior	10.1250	--	--	1.0682	10.8153	1.0106	10.2324
		Metatarsals 1-2	7.8750	--	--	1.1315	8.9107	0.9855	7.7612
		Metatarsals 3-5	20.2500	--	--	1.0677	24.0128	1.0063	22.7442
		Toe 1	--	--	--	--	--	--	--
		Toe 2	--	--	--	--	--	--	--
		Toes 3-5	--	--	--	--	--	--	--

Time instant	Images: • Threshold insole – 1 is active sensor, 0 is inactive. • Ellipses fitted to the active sensors	Anatomical Location	Sensor Area (cm)	Normalized Area					
				Rectangle		Boundaries		Neighbors	
				Norm. Area	Area (cm ²)	Norm. Area	Area (cm ²)	Norm. Area	Area (cm ²)
19		Heel	21.3750	--	--	1.1481	24.5404	1.0081	21.5486
		Midfoot Posterior	11.2500	--	--	1.0987	12.3602	1.0152	11.4211
		Midfoot Anterior	10.1250	--	--	1.0682	10.8153	1.0106	10.2324
		Metatarsals 1-2	7.8750	--	--	1.1315	8.9107	0.9855	7.7612
		Metatarsals 3-5	20.2500	--	--	1.0677	24.0128	1.0063	22.7442
		Toe 1	--	--	--	--	--	--	--
		Toe 2	--	--	--	--	--	--	--
		Toes 3-5	--	--	--	--	--	--	--
20		Heel	21.3750	--	--	1.1481	24.5404	1.0081	21.5486
		Midfoot Posterior	11.2500	--	--	1.0987	12.3602	1.0152	11.4211
		Midfoot Anterior	10.1250	--	--	1.0682	10.8153	1.0106	10.2324
		Metatarsals 1-2	7.8750	--	--	1.1315	8.9107	0.9855	7.7612
		Metatarsals 3-5	20.2500	--	--	1.0677	24.0128	1.0063	22.7442
		Toe 1	--	--	--	--	--	--	--
		Toe 2	--	--	--	--	--	--	--
		Toes 3-5	--	--	--	--	--	--	--

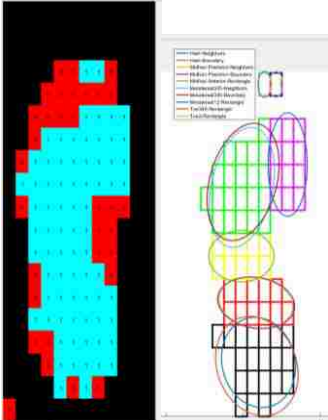
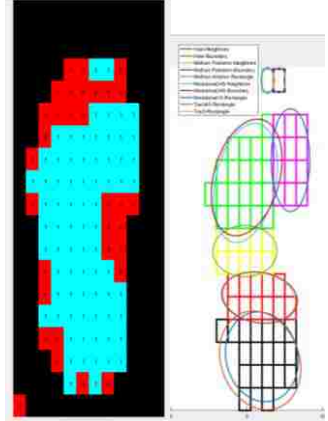
Time instant	Images: • Threshold insole – 1 is active sensor, 0 is inactive. • Ellipses fitted to the active sensors		Anatomical Location	Sensor Area (cm)	Normalized Area					
					Rectangle		Boundaries		Neighbors	
					Norm. Area	Area (cm ²)	Norm. Area	Area (cm ²)	Norm. Area	Area (cm ²)
21		Heel	21.3750	--	--	1.1481	24.5404	1.0081	21.5486	
		Midfoot Posterior	11.2500	--	--	1.0987	12.3602	1.0152	11.4211	
		Midfoot Anterior	10.1250	--	--	1.0682	10.8153	1.0106	10.2324	
		Metatarsals 1-2	7.8750	--	--	1.1315	8.9107	0.9855	7.7612	
		Metatarsals 3-5	20.2500	--	--	1.0677	24.0128	1.0063	22.7442	
		Toe 1	--	--	--	--	--	--	--	
		Toe 2	--	--	--	--	--	--	--	
		Toes 3-5	--	--	--	--	--	--	--	
22		Heel	21.3750	--	--	1.1481	24.5404	1.0081	21.5486	
		Midfoot Posterior	11.2500	--	--	1.0987	12.3602	1.0152	11.4211	
		Midfoot Anterior	10.1250	--	--	1.0682	10.8153	1.0106	10.2324	
		Metatarsals 1-2	9.0000	--	--	1.1181	10.0626	1.1448	10.3036	
		Metatarsals 3-5	20.2500	--	--	1.0677	24.0128	1.0063	22.7442	
		Toe 1	--	--	--	--	--	--	--	
		Toe 2	--	--	--	--	--	--	--	
		Toes 3-5	--	--	--	--	--	--	--	

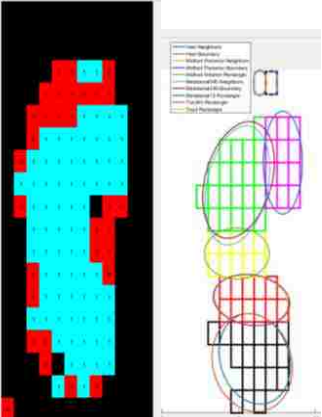
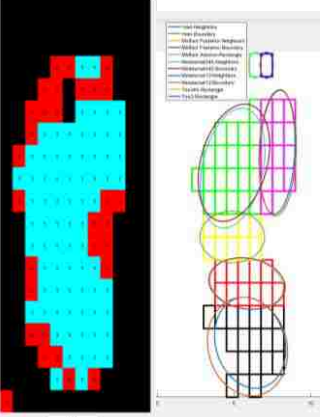
Time instant	<p>Images:</p> <ul style="list-style-type: none"> Threshold insole – 1 is active sensor, 0 is inactive. Ellipses fitted to the active sensors 	Anatomical Location	Sensor Area (cm)	Normalized Area					
				Rectangle		Boundaries		Neighbors	
				Norm. Area	Area (cm ²)	Norm. Area	Area (cm ²)	Norm. Area	Area (cm ²)
23		Heel	21.3750	--	--	1.1481	24.5404	1.0081	21.5486
		Midfoot Posterior	11.2500	--	--	1.0987	12.3602	1.0152	11.4211
		Midfoot Anterior	10.1250	--	--	1.0682	10.8153	1.0106	10.2324
		Metatarsals 1-2	9.0000	--	--	1.1181	10.0626	1.1448	10.3036
		Metatarsals 3-5	20.2500	--	--	1.0677	24.0128	1.0063	22.7442
		Toe 1	--	--	--	--	--	--	--
		Toe 2	--	--	--	--	--	--	--
		Toes 3-5	--	--	--	--	--	--	--
24		Heel	21.3750	--	--	1.1481	24.5404	1.0081	21.5486
		Midfoot Posterior	11.2500	--	--	1.0987	12.3602	1.0152	11.4211
		Midfoot Anterior	10.1250	--	--	1.0682	10.8153	1.0106	10.2324
		Metatarsals 1-2	9.0000	--	--	1.1181	10.0626	1.1448	10.3036
		Metatarsals 3-5	20.2500	--	--	1.0677	24.0128	1.0063	22.7442
		Toe 1	--	--	--	--	--	--	--
		Toe 2	--	--	--	--	--	--	--
		Toes 3-5	--	--	--	--	--	--	--

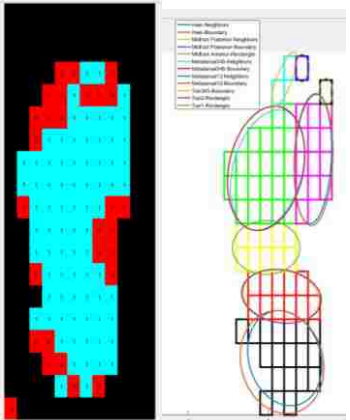
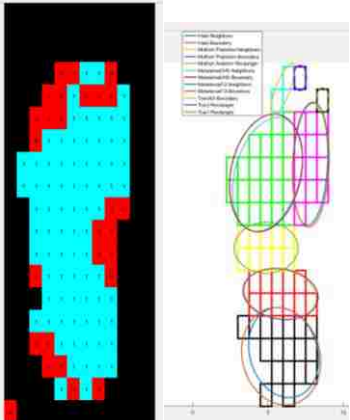
Time instant	Images: <ul style="list-style-type: none"> • Threshold insole – 1 is active sensor, 0 is inactive. • Ellipses fitted to the active sensors 	Anatomical Location	Sensor Area (cm)	Normalized Area					
				Rectangle		Boundaries		Neighbors	
				Norm. Area	Area (cm ²)	Norm. Area	Area (cm ²)	Norm. Area	Area (cm ²)
25		Heel	21.3750	--	--	1.1481	24.5404	1.0081	21.5486
		Midfoot Posterior	11.2500	--	--	1.0987	12.3602	1.0152	11.4211
		Midfoot Anterior	10.1250	--	--	1.0682	10.8153	1.0106	10.2324
		Metatarsals 1-2	11.2500	--	--	1.1772	13.2437	0.9995	11.2448
		Metatarsals 3-5	20.2500	--	--	1.0677	24.0128	1.0063	22.7442
		Toe 1	--	--	--	--	--	--	--
		Toe 2	--	--	--	--	--	--	--
		Toes 3-5	--	--	--	--	--	--	--
26		Heel	21.3750	--	--	1.1481	24.5404	1.0081	21.5486
		Midfoot Posterior	12.3750	--	--	1.0617	13.1391	1.0122	12.5262
		Midfoot Anterior	10.1250	--	--	1.0682	10.8153	1.0106	10.2324
		Metatarsals 1-2	11.2500	--	--	1.1772	13.2437	0.9995	11.2448
		Metatarsals 3-5	20.2500	--	--	1.0677	24.0128	1.0063	22.7442
		Toe 1	1.1250	1.0000	1.1250	--	--	--	--
		Toe 2	--	--	--	--	--	--	--
		Toes 3-5	--	--	--	--	--	--	--

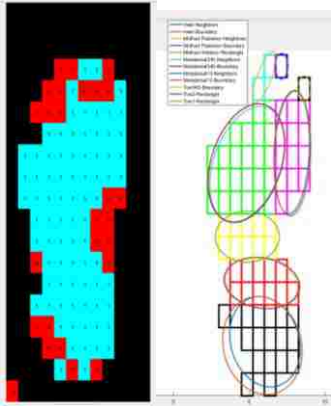
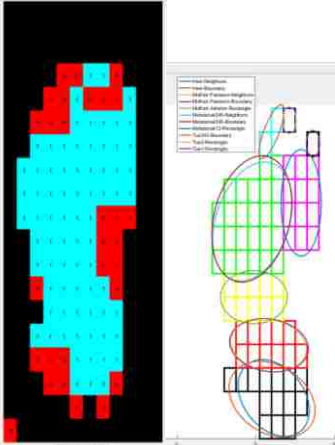
Time instant	Images: • Threshold insole – 1 is active sensor, 0 is inactive. • Ellipses fitted to the active sensors	Anatomical Location	Sensor Area (cm)	Normalized Area					
				Rectangle		Boundaries		Neighbors	
				Norm. Area	Area (cm ²)	Norm. Area	Area (cm ²)	Norm. Area	Area (cm ²)
27		Heel	21.3750			1.1481	24.5404	1.0081	21.5486
		Midfoot Posterior	12.3750	--	--	1.0617	13.1391	1.0122	12.5262
		Midfoot Anterior	10.1250	--	--	1.0682	10.8153	1.0106	10.2324
		Metatarsals 1-2	11.2500	--	--	1.1772	13.2437	0.9995	11.2448
		Metatarsals 3-5	20.2500	--	--	1.0677	24.0128	1.0063	22.7442
		Toe 1	1.1250	1.0000	1.1250	--	--	--	--
		Toe 2	--	--	--	--	--	--	--
		Toes 3-5	--	--	--	--	--	--	--
28		Heel	20.25	--	--	1.1978	24.2550	1.0197	20.6490
		Midfoot Posterior	12.3750	--	--	1.0617	13.1391	1.0122	12.5262
		Midfoot Anterior	10.1250	--	--	1.0682	10.8153	1.0106	10.2324
		Metatarsals 1-2	11.2500	--	--	1.1772	13.2437	0.9995	11.2448
		Metatarsals 3-5	20.2500	--	--	1.0677	24.0128	1.0063	22.7442
		Toe 1	1.1250	1.0000	1.1250	--	--	--	--
		Toe 2	--	--	--	--	--	--	--
		Toes 3-5	--	--	--	--	--	--	--

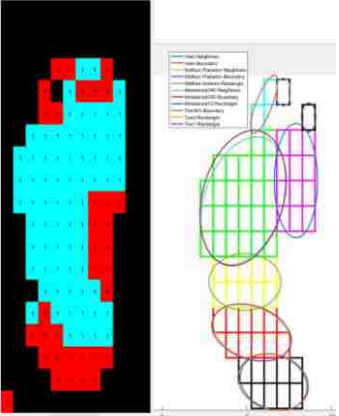
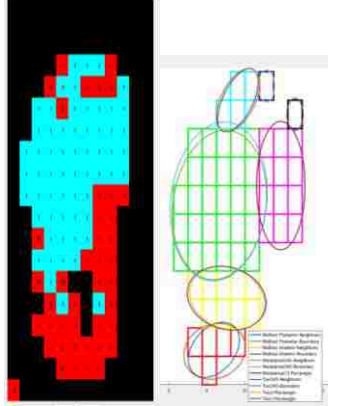
Time instant	<p>Images:</p> <ul style="list-style-type: none"> • Threshold insole – 1 is active sensor, 0 is inactive. • Ellipses fitted to the active sensors 	Anatomical Location	Sensor Area (cm)	Rectangle		Normalized Area		Neighbors	
				Norm. Area	Area (cm ²)	Boundaries		Norm. Area	Area (cm ²)
						Norm. Area	Area (cm ²)		
29		Heel	21.3750	--	--	1.2639	27.0162	1.0388	22.2037
		Midfoot Posterior	12.3750	--	--	1.0617	13.1391	1.0122	12.5262
		Midfoot Anterior	10.1250	--	--	1.0682	10.8153	1.0106	10.2324
		Metatarsals 1-2	12.3750	--	--	1.0956	13.5582	0.9907	12.2600
		Metatarsals 3-5	23.6250	--	--	1.1373	26.8689	1.0564	24.9569
		Toe 1	1.1250	1.0000	1.1250	--	--	--	--
		Toe 2	--	--	--	--	--	--	--
		Toes 3-5	--	--	--	--	--	--	--
30		Heel	21.3750	--	--	1.2639	27.0162	1.0388	22.2037
		Midfoot Posterior	12.3750	--	--	1.0617	13.1391	1.0122	12.5262
		Midfoot Anterior	11.2500	1.0000	11.2500	--	--	--	--
		Metatarsals 1-2	13.5000	1.0000	13.5000	--	--	--	--
		Metatarsals 3-5	23.6250	--	--	1.1373	26.8689	1.0564	24.9569
		Toe 1	--	--	--	--	--	--	--
		Toe 2	1.1250	1.0000	1.1250	--	--	--	--
		Toes 3-5	1.1250	1.0000	1.1250	--	--	--	--

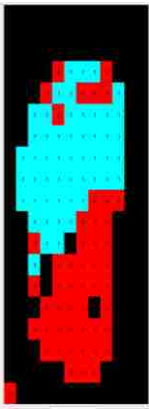
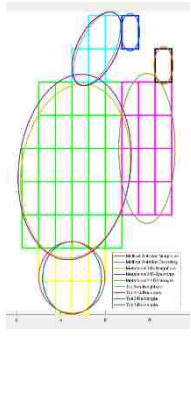
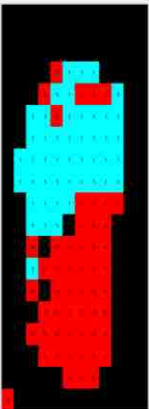
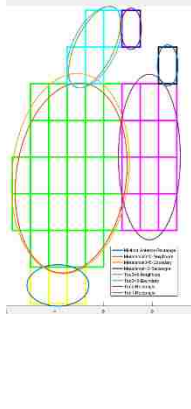
Time instant	Images: • Threshold insole – 1 is active sensor, 0 is inactive. • Ellipses fitted to the active sensors	Anatomical Location	Sensor Area (cm)	Normalized Area					
				Rectangle		Boundaries		Neighbors	
				Norm. Area	Area (cm ²)	Norm. Area	Area (cm ²)	Norm. Area	Area (cm ²)
31		Heel	21.3750	--	--	1.2639	27.0162	1.0388	22.2037
		Midfoot Posterior	12.3750	--	--	1.0617	13.1391	1.0122	12.5262
		Midfoot Anterior	11.2500	1.0000	11.2500	--	--	--	--
		Metatarsals 1-2	13.5000	1.0000	13.5000	--	--	--	--
		Metatarsals 3-5	23.6250	--	--	1.1373	26.8689	1.0564	24.9569
		Toe 1	--	--	--	--	--	--	--
		Toe 2	1.1250	1.0000	1.1250	--	--	--	--
		Toes 3-5	1.1250	1.0000	1.1250	--	--	--	--
32		Heel	21.3750	--	--	1.2639	27.0162	1.0388	22.2037
		Midfoot Posterior	12.3750	--	--	1.0617	13.1391	1.0122	12.5262
		Midfoot Anterior	11.2500	1.0000	11.2500	--	--	--	--
		Metatarsals 1-2	13.5000	1.0000	13.5000	--	--	--	--
		Metatarsals 3-5	23.6250	--	--	1.1373	26.8689	1.0564	24.9569
		Toe 1	--	--	--	--	--	--	--
		Toe 2	1.1250	1.0000	1.1250	--	--	--	--
		Toes 3-5	1.1250	1.0000	1.1250	--	--	--	--

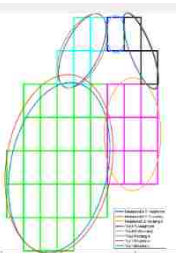
Time instant	Images: <ul style="list-style-type: none"> • Threshold insole – 1 is active sensor, 0 is inactive. • Ellipses fitted to the active sensors 	Anatomical Location	Sensor Area (cm)	Normalized Area					
				Rectangle		Boundaries		Neighbors	
				Norm. Area	Area (cm ²)	Norm. Area	Area (cm ²)	Norm. Area	Area (cm ²)
33		Heel	20.2500	--	--	1.3060	26.4463	1.0628	21.5219
		Midfoot Posterior	12.3750	--	--	1.0617	13.1391	1.0122	12.5262
		Midfoot Anterior	11.2500	1.0000	11.2500	--	--	--	--
		Metatarsals 1-2	13.5000	1.0000	13.5000	--	--	--	--
		Metatarsals 3-5	23.6250	--	--	1.1373	26.8689	1.0564	24.9569
		Toe 1	--	--	--	--	--	--	--
		Toe 2	1.1250	1.0000	1.1250	--	--	--	--
		Toes 3-5	1.1250	1.0000	1.1250	--	--	--	--
34		Heel	20.2500	--	--	1.3060	26.4463	1.0628	21.5219
		Midfoot Posterior	12.3750	--	--	1.0617	13.1391	1.0122	12.5262
		Midfoot Anterior	11.2500	1.0000	11.2500	--	--	--	--
		Metatarsals 1-2	14.6250	--	--	1.0711	15.6650	1.0077	14.7378
		Metatarsals 3-5	23.6250	--	--	1.1373	26.8689	1.0564	24.9569
		Toe 1	--	--	--	--	--	--	--
		Toe 2	1.1250	1.0000	1.1250	--	--	--	--
		Toes 3-5	1.1250	1.0000	1.1250	--	--	--	--

Time instant	Images: <ul style="list-style-type: none"> • Threshold insole – 1 is active sensor, 0 is inactive. • Ellipses fitted to the active sensors 	Anatomical Location	Sensor Area (cm)	Normalized Area					
				Rectangle		Boundaries		Neighbors	
				Norm. Area	Area (cm ²)	Norm. Area	Area (cm ²)	Norm. Area	Area (cm ²)
35		Heel	20.2500	--	--	1.3060	26.4463	1.0628	21.5219
		Midfoot Posterior	12.3750	--	--	1.0617	13.1391	1.0122	12.5262
		Midfoot Anterior	11.2500	1.0000	11.2500	--	--	--	--
		Metatarsals 1-2	14.6250	--	--	1.0711	15.6650	1.0077	14.7378
		Metatarsals 3-5	25.8750	--	--	1.1194	28.9633	1.0193	26.3737
		Toe 1	1.1250	1.0000	1.1250	--	--	--	--
		Toe 2	1.1250	1.0000	1.1250	--	--	--	--
		Toes 3-5	2.2500	--	--	1.2192	2.7431	1.2536	2.8207
36		Heel	20.2500	--	--	1.3060	26.4463	1.0628	21.5219
		Midfoot Posterior	12.3750	--	--	1.0617	13.1391	1.0122	12.5262
		Midfoot Anterior	11.2500	1.0000	11.2500	--	--	--	--
		Metatarsals 1-2	14.6250	--	--	1.0711	15.6650	1.0077	14.7378
		Metatarsals 3-5	25.8750	--	--	1.1194	28.9633	1.0193	26.3737
		Toe 1	1.1250	1.0000	1.1250	--	--	--	--
		Toe 2	1.1250	1.0000	1.1250	--	--	--	--
		Toes 3-5	2.2500	--	--	1.2192	2.7431	1.2536	2.8207

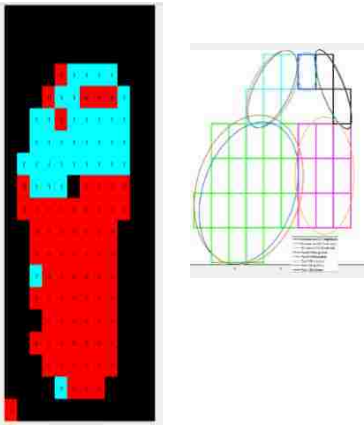
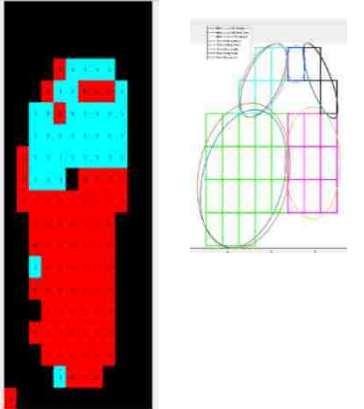
Time instant	Images: • Threshold insole – 1 is active sensor, 0 is inactive. • Ellipses fitted to the active sensors	Anatomical Location	Sensor Area (cm)	Normalized Area					
				Rectangle		Boundaries		Neighbors	
				Norm. Area	Area (cm ²)	Norm. Area	Area (cm ²)	Norm. Area	Area (cm ²)
37		Heel	20.2500	--	--	1.3060	26.4463	1.0628	21.5219
		Midfoot Posterior	12.3750	--	--	1.0617	13.1391	1.0122	12.5262
		Midfoot Anterior	11.2500	1.0000	11.2500	--	--	--	--
		Metatarsals 1-2	14.6250	--	--	1.0711	15.6650	1.0077	14.7378
		Metatarsals 3-5	27.0000	--	--	1.0889	29.3991	1.0176	27.4763
		Toe 1	1.1250	1.0000	1.1250	--	--	--	--
		Toe 2	1.1250	1.0000	1.1250	--	--	--	--
		Toes 3-5	2.2500	--	--	1.2192	2.7431	1.2536	2.8207
38		Heel	15.7500	--	--	1.2627	19.8881	1.0372	16.3353
		Midfoot Posterior	12.3750	--	--	1.0617	13.1391	1.0122	11.3197
		Midfoot Anterior	11.2500	1.0000	11.2500	--	--	--	--
		Metatarsals 1-2	13.5000	1.0000	13.5000	--	--	--	--
		Metatarsals 3-5	28.1250	--	--	1.0982	30.8857	1.0148	28.5419
		Toe 1	1.1250	1.0000	1.1250	--	--	--	--
		Toe 2	1.1250	1.0000	1.1250	--	--	--	--
		Toes 3-5	2.2500	--	--	1.2192	2.7431	1.2536	2.8207

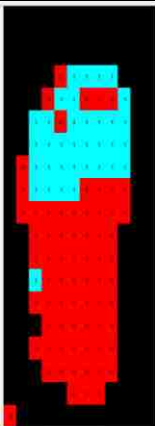
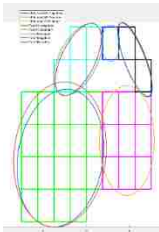
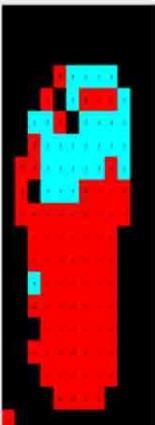
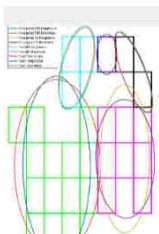
Time instant	Images: • Threshold insole – 1 is active sensor, 0 is inactive. • Ellipses fitted to the active sensors	Anatomical Location	Sensor Area (cm)	Normalized Area					
				Rectangle		Boundaries		Neighbors	
				Norm. Area	Area (cm ²)	Norm. Area	Area (cm ²)	Norm. Area	Area (cm ²)
39		Heel	10.1250	--	--	1.0706	10.8399	1.0106	10.2324
		Midfoot Posterior	11.2500	--	--	1.0644	11.9749	1.0062	5.7051
		Midfoot Anterior	11.2500	1.0000	11.2500	--	--	--	--
		Metatarsals 1-2	13.5000	1.0000	13.5000	--	--	--	--
		Metatarsals 3-5	28.1250	--	--	1.0982	30.8857	1.0148	28.5419
		Toe 1	1.1250	1.0000	1.1250	--	--	--	--
		Toe 2	1.1250	1.0000	1.1250	--	--	--	--
		Toes 3-5	2.2500	--	--	1.2192	2.7431	1.2536	2.8207
40		Heel	--	--	--	--	--	--	
		Midfoot Posterior	5.6250	--	--	1.3170	7.4080	1.0142	5.7051
		Midfoot Anterior	10.1250	--	--	1.0706	10.8399	1.0106	10.2324
		Metatarsals 1-2	13.5000	1.0000	13.5000	--	--	--	--
		Metatarsals 3-5	30.3750	--	--	1.0978	33.3449	1.0000	30.3758
		Toe 1	1.1250	1.0000	1.1250	--	--	--	--
		Toe 2	1.1250	1.0000	1.1250	--	--	--	--
		Toes 3-5	4.5000	--	--	1.1251	5.0628	0.9954	4.4792

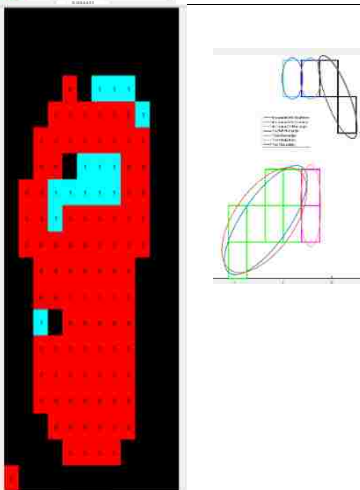
Time instant	Images: <ul style="list-style-type: none"> • Threshold insole – 1 is active sensor, 0 is inactive. • Ellipses fitted to the active sensors 		Anatomical Location	Sensor Area (cm)	Normalized Area					
					Rectangle		Boundaries		Neighbors	
					Norm. Area	Area (cm ²)	Norm. Area	Area (cm ²)	Norm. Area	Area (cm ²)
41			Heel	--	--	--	--	--	--	--
			Midfoot Posterior	--	--	--	--	--	--	--
			Midfoot Anterior	6.7500	--	--	1.1232	7.5814	1.0133	6.8395
			Metatarsals 1-2	13.5000	1.0000	13.5000	--	--	--	--
			Metatarsals 3-5	30.3750	--	--	1.0978	33.3449	1.0000	30.3758
			Toe 1	1.1250	1.0000	1.1250	--	--	--	--
			Toe 2	1.1250	1.0000	1.1250	--	--	--	--
			Toes 3-5	4.5000	--	--	1.1251	5.0628	0.9954	4.4792
42			Heel	--	--	--	--	--	--	--
			Midfoot Posterior	--	--	--	--	--	--	--
			Midfoot Anterior	3.3750	1.0000	3.3750	--	--	--	--
			Metatarsals 1-2	13.5000	1.0000	13.5000	--	--	--	--
			Metatarsals 3-5	28.1250	--	--	1.1008	30.9592	0.9862	27.7362
			Toe 1	1.1250	1.0000	1.1250	--	--	--	--
			Toe 2	1.1250	1.0000	1.1250	--	--	--	--
			Toes 3-5	4.5000	--	--	1.1251	5.0628	0.9954	4.4792

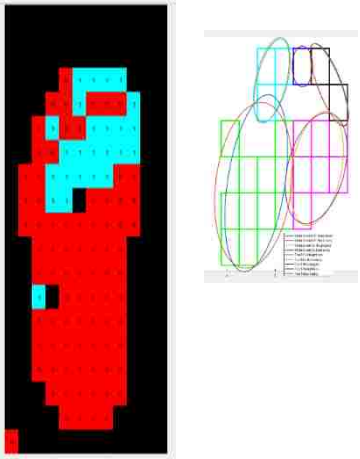
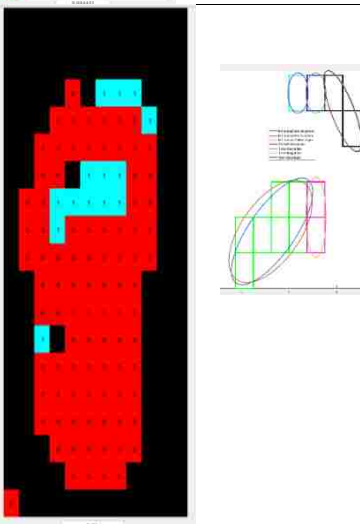
Time instant	Images: • Threshold insole – 1 is active sensor, 0 is inactive. • Ellipses fitted to the active sensors	Anatomical Location	Sensor Area (cm)	Normalized Area							
				Rectangle		Boundaries		Neighbors			
				Norm. Area	Area (cm ²)	Norm. Area	Area (cm ²)	Norm. Area	Area (cm ²)		
43			Heel	--	--	--	--	--	--	--	
			Midfoot Posterior	--	--	--	--	--	--	--	--
			Midfoot Anterior	2.2500	1.0000	2.2500	--	--	--	--	--
			Metatarsals 1-2	12.3750	--	--	1.0475	12.9623	0.9969	12.3365	
			Metatarsals 3-5	28.1250	--	--	1.1008	30.9592	0.9862	27.7362	
			Toe 1	2.2500	--	--	1.2192	--	1.2536	--	
			Toe 2	1.1250	1.0000	1.1250	--	--	--	--	
			Toes 3-5	4.5000	--	--	1.1251	5.0628	0.9954	4.4792	
44			Heel	--	--	--	--	--	--	--	
			Midfoot Posterior	--	--	--	--	--	--	--	--
			Midfoot Anterior	--	--	--	--	--	--	--	--
			Metatarsals 1-2	10.1250	1.0000	10.1250	--	--	--	--	
			Metatarsals 3-5	27	--	--	1.1183	30.1934	0.9839	26.5659	
			Toe 1	2.2500	--	--	1.2192	--	1.2536	--	
			Toe 2	1.1250	1.0000	1.1250	--	--	--	--	
			Toes 3-5	4.5000	--	--	1.1251	5.0628	0.9954	4.4792	

Time instant	Images: • Threshold insole – 1 is active sensor, 0 is inactive. • Ellipses fitted to the active sensors	Anatomical Location	Sensor Area (cm)	Normalized Area					
				Rectangle		Boundaries		Neighbors	
				Norm. Area	Area (cm ²)	Norm. Area	Area (cm ²)	Norm. Area	Area (cm ²)
45		Heel	--	--	--	--	--	--	--
		Midfoot Posterior	--	--	--	--	--	--	--
		Midfoot Anterior	--	--	--	--	--	--	--
		Metatarsals 1-2	10.1250	1.0000	10.1250	--	--	--	--
		Metatarsals 3-5	24.7500	--	--	1.1433	28.2975	0.9810	24.2802
		Toe 1	2.2500	--	--	1.2192	--	1.2536	--
		Toe 2	1.1250	1.0000	1.1250	--	--	--	--
		Toes 3-5	4.5000	--	--	1.1251	5.0628	0.9954	4.4792
46		Heel	--	--	--	--	--	--	
		Midfoot Posterior	--	--	--	--	--	--	--
		Midfoot Anterior	--	--	--	--	--	--	--
		Metatarsals 1-2	10.1250	1.0000	10.1250	--	--	--	--
		Metatarsals 3-5	22.5000	--	--	1.1221	25.2469	0.9988	22.4725
		Toe 1	2.2500	--	--	1.2192	--	1.2536	--
		Toe 2	1.1250	1.0000	1.1250	--	--	--	--
		Toes 3-5	4.5000	--	--	1.1251	5.0628	0.9954	4.4792

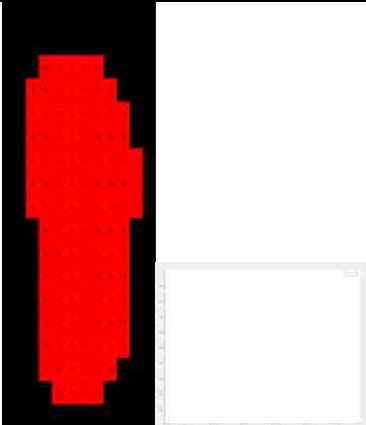
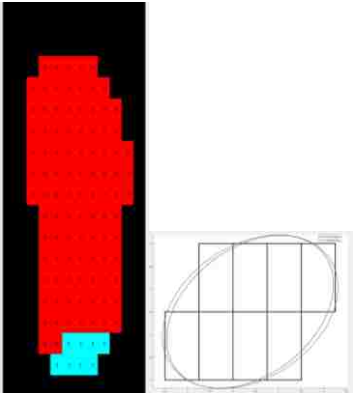
Time instant	Images: <ul style="list-style-type: none"> • Threshold insole – 1 is active sensor, 0 is inactive. • Ellipses fitted to the active sensors 	Anatomical Location	Sensor Area (cm)	Normalized Area					
				Rectangle		Boundaries		Neighbors	
				Norm. Area	Area (cm ²)	Norm. Area	Area (cm ²)	Norm. Area	Area (cm ²)
47		Heel	--	--	--	--	--	--	--
		Midfoot Posterior	--	--	--	--	--	--	--
		Midfoot Anterior	--	--	--	--	--	--	--
		Metatarsals 1-2	10.1250	1.0000	10.1250	--	--	--	--
		Metatarsals 3-5	20.2500	--	--	1.1582	23.4528	0.9770	19.7850
		Toe 1	2.2500	--	--	1.2192	--	1.2536	--
		Toe 2	1.1250	1.0000	1.1250	--	--	--	--
		Toes 3-5	4.5000	--	--	1.1251	5.0628	0.9954	4.4792
48		Heel	--	--	--	--	--	--	
		Midfoot Posterior	--	--	--	--	--	--	--
		Midfoot Anterior	--	--	--	--	--	--	--
		Metatarsals 1-2	10.1250	1.0000	10.1250	--	--	--	--
		Metatarsals 3-5	19.1250	--	--	1.1346	21.6992	0.9782	18.7088
		Toe 1	2.2500	--	--	1.2192	--	1.2536	--
		Toe 2	1.1250	1.0000	1.1250	--	--	--	--
		Toes 3-5	4.5000	--	--	1.1251	5.0628	0.9954	4.4792

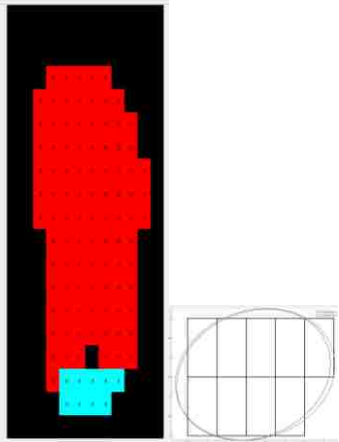
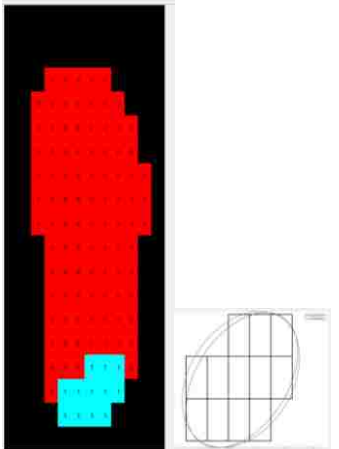
Time instant	Images: <ul style="list-style-type: none"> • Threshold insole – 1 is active sensor, 0 is inactive. • Ellipses fitted to the active sensors 		Anatomical Location	Sensor Area (cm)	Normalized Area					
					Rectangle		Boundaries		Neighbors	
					Norm. Area	Area (cm ²)	Norm. Area	Area (cm ²)	Norm. Area	Area (cm ²)
49			Heel	--	--	--	--	--	--	--
			Midfoot Posterior	--	--	--	--	--	--	--
			Midfoot Anterior	--	--	--	--	--	--	--
			Metatarsals 1-2	10.1250	1.0000	10.1250	--	--	--	--
			Metatarsals 3-5	20.2500	--	--	1.1126	22.5311	0.9776	19.7961
			Toe 1	2.2500	--	--	1.2192	--	1.2536	--
			Toe 2	1.1250	1.0000	1.1250	--	--	--	--
			Toes 3-5	4.5000	--	--	1.1251	5.0628	0.9954	4.4792
50			Heel	--	--	--	--	--	--	--
			Midfoot Posterior	--	--	--	--	--	--	--
			Midfoot Anterior	--	--	--	--	--	--	--
			Metatarsals 1-2	9.0000	--	--	1.0866	9.7795	1.1448	10.3036
			Metatarsals 3-5	15.7500	--	--	1.3267	20.8960	1.0828	17.0549
			Toe 1	2.2500	--	--	1.2192	--	1.2536	--
			Toe 2	1.1250	1.0000	1.1250	--	--	--	--
			Toes 3-5	3.3750	--	--	1.1090	3.7429	1.0248	3.4588

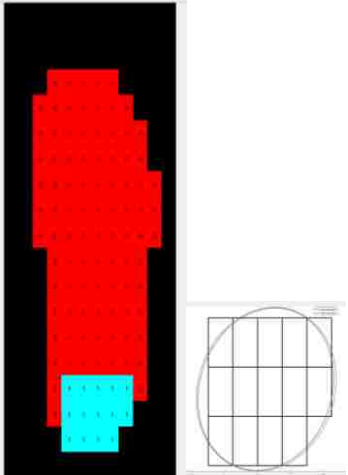
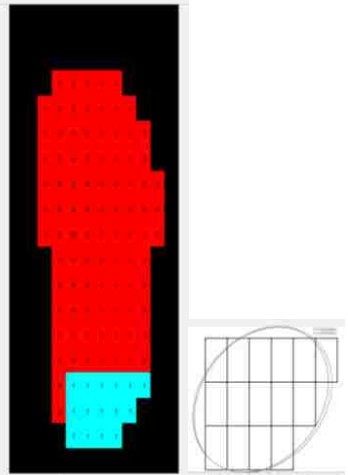
Time instant	Images: <ul style="list-style-type: none"> • Threshold insole – 1 is active sensor, 0 is inactive. • Ellipses fitted to the active sensors 	Anatomical Location	Sensor Area (cm)	Normalized Area					
				Rectangle		Boundaries		Neighbors	
				Norm. Area	Area (cm ²)	Norm. Area	Area (cm ²)	Norm. Area	Area (cm ²)
51		Heel	--	--	--	--	--	--	--
		Midfoot Posterior	--	--	--	--	--	--	--
		Midfoot Anterior	--	--	--	--	--	--	--
		Metatarsals 1-2	7.8750	--	--	1.1077	8.7231	0.9855	7.7612
		Metatarsals 3-5	12.3750	--	--	1.3830	17.1143	1.1224	13.8896
		Toe 1	2.2500	--	--	1.2192	--	1.2536	--
		Toe 2	1.1250	1.0000	1.1250	--	--	--	--
		Toes 3-5	3.3750	--	--	1.1090	3.7429	1.0248	3.4588
52		Heel	--	--	--	--	--	--	
		Midfoot Posterior	--	--	--	--	--	--	--
		Midfoot Anterior	--	--	--	--	--	--	--
		Metatarsals 1-2	2.2500	1.0000	--	--	--	--	--
		Metatarsals 3-5	7.8750	--	--	1.2324	9.7054	1.0306	8.1163
		Toe 1	2.2500	--	--	1.2192	--	1.2536	--
		Toe 2	1.1250	1.0000	1.1250	--	--	--	--
		Toes 3-5	1.1250	1.0000	1.1250	--	--	--	--

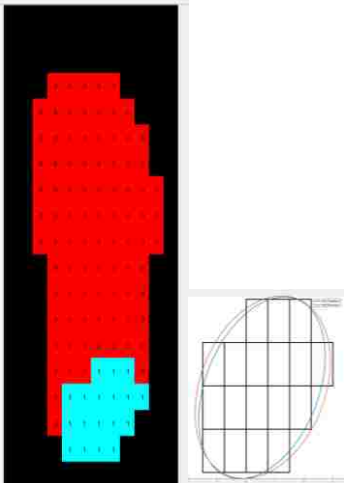
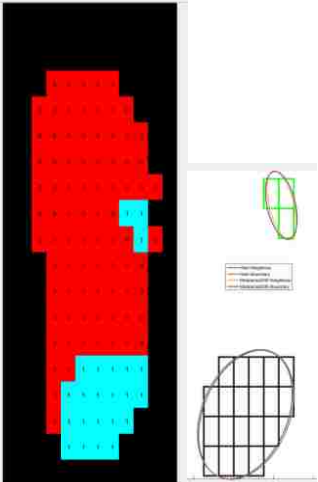
Time instant	Images: <ul style="list-style-type: none"> • Threshold insole – 1 is active sensor, 0 is inactive. • Ellipses fitted to the active sensors 	Anatomical Location	Sensor Area (cm)	Normalized Area					
				Rectangle		Boundaries		Neighbors	
				Norm. Area	Area (cm ²)	Norm. Area	Area (cm ²)	Norm. Area	Area (cm ²)
51		Heel	--	--	--	--	--	--	--
		Midfoot Posterior	--	--	--	--	--	--	--
		Midfoot Anterior	--	--	--	--	--	--	--
		Metatarsals 1-2	7.8750	--	--	1.1077	8.7231	0.9855	7.7612
		Metatarsals 3-5	12.3750	--	--	1.3830	17.1143	1.1224	13.8896
		Toe 1	2.2500	--	--	1.2192	--	1.2536	--
		Toe 2	1.1250	1.0000	1.1250	--	--	--	--
		Toes 3-5	3.3750	--	--	1.1090	3.7429	1.0248	3.4588
52		Heel	--	--	--	--	--	--	
		Midfoot Posterior	--	--	--	--	--	--	--
		Midfoot Anterior	--	--	--	--	--	--	--
		Metatarsals 1-2	2.2500	1.0000	--	--	--	--	--
		Metatarsals 3-5	7.8750	--	--	1.2324	9.7054	1.0306	8.1163
		Toe 1	2.2500	--	--	1.2192	--	1.2536	--
		Toe 2	1.1250	1.0000	1.1250	--	--	--	--
		Toes 3-5	1.1250	1.0000	1.1250	--	--	--	--

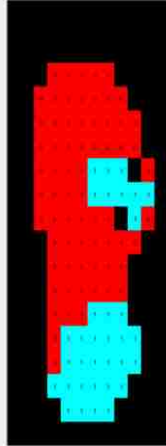
Appendix G – Results of Ellipse Fitting for Participant 112, Trial 1 – Right Foot

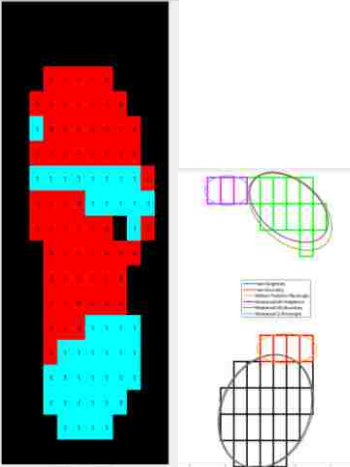
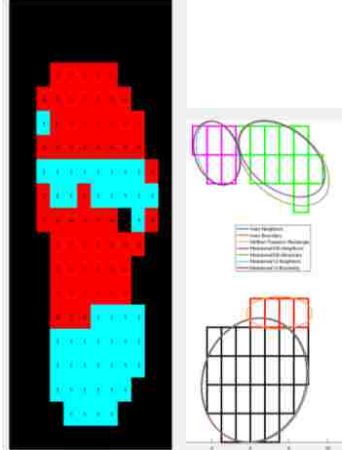
Time instant	Images: <ul style="list-style-type: none"> • Threshold insole – 1 is active sensor, 0 is inactive. • Ellipses fitted to the active sensors 	Anatomical Location	Sensor Area (cm)	Normalized Area					
				Rectangle		Boundaries		Neighbors	
				Norm. Area	Area (cm ²)	Norm. Area	Area (cm ²)	Norm. Area	Area (cm ²)
1		Heel	--	--	--	--	--	--	--
		Midfoot Posterior	--	--	--	--	--	--	--
		Midfoot Anterior	--	--	--	--	--	--	--
		Metatarsals 1-2	--	--	--	--	--	--	--
		Metatarsals 3-5	--	--	--	--	--	--	--
		Toe 1	--	--	--	--	--	--	--
		Toe 2	--	--	--	--	--	--	--
		Toes 3-5	--	--	--	--	--	--	--
2		Heel	9.0000	--	--	1.0748	9.6731	1.0025	9.0221
		Midfoot Posterior	--	--	--	--	--	--	--
		Midfoot Anterior	--	--	--	--	--	--	--
		Metatarsals 1-2	--	--	--	--	--	--	--
		Metatarsals 3-5	--	--	--	--	--	--	--
		Toe 1	--	--	--	--	--	--	--
		Toe 2	--	--	--	--	--	--	--
		Toes 3-5	--	--	--	--	--	--	--


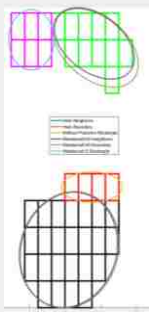
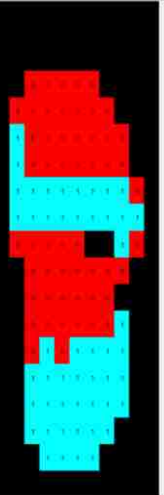
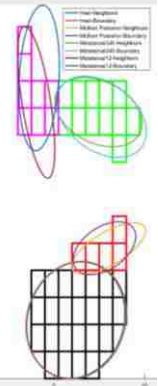
Time instant	Images: <ul style="list-style-type: none"> • Threshold insole – 1 is active sensor, 0 is inactive. • Ellipses fitted to the active sensors 	Anatomical Location	Sensor Area (cm)	Normalized Area					
				Rectangle		Boundaries		Neighbors	
				Norm. Area	Area (cm ²)	Norm. Area	Area (cm ²)	Norm. Area	Area (cm ²)
3		Heel	10.1250	--	--	1.0596	10.7286	1.0106	10.2324
		Midfoot Posterior	--	--	--	--	--	--	--
		Midfoot Anterior	--	--	--	--	--	--	--
		Metatarsals 1-2	--	--	--	--	--	--	--
		Metatarsals 3-5	--	--	--	--	--	--	--
		Toe 1	--	--	--	--	--	--	--
		Toe 2	--	--	--	--	--	--	--
		Toes 3-5	--	--	--	--	--	--	--
4		Heel	13.5000	--	--	1.1052	14.9203	0.9997	13.4963
		Midfoot Posterior	--	--	--	--	--	--	--
		Midfoot Anterior	--	--	--	--	--	--	--
		Metatarsals 1-2	--	--	--	--	--	--	--
		Metatarsals 3-5	--	--	--	--	--	--	--
		Toe 1	--	--	--	--	--	--	--
		Toe 2	--	--	--	--	--	--	--
		Toes 3-5	--	--	--	--	--	--	--

Time instant	Images: • Threshold insole – 1 is active sensor, 0 is inactive. • Ellipses fitted to the active sensors	Anatomical Location	Sensor Area (cm)	Normalized Area					
				Rectangle		Boundaries		Neighbors	
				Norm. Area	Area (cm ²)	Norm. Area	Area (cm ²)	Norm. Area	Area (cm ²)
5		Heel	15.7500	--	--	1.0527	16.5808	1.0090	15.8918
		Midfoot Posterior	--	--	--	--	--	--	--
		Midfoot Anterior	--	--	--	--	--	--	--
		Metatarsals 1-2	--	--	--	--	--	--	--
		Metatarsals 3-5	--	--	--	--	--	--	--
		Toe 1	--	--	--	--	--	--	--
		Toe 2	--	--	--	--	--	--	--
		Toes 3-5	--	--	--	--	--	--	--
6		Heel	16.8750	--	--	1.0688	18.0360	1.0205	17.2207
		Midfoot Posterior	--	--	--	--	--	--	--
		Midfoot Anterior	--	--	--	--	--	--	--
		Metatarsals 1-2	--	--	--	--	--	--	--
		Metatarsals 3-5	--	--	--	--	--	--	--
		Toe 1	--	--	--	--	--	--	--
		Toe 2	--	--	--	--	--	--	--
		Toes 3-5	--	--	--	--	--	--	--

Time instant	Images: <ul style="list-style-type: none"> • Threshold insole – 1 is active sensor, 0 is inactive. • Ellipses fitted to the active sensors 	Anatomical Location	Sensor Area (cm)	Normalized Area					
				Rectangle		Boundaries		Neighbors	
				Norm. Area	Area (cm ²)	Norm. Area	Area (cm ²)	Norm. Area	Area (cm ²)
7		Heel	20.2500	--	--	1.1025	22.3249	1.0014	20.2777
		Midfoot Posterior	--	--	--	--	--	--	--
		Midfoot Anterior	--	--	--	--	--	--	--
		Metatarsals 1-2	--	--	--	--	--	--	--
		Metatarsals 3-5	--	--	--	--	--	--	--
		Toe 1	--	--	--	--	--	--	--
		Toe 2	--	--	--	--	--	--	--
		Toes 3-5	--	--	--	--	--	--	--
8		Heel	22.5000	--	--	1.0501	23.6269	1.0037	22.5823
		Midfoot Posterior	--	--	--	--	--	--	--
		Midfoot Anterior	--	--	--	--	--	--	--
		Metatarsals 1-2	--	--	--	--	--	--	--
		Metatarsals 3-5	3.3750	--	--	1.1500	3.8813	1.0248	3.4588
		Toe 1	--	--	--	--	--	--	--
		Toe 2	--	--	--	--	--	--	--
		Toes 3-5	--	--	--	--	--	--	--

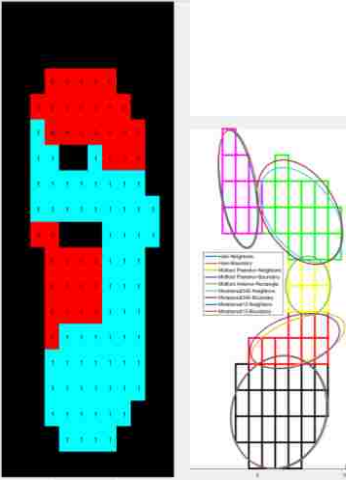
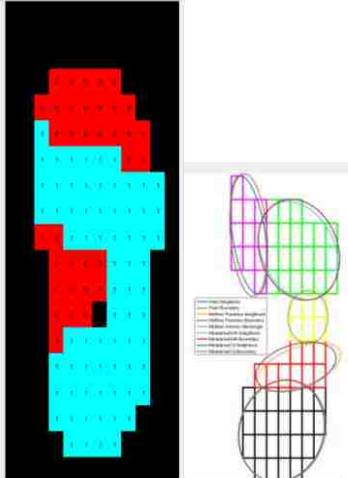
Time instant	Images: <ul style="list-style-type: none"> • Threshold insole – 1 is active sensor, 0 is inactive. • Ellipses fitted to the active sensors 	Anatomical Location	Sensor Area (cm)	Normalized Area					
				Rectangle		Boundaries		Neighbors	
				Norm. Area	Area (cm ²)	Norm. Area	Area (cm ²)	Norm. Area	Area (cm ²)
9		Heel	24.7500	--	--	1.0880	26.9286	1.0053	24.8818
		Midfoot Posterior	--	--	--	--	--	--	--
		Midfoot Anterior	--	--	--	--	--	--	--
		Metatarsals 1-2	--	--	--	--	--	--	--
		Metatarsals 3-5	5.6250	--	--	1.3223	7.4377	1.0142	5.7051
		Toe 1	--	--	--	--	--	--	--
		Toe 2	--	--	--	--	--	--	--
		Toes 3-5	--	--	--	--	--	--	--
10		Heel	24.7500	--	--	1.0880	26.9286	1.0053	24.8818
		Midfoot Posterior	3.3750	1.0000	3.3750	--	--	--	--
		Midfoot Anterior	--	--	--	--	--	--	--
		Metatarsals 1-2	--	--	--	--	--	--	--
		Metatarsals 3-5	10.1250	--	--	1.2891	13.0519	1.0160	10.2875
		Toe 1	--	--	--	--	--	--	--
		Toe 2	--	--	--	--	--	--	--
		Toes 3-5	--	--	--	--	--	--	--

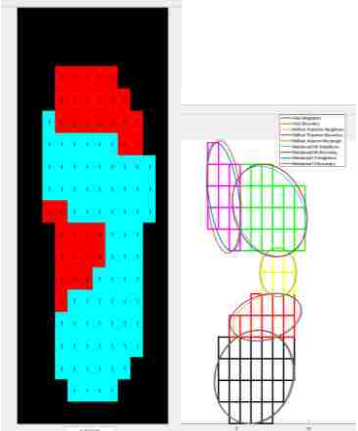
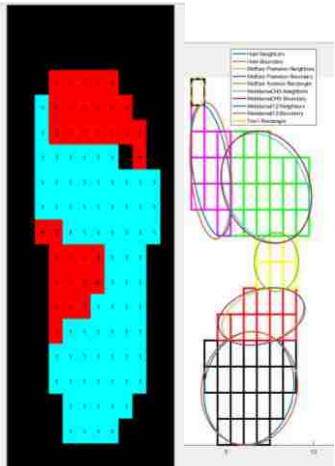
Time instant	Images: <ul style="list-style-type: none"> • Threshold insole – 1 is active sensor, 0 is inactive. • Ellipses fitted to the active sensors 	Anatomical Location	Sensor Area (cm)	Normalized Area					
				Rectangle		Boundaries		Neighbors	
				Norm. Area	Area (cm ²)	Norm. Area	Area (cm ²)	Norm. Area	Area (cm ²)
11		Heel	25.8750	--	--	1.0479	27.1148	1.0052	26.0091
		Midfoot Posterior	4.5000	1.0000	4.5000	--	--	--	--
		Midfoot Anterior	--	--	--	--	--	--	--
		Metatarsals 1-2	3.3750	1.0000	3.3750	--	--	--	--
		Metatarsals 3-5	12.3750	--	--	1.2210	15.1104	1.0119	12.5227
		Toe 1	--	--	--	--	--	--	--
		Toe 2	--	--	--	--	--	--	--
		Toes 3-5	--	--	--	--	--	--	--
12		Heel	27.0000	--	--	1.0482	28.3002	1.0140	27.3769
		Midfoot Posterior	4.5000	1.0000	4.5000	--	--	--	--
		Midfoot Anterior	--	--	--	--	--	--	--
		Metatarsals 1-2	5.6250	--	--	1.0995	6.1848	1.0050	5.6530
		Metatarsals 3-5	12.3750	--	--	1.2210	15.1104	1.0119	12.5227
		Toe 1	--	--	--	--	--	--	--
		Toe 2	--	--	--	--	--	--	--
		Toes 3-5	--	--	--	--	--	--	--

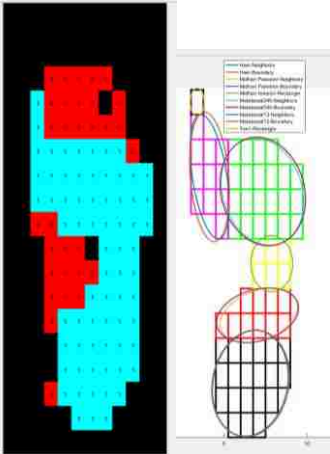
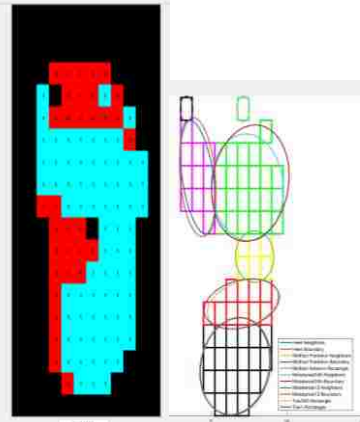
Time instant	Images: • Threshold insole – 1 is active sensor, 0 is inactive. • Ellipses fitted to the active sensors		Anatomical Location	Sensor Area (cm)	Normalized Area					
					Rectangle		Boundaries		Neighbors	
					Norm. Area	Area (cm ²)	Norm. Area	Area (cm ²)	Norm. Area	Area (cm ²)
13			Heel	27.0000	--	--	1.0482	28.3002	1.0140	27.3769
			Midfoot Posterior	4.5000	1.0000	4.5000	--	--	--	--
			Midfoot Anterior	--	--	--	--	--	--	--
			Metatarsals 1-2	6.7500	1.0000	6.7500	--	--	--	--
			Metatarsals 3-5	12.3750	--	--	1.2210	15.1104	1.0119	12.5227
			Toe 1	--	--	--	--	--	--	--
			Toe 2	--	--	--	--	--	--	--
			Toes 3-5	--	--	--	--	--	--	--
14			Heel	27.0000	--	--	1.0482	28.3002	1.0140	27.3769
			Midfoot Posterior	5.6250	--	--	1.2722	7.1562	1.1709	6.5861
			Midfoot Anterior	--	--	--	--	--	--	--
			Metatarsals 1-2	9.0000	--	--	1.5478	13.9299	1.1778	10.6005
			Metatarsals 3-5	13.5000	--	--	1.2159	16.4145	1.0201	13.7717
			Toe 1	--	--	--	--	--	--	--
			Toe 2	--	--	--	--	--	--	--
			Toes 3-5	--	--	--	--	--	--	--

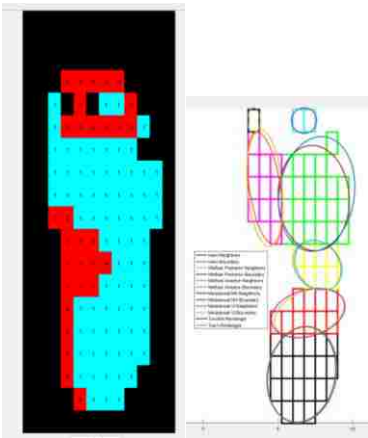
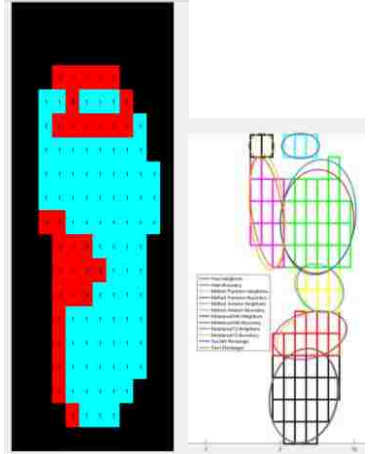
Time instant	Images: <ul style="list-style-type: none"> • Threshold insole – 1 is active sensor, 0 is inactive. • Ellipses fitted to the active sensors 	Anatomical Location	Sensor Area (cm)	Normalized Area					
				Rectangle		Boundaries		Neighbors	
				Norm. Area	Area (cm ²)	Norm. Area	Area (cm ²)	Norm. Area	Area (cm ²)
15		Heel	27.0000	--	--	1.0482	28.3002	1.0140	27.3769
		Midfoot Posterior	5.6250	--	--	1.2722	7.1562	1.1709	6.5861
		Midfoot Anterior	--	--	--	--	--	--	--
		Metatarsals 1-2	9.0000	--	--	1.5478	13.9299	1.1778	10.6005
		Metatarsals 3-5	13.5000	--	--	1.2159	16.4145	1.0201	13.7717
		Toe 1	--	--	--	--	--	--	--
		Toe 2	--	--	--	--	--	--	--
		Toes 3-5	--	--	--	--	--	--	--
16		Heel	27.0000	--	--	1.0482	28.3002	1.0140	27.3769
		Midfoot Posterior	7.8750	1.0000	7.8750	--	--	--	--
		Midfoot Anterior	--	--	--	--	--	--	--
		Metatarsals 1-2	9.0000	--	--	1.5478	13.9299	1.1778	10.6005
		Metatarsals 3-5	14.6250	--	--	1.1889	17.3874	0.9989	14.6091
		Toe 1	--	--	--	--	--	--	--
		Toe 2	--	--	--	--	--	--	--
		Toes 3-5	--	--	--	--	--	--	--

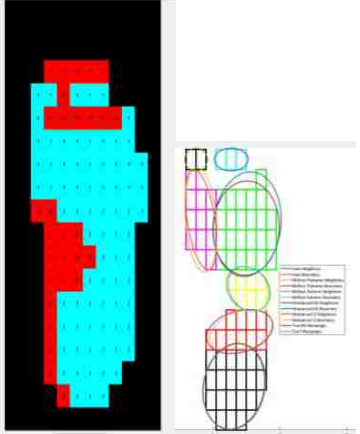
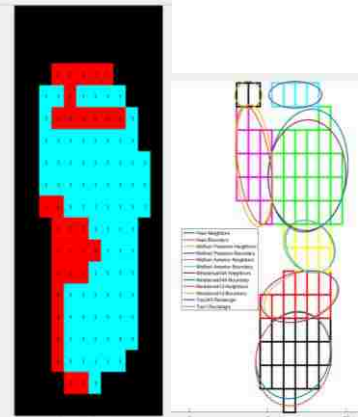
Time instant	Images: • Threshold insole – 1 is active sensor, 0 is inactive. • Ellipses fitted to the active sensors	Anatomical Location	Sensor Area (cm)	Normalized Area					
				Rectangle		Boundaries		Neighbors	
				Norm. Area	Area (cm ²)	Norm. Area	Area (cm ²)	Norm. Area	Area (cm ²)
17		Heel	27.0000	--	--	1.0482	28.3002	1.0140	27.3769
		Midfoot Posterior	10.1250	--	--	1.1645	11.7909	1.8260	10.9610
		Midfoot Anterior	3.3750	--	--	1.1500	3.8813	1.0248	3.4588
		Metatarsals 1-2	9.0000	--	--	1.5478	13.9299	1.1778	10.6005
		Metatarsals 3-5	14.6250	--	--	1.1889	17.3874	0.9989	14.6091
		Toe 1	--	--	--	--	--	--	--
		Toe 2	--	--	--	--	--	--	--
18		Heel	27.0000	--	--	1.0482	28.3002	1.0140	27.3769
		Midfoot Posterior	10.1250	--	--	1.1645	11.7909	1.8260	10.9610
		Midfoot Anterior	6.7500	1.0000	6.7500	--	--	--	--
		Metatarsals 1-2	10.1250	--	--	1.1164	11.3033	1.0262	10.3907
		Metatarsals 3-5	18	--	--	1.1715	21.0870	1.0053	18.0960
		Toe 1	--	--	--	--	--	--	--
		Toe 2	--	--	--	--	--	--	--
Toes 3-5	--	--	--	--	--	--	--		

Time instant	Images: • Threshold insole – 1 is active sensor, 0 is inactive. • Ellipses fitted to the active sensors	Anatomical Location	Sensor Area (cm)	Normalized Area					
				Rectangle		Boundaries		Neighbors	
				Norm. Area	Area (cm ²)	Norm. Area	Area (cm ²)	Norm. Area	Area (cm ²)
19		Heel	27.0000	--	--	1.0482	28.3002	1.0140	27.3769
		Midfoot Posterior	10.1250	--	--	1.1645	11.7909	1.8260	10.9610
		Midfoot Anterior	6.7500	1.0000	6.7500	--	--	--	--
		Metatarsals 1-2	10.1250	--	--	1.1164	11.3033	1.0262	10.3907
		Metatarsals 3-5	18	--	--	1.1715	25.7553	1.0053	18.0960
		Toe 1	--	--	--	--	--	--	--
		Toe 2	--	--	--	--	--	--	--
		Toes 3-5	--	--	--	--	--	--	--
20		Heel	27.0000	--	--	1.0482	28.3002	1.0140	27.3769
		Midfoot Posterior	10.1250	--	--	1.1645	11.7909	1.8260	10.9610
		Midfoot Anterior	6.7500	1.0000	6.7500	--	--	--	--
		Metatarsals 1-2	12.3750	--	--	1.1542	14.2833	1.0051	12.4381
		Metatarsals 3-5	23.6250	--	--	1.0902	25.7553	1.0131	23.9348
		Toe 1	--	--	--	--	--	--	--
		Toe 2	--	--	--	--	--	--	--
		Toes 3-5	--	--	--	--	--	--	--

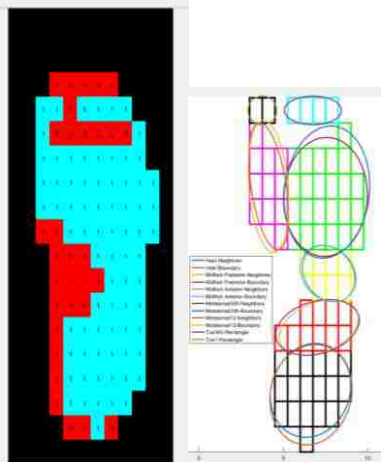
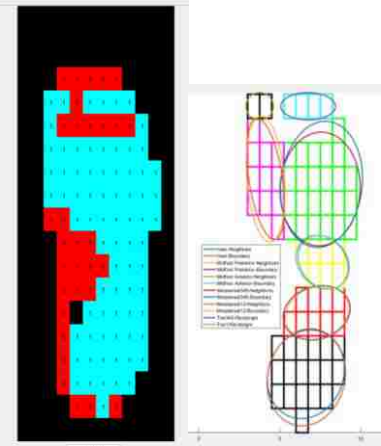
Time instant	Images: • Threshold insole – 1 is active sensor, 0 is inactive. • Ellipses fitted to the active sensors	Anatomical Location	Sensor Area (cm)	Normalized Area					
				Rectangle		Boundaries		Neighbors	
				Norm. Area	Area (cm ²)	Norm. Area	Area (cm ²)	Norm. Area	Area (cm ²)
21		Heel	27.0000	--	--	1.0482	28.3002	1.0140	27.3769
		Midfoot Posterior	11.2500	--	--	1.1013	12.3900	1.0152	11.4211
		Midfoot Anterior	6.7500	1.0000	6.7500	--	--	--	--
		Metatarsals							
		1-2	12.3750	--	--	1.1542	14.2833	1.0051	12.4381
		3-5	23.6250	--	--	1.0902	25.7553	1.0131	23.9348
		Toe 1	--	--	--	--	--	--	--
		Toe 2	--	--	--	--	--	--	--
		Toes 3-5	--	--	--	--	--	--	--
22		Heel	25.8750	--	--	1.0918	28.2510	1.0157	26.2815
		Midfoot Posterior	11.2500	--	--	1.1013	12.3900	1.0152	11.4211
		Midfoot Anterior	6.7500	1.0000	6.7500	--	--	--	--
		Metatarsals							
		1-2	12.3750	--	--	1.1542	14.2833	1.0051	12.4381
		3-5	23.6250	--	--	1.0902	26.3659	1.0131	23.9348
		Toe 1	1.1250	1.0000	1.1250	--	--	--	--
		Toe 2	--	--	--	--	--	--	--
		Toes 3-5	--	--	--	--	--	--	--

Time instant	Images: • Threshold insole – 1 is active sensor, 0 is inactive. • Ellipses fitted to the active sensors	Anatomical Location	Sensor Area (cm)	Normalized Area						
				Rectangle		Boundaries		Neighbors		
				Norm. Area	Area (cm ²)	Norm. Area	Area (cm ²)	Norm. Area	Area (cm ²)	
23		Heel	22.5000	--	--	1.0527	23.6851	1.0120	22.7706	
		Midfoot Posterior	11.2500	--	--	1.1013	12.3900	1.0152	11.4211	
		Midfoot Anterior	6.7500	1.0000	6.7500	--	--	--	--	
		Metatarsals	12.3750	--	--	1.1542	14.2833	1.0051	12.4381	
		1-2	24.7500	--	--	1.0653	30.6088	1.0095	24.9849	
		3-5	Toe 1	1.1250	1.0000	1.1250	--	--	--	--
		Toe 2	--	--	--	--	--	--	--	
		Toes 3-5	--	--	--	--	--	--	--	
24		Heel	22.5000	--	--	1.0527	23.6851	1.0120	22.7706	
		Midfoot Posterior	11.2500	--	--	1.1013	12.3900	1.0152	11.4211	
		Midfoot Anterior	6.7500	1.0000	6.7500	--	--	--	--	
		Metatarsals	12.3750	--	--	1.1542	14.2833	1.0051	12.4381	
		1-2	24.7500	--	--	1.1830	30.6088	1.0193	26.3749	
		3-5	Toe 1	1.1250	1.0000	1.1250	--	--	--	--
		Toe 2	--	--	--	--	--	--	--	
		Toes 3-5	1.1250	1.0000	1.1250	--	--	--	--	

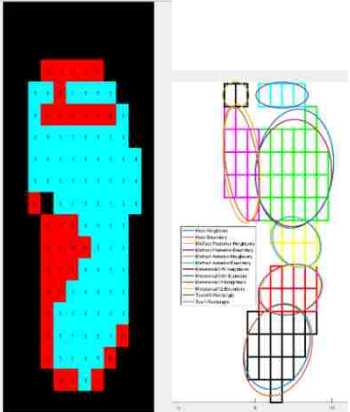
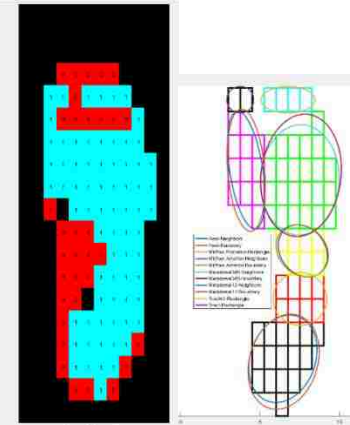
Time instant	Images: <ul style="list-style-type: none"> • Threshold insole – 1 is active sensor, 0 is inactive. • Ellipses fitted to the active sensors 	Anatomical Location	Sensor Area (cm)	Normalized Area					
				Rectangle		Boundaries		Neighbors	
				Norm. Area	Area (cm ²)	Norm. Area	Area (cm ²)	Norm. Area	Area (cm ²)
25		Heel	22.5000	--	--	1.0527	23.6851	1.0120	22.7706
		Midfoot Posterior	11.2500	--	--	1.1013	12.3900	1.0152	11.4211
		Midfoot Anterior	7.875	--	--	1.0811	8.5136	1.0083	7.9402
		Metatarsals	12.3750	--	--	1.1542	14.2833	1.0051	12.4381
		1-2 Metatarsals	25.8750	--	--	1.1830	30.6088	1.0193	26.3749
		3-5							
		Toe 1	1.1250	1.0000	1.1250	--	--	--	--
		Toe 2	--	--	--	--	--	--	--
		Toes 3-5	2.2500	1.0000	2.2500	--	--	--	--
26		Heel	22.5000	--	--	1.0527	23.6851	1.0120	22.7706
		Midfoot Posterior	11.2500	--	--	1.1013	12.3900	1.0152	11.4211
		Midfoot Anterior	7.875	--	--	1.0811	8.5136	1.0083	7.9402
		Metatarsals	12.3750	--	--	1.1542	14.2833	1.0051	12.4381
		1-2 Metatarsals	27.0000	--	--	1.1507	31.0682	1.0198	27.5352
		3-5							
		Toe 1	2.2500	1.0000	2.2500	--	--	--	--
		Toe 2	--	--	--	--	--	--	--
		Toes 3-5	3.3750	1.0000	3.3750	--	--	--	--

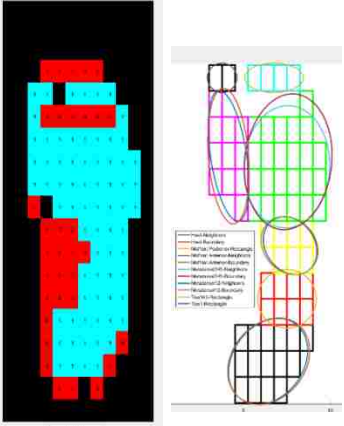
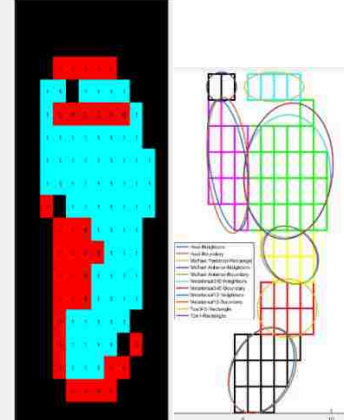
Time instant	Images: • Threshold insole – 1 is active sensor, 0 is inactive. • Ellipses fitted to the active sensors	Anatomical Location	Sensor Area (cm)	Normalized Area					
				Rectangle		Boundaries		Neighbors	
				Norm. Area	Area (cm ²)	Norm. Area	Area (cm ²)	Norm. Area	Area (cm ²)
27		Heel	22.5000	--	--	1.0527	23.6851	1.0120	22.7706
		Midfoot Posterior	11.2500	--	--	1.1013	12.3900	1.0152	11.4211
		Midfoot Anterior	7.875	--	--	1.0811	8.5136	1.0083	7.9402
		Metatarsals 1-2	12.3750	--	--	1.1542	14.2833	1.0051	12.4381
		Metatarsals 3-5	27.0000	--	--	1.1507	31.0682	1.0198	27.5352
		Toe 1	2.2500	1.0000	2.2500	--	--	--	--
		Toe 2	--	--	--	--	--	--	--
		Toes 3-5	3.3750	1.0000	3.3750	--	--	--	--
28		Heel	20.2500	--	--	1.1273	22.8283	1.0119	20.4914
		Midfoot Posterior	11.2500	--	--	1.1013	12.3900	1.0152	11.4211
		Midfoot Anterior	7.875	--	--	1.0811	8.5136	1.0083	7.9402
		Metatarsals 1-2	12.3750	--	--	1.1542	14.2833	1.0051	12.4381
		Metatarsals 3-5	27.0000	--	--	1.1507	31.0682	1.0198	27.5352
		Toe 1	2.2500	1.0000	2.2500	--	--	--	--
		Toe 2	--	--	--	--	--	--	--
		Toes 3-5	4.5000	1.0000	4.5000	--	--	--	--

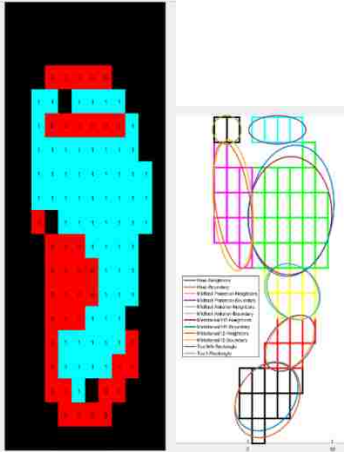
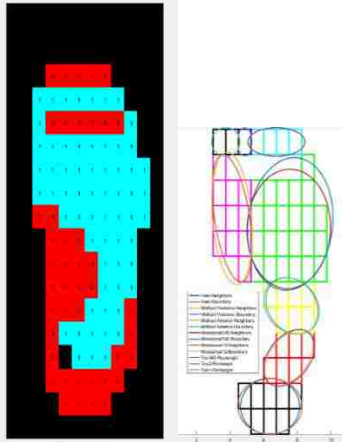
Time instant	Images: <ul style="list-style-type: none"> • Threshold insole – 1 is active sensor, 0 is inactive. • Ellipses fitted to the active sensors 	Anatomical Location	Sensor Area (cm)	Normalized Area					
				Rectangle		Boundaries		Neighbors	
				Norm. Area	Area (cm ²)	Norm. Area	Area (cm ²)	Norm. Area	Area (cm ²)
27		Heel	22.5000	--	--	1.0527	23.6851	1.0120	22.7706
		Midfoot Posterior	11.2500	--	--	1.1013	12.3900	1.0152	11.4211
		Midfoot Anterior	7.875	--	--	1.0811	8.5136	1.0083	7.9402
		Metatarsals 1-2	12.3750	--	--	1.1542	14.2833	1.0051	12.4381
		Metatarsals 3-5	27.0000	--	--	1.1507	31.0682	1.0198	27.5352
		Toe 1	2.2500	1.0000	2.2500	--	--	--	--
		Toe 2	--	--	--	--	--	--	--
		Toes 3-5	3.3750	1.0000	3.3750	--	--	--	--
28		Heel	20.2500	--	--	1.1273	22.8283	1.0119	20.4914
		Midfoot Posterior	11.2500	--	--	1.1013	12.3900	1.0152	11.4211
		Midfoot Anterior	7.875	--	--	1.0811	8.5136	1.0083	7.9402
		Metatarsals 1-2	12.3750	--	--	1.1542	14.2833	1.0051	12.4381
		Metatarsals 3-5	27.0000	--	--	1.1507	31.0682	1.0198	27.5352
		Toe 1	2.2500	1.0000	2.2500	--	--	--	--
		Toe 2	--	--	--	--	--	--	--
		Toes 3-5	4.5000	1.0000	4.5000	--	--	--	--

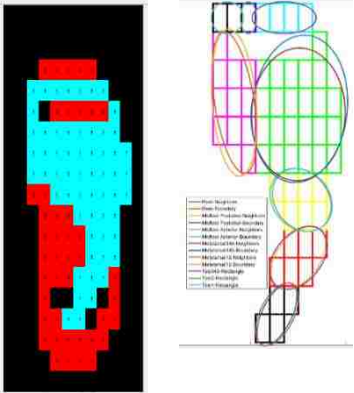
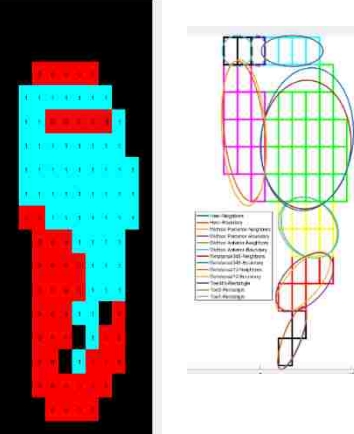
Time instant	Images: <ul style="list-style-type: none"> • Threshold insole – 1 is active sensor, 0 is inactive. • Ellipses fitted to the active sensors 	Anatomical Location	Sensor Area (cm)	Normalized Area					
				Rectangle		Boundaries		Neighbors	
				Norm. Area	Area (cm ²)	Norm. Area	Area (cm ²)	Norm. Area	Area (cm ²)
29		Heel	20.2500	--	--	1.1273	22.8283	1.0119	20.4914
		Midfoot Posterior	11.2500	--	--	1.1013	12.3900	1.0152	11.4211
		Midfoot Anterior	7.875	--	--	1.0811	8.5136	1.0083	7.9402
		Metatarsals	12.3750	--	--	1.1542	14.2833	1.0051	12.4381
		1-2 Metatarsals	27.0000	--	--	1.1507	31.0682	1.0198	27.5352
		3-5	2.2500	1.0000	2.2500	--	--	--	--
		Toe 1	--	--	--	--	--	--	--
		Toe 2	--	--	--	--	--	--	--
30		Heel	20.2500	--	--	1.1273	22.8283	1.0119	20.4914
		Midfoot Posterior	10.1250	--	--	1.0706	10.8399	1.0106	10.2324
		Midfoot Anterior	7.875	--	--	1.0811	8.5136	1.0083	7.9402
		Metatarsals	12.3750	--	--	1.1542	14.2833	1.0051	12.4381
		1-2 Metatarsals	27.0000	--	--	1.1507	31.0682	1.0198	27.5352
		3-5	2.2500	1.0000	2.2500	--	--	--	--
		Toe 1	--	--	--	--	--	--	--
		Toe 2	--	--	--	--	--	--	--
Toes 3-5	4.5000	1.0000	4.5000	--	--	--	--		

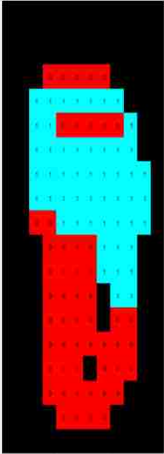
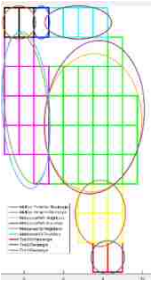
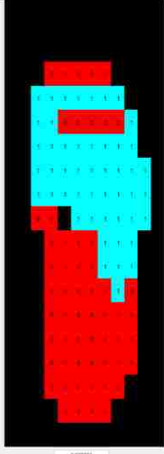
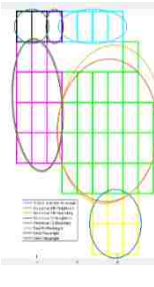
Time instant	Images: <ul style="list-style-type: none"> • Threshold insole – 1 is active sensor, 0 is inactive. • Ellipses fitted to the active sensors 	Anatomical Location	Sensor Area (cm)	Normalized Area					
				Rectangle		Boundaries		Neighbors	
				Norm. Area	Area (cm ²)	Norm. Area	Area (cm ²)	Norm. Area	Area (cm ²)
31		Heel	19.1250	--	--	1.1677	22.3319	1.0188	19.4845
		Midfoot Posterior	10.1250	--	--	1.0706	10.8399	1.0106	10.2324
		Midfoot Anterior	7.875	--	--	1.0811	8.5136	1.0083	7.9402
		Metatarsals 1-2	12.3750	--	--	1.1542	14.2833	1.0051	12.4381
		Metatarsals 3-5	27.0000	--	--	1.1507	31.0682	1.0198	27.5352
		Toe 1	2.2500	1.0000	2.2500	--	--	--	--
		Toe 2	--	--	--	--	--	--	--
		Toes 3-5	4.5000	1.0000	4.5000	--	--	--	--
32		Heel	18.0000	--	--	1.1658	20.9848	1.0284	18.5114
		Midfoot Posterior	10.1250	--	--	1.0706	10.8399	1.0106	10.2324
		Midfoot Anterior	7.875	--	--	1.0811	8.5136	1.0083	7.9402
		Metatarsals 1-2	12.3750	--	--	1.1542	14.2833	1.0051	12.4381
		Metatarsals 3-5	27.0000	--	--	1.1507	31.0682	1.0198	27.5352
		Toe 1	2.2500	1.0000	2.2500	--	--	--	--
		Toe 2	--	--	--	--	--	--	--
		Toes 3-5	4.5000	1.0000	4.5000	--	--	--	--

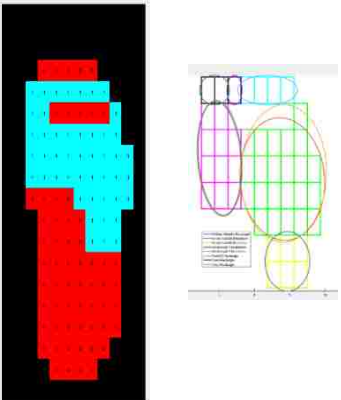
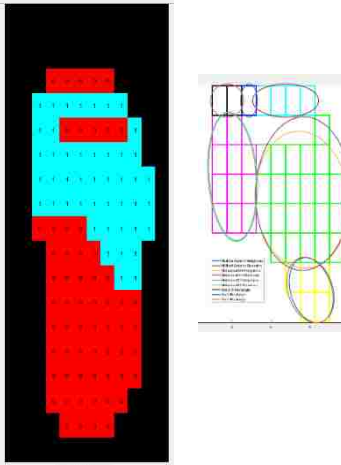
Time instant	Images: <ul style="list-style-type: none"> • Threshold insole – 1 is active sensor, 0 is inactive. • Ellipses fitted to the active sensors 	Anatomical Location	Sensor Area (cm)	Normalized Area					
				Rectangle		Boundaries		Neighbors	
				Norm. Area	Area (cm ²)	Norm. Area	Area (cm ²)	Norm. Area	Area (cm ²)
33		Heel	18.0000	--	--	1.1658	20.9848	1.0284	18.5114
		Midfoot Posterior	10.1250	--	--	1.0706	10.8399	1.0106	10.2324
		Midfoot Anterior	7.875	--	--	1.0811	8.5136	1.0083	7.9402
		Metatarsals 1-2	12.3750	--	--	1.1542	14.2833	1.0051	12.4381
		Metatarsals 3-5	27.0000	--	--	1.1507	31.0682	1.0198	27.5352
		Toe 1	2.2500	1.0000	2.2500	--	--	--	--
		Toe 2	--	--	--	--	--	--	--
		Toes 3-5	4.5000	1.0000	4.5000	--	--	--	--
34		Heel	18.0000	--	--	1.1658	20.9848	1.0284	18.5114
		Midfoot Posterior	9.0000	1.0000	9.0000	--	--	--	--
		Midfoot Anterior	7.875	--	--	1.0811	8.5136	1.0083	7.9402
		Metatarsals 1-2	12.3750	--	--	1.1542	14.2833	1.0051	12.4381
		Metatarsals 3-5	27.0000	--	--	1.1507	31.0682	1.0198	27.5352
		Toe 1	2.2500	1.0000	2.2500	--	--	--	--
		Toe 2	--	--	--	--	--	--	--
		Toes 3-5	4.5000	1.0000	4.5000	--	--	--	--

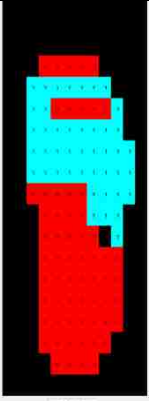
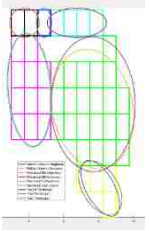
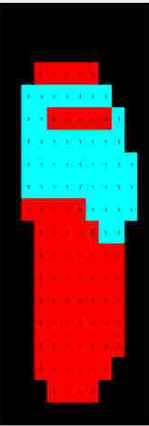
Time instant	Images: • Threshold insole – 1 is active sensor, 0 is inactive. • Ellipses fitted to the active sensors	Anatomical Location	Sensor Area (cm)	Normalized Area					
				Rectangle		Boundaries		Neighbors	
				Norm. Area	Area (cm ²)	Norm. Area	Area (cm ²)	Norm. Area	Area (cm ²)
35		Heel	16.8750	--	--	1.0688	18.0360	1.0205	17.2207
		Midfoot Posterior	9.0000	1.0000	9.0000	--	--	--	--
		Midfoot Anterior	7.875	--	--	1.0811	8.5136	1.0083	7.9402
		Metatarsals 1-2	12.3750	--	--	1.1542	14.2833	1.0051	12.4381
		Metatarsals 3-5	27.0000	--	--	1.1507	31.0682	1.0198	27.5352
		Toe 1	2.2500	1.0000	2.2500	--	--	--	--
		Toe 2	--	--	--	--	--	--	--
Toes 3-5	4.5000	1.0000	4.5000	--	--	--	--		
36		Heel	13.5000	--	--	1.0750	14.5131	1.0185	13.7493
		Midfoot Posterior	9.0000	1.0000	9.0000	--	--	--	--
		Midfoot Anterior	7.875	--	--	1.0811	8.5136	1.0083	7.9402
		Metatarsals 1-2	12.3750	--	--	1.1542	14.2833	1.0051	12.4381
		Metatarsals 3-5	27.0000	--	--	1.1507	31.0682	1.0198	27.5352
		Toe 1	2.2500	1.0000	2.2500	--	--	--	--
		Toe 2	--	--	--	--	--	--	--
Toes 3-5	4.5000	1.0000	4.5000	--	--	--	--		

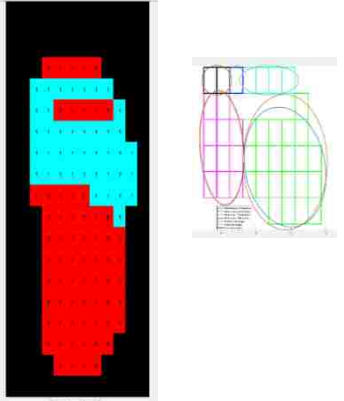
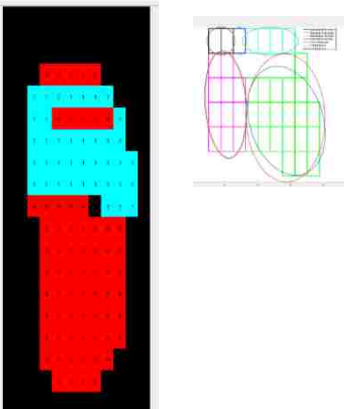
Time instant	Images: <ul style="list-style-type: none"> • Threshold insole – 1 is active sensor, 0 is inactive. • Ellipses fitted to the active sensors 	Anatomical Location	Sensor Area (cm)	Normalized Area					
				Rectangle		Boundaries		Neighbors	
				Norm. Area	Area (cm ²)	Norm. Area	Area (cm ²)	Norm. Area	Area (cm ²)
37		Heel	11.2500	--	--	1.1875	13.3592	1.0221	11.4990
		Midfoot Posterior	6.7500	--	--	1.0915	7.3675	0.9978	6.7354
		Midfoot Anterior	7.875	--	--	1.0811	8.5136	1.0083	7.9402
		Metatarsals 1-2	12.3750	--	--	1.1542	14.2833	1.0051	12.4381
		Metatarsals 3-5	27.0000	--	--	1.1507	31.0682	1.0198	27.5352
		Toe 1	2.2500	1.0000	2.2500	--	--	--	--
		Toe 2	--	--	--	--	--	--	--
Toes 3-5	4.5000	1.0000	4.5000	--	--	--	--		
38		Heel	9.0000	--	--	1.0968	9.8708	1.0114	9.1026
		Midfoot Posterior	6.7500	--	--	1.0915	7.3675	0.9978	6.7354
		Midfoot Anterior	7.875	--	--	1.0811	8.5136	1.0083	7.9402
		Metatarsals 1-2	12.3750	--	--	1.1542	14.2833	1.0051	12.4381
		Metatarsals 3-5	27.0000	--	--	1.1507	31.0682	1.0198	27.5352
		Toe 1	2.2500	1.0000	2.2500	--	--	--	--
		Toe 2	1.1250	1.0000	1.1250	--	--	--	--
Toes 3-5	4.5000	1.0000	4.5000	--	--	--	--		

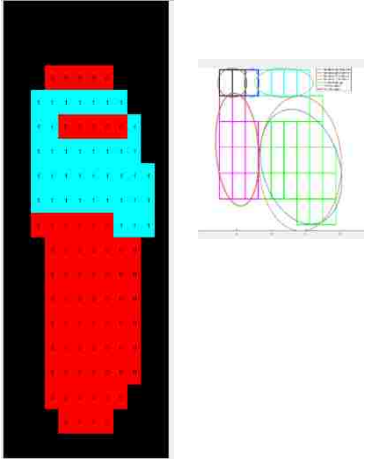
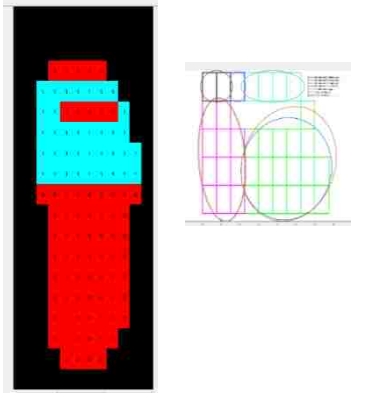
Time instant	Images: • Threshold insole – 1 is active sensor, 0 is inactive. • Ellipses fitted to the active sensors	Anatomical Location	Sensor Area (cm)	Normalized Area					
				Rectangle		Boundaries		Neighbors	
				Norm. Area	Area (cm ²)	Norm. Area	Area (cm ²)	Norm. Area	Area (cm ²)
39		Heel	4.5000	--	--	1.1251	5.0628	0.9954	4.4792
		Midfoot Posterior	6.7500	--	--	1.0915	7.3675	0.9978	6.7354
		Midfoot Anterior	7.875	--	--	1.0811	8.5136	1.0083	7.9402
		Metatarsals 1-2	12.3750	--	--	1.1542	14.2833	1.0051	12.4381
		Metatarsals 3-5	27.0000	--	--	1.1507	31.0682	1.0198	27.5352
		Toe 1	2.2500	1.0000	2.2500	--	--	--	--
		Toe 2	1.1250	1.0000	1.1250	--	--	--	--
Toes 3-5	4.5000	1.0000	4.5000	--	--	--	--		
40		Heel	2.2500	--	--	1.2192	2.7431	1.2536	2.8207
		Midfoot Posterior	5.6250	--	--	1.2234	6.8818	1.0054	5.6553
		Midfoot Anterior	7.875	--	--	1.0811	8.5136	1.0083	7.9402
		Metatarsals 1-2	13.5000	--	--	1.1285	15.2341	0.9984	13.4783
		Metatarsals 3-5	27.0000	--	--	1.1507	31.0682	1.0198	27.5352
		Toe 1	2.2500	1.0000	2.2500	--	--	--	--
		Toe 2	1.1250	1.0000	1.1250	--	--	--	--
Toes 3-5	4.5000	1.0000	4.5000	--	--	--	--		

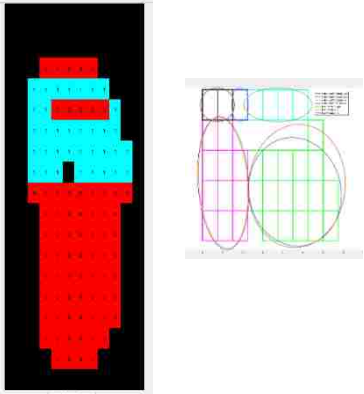
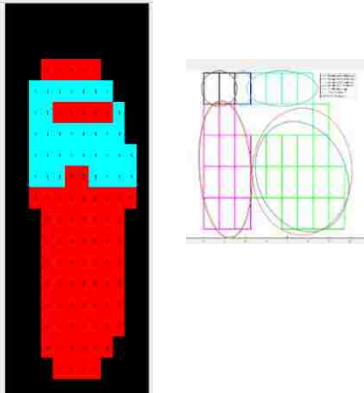
Time instant	Images: <ul style="list-style-type: none"> • Threshold insole – 1 is active sensor, 0 is inactive. • Ellipses fitted to the active sensors 	Anatomical Location	Sensor Area (cm)	Normalized Area					
				Rectangle		Boundaries		Neighbors	
				Norm. Area	Area (cm ²)	Norm. Area	Area (cm ²)	Norm. Area	Area (cm ²)
41	 	Heel	--	--	--	--	--	--	--
		Midfoot Posterior	2.2500	1.0000	2.2500	--	--	--	--
		Midfoot Anterior	6.7500	1.0000	6.7500	--	--	--	--
		Metatarsals 1-2	13.5000	--	--	1.1285	15.2341	0.9984	13.4783
		Metatarsals 3-5	27.0000	--	--	1.1507	31.0682	1.0198	27.5352
		Toe 1	2.2500	1.0000	2.2500	--	--	--	--
		Toe 2	1.1250	1.0000	1.1250	--	--	--	--
Toes 3-5	4.5000	1.0000	4.5000	--	--	--	--		
42	 	Heel	--	--	--	--	--	--	
		Midfoot Posterior	--	--	--	--	--	--	--
		Midfoot Anterior	6.7500	1.0000	6.7500	--	--	--	--
		Metatarsals 1-2	12.3750	--	--	1.0552	13.0582	0.9969	12.3365
		Metatarsals 3-5	27.0000	--	--	1.1507	31.0682	1.0198	27.5352
		Toe 1	2.2500	1.0000	2.2500	--	--	--	--
		Toe 2	1.1250	1.0000	1.1250	--	--	--	--
Toes 3-5	4.5000	1.0000	4.5000	--	--	--	--		

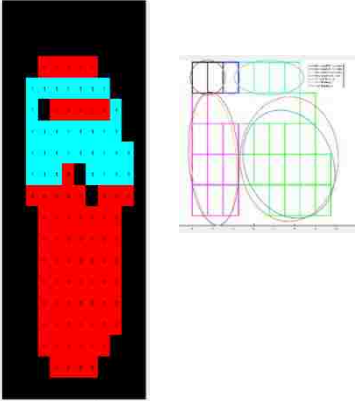
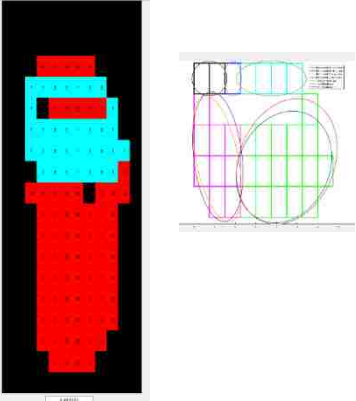
Time instant	Images: • Threshold insole – 1 is active sensor, 0 is inactive. • Ellipses fitted to the active sensors	Anatomical Location	Sensor Area (cm)	Normalized Area					
				Rectangle		Boundaries		Neighbors	
				Norm. Area	Area (cm ²)	Norm. Area	Area (cm ²)	Norm. Area	Area (cm ²)
43		Heel	--	--	--	--	--	--	--
		Midfoot Posterior	--	--	--	--	--	--	--
		Midfoot Anterior	6.7500	1.0000	6.7500	--	--	--	--
		Metatarsals 1-2	12.3750	--	--	1.0552	13.0582	0.9969	12.3365
		Metatarsals 3-5	25.8750	--	--	1.1568	29.9321	1.0156	26.2798
		Toe 1	2.2500	1.0000	2.2500	--	--	--	--
		Toe 2	1.1250	1.0000	1.1250	--	--	--	--
	Toes 3-5	4.5000	1.0000	4.5000	--	--	--	--	
44		Heel	--	--	--	--	--	--	--
		Midfoot Posterior	--	--	--	--	--	--	--
		Midfoot Anterior	5.6250	--	--	1.0995	6.1848	1.0050	5.6530
		Metatarsals 1-2	12.3750	--	--	1.0552	13.0582	0.9969	12.3365
		Metatarsals 3-5	25.8750	--	--	1.1568	29.9321	1.0156	26.2798
		Toe 1	2.2500	1.0000	2.2500	--	--	--	--
		Toe 2	1.1250	1.0000	1.1250	--	--	--	--
	Toes 3-5	4.5000	1.0000	4.5000	--	--	--	--	

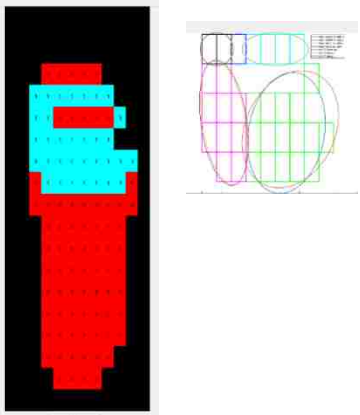
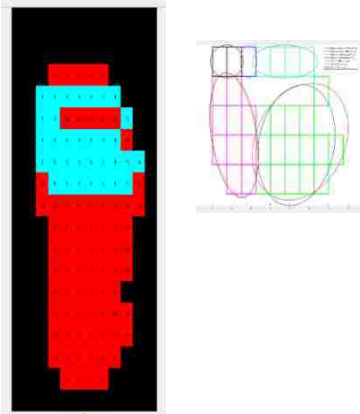
Time instant	Images: • Threshold insole – 1 is active sensor, 0 is inactive. • Ellipses fitted to the active sensors	Anatomical Location	Sensor Area (cm)	Normalized Area							
				Rectangle		Boundaries		Neighbors			
				Norm. Area	Area (cm ²)	Norm. Area	Area (cm ²)	Norm. Area	Area (cm ²)		
45			Heel	--	--	--	--	--	--	--	
			Midfoot Posterior	--	--	--	--	--	--	--	--
			Midfoot Anterior	4.5000	--	--	1.2198	5.4891	1.0074	4.5334	
			Metatarsals 1-2	12.3750	--	--	1.0552	13.0582	0.9969	12.3365	
			Metatarsals 3-5	24.7500	--	--	1.1946	29.5656	1.0148	25.1166	
			Toe 1	2.2500	1.0000	2.2500	--	--	--	--	
			Toe 2	1.1250	1.0000	1.1250	--	--	--	--	
			Toes 3-5	4.5000	1.0000	4.5000	--	--	--	--	
46			Heel	--	--	--	--	--	--	--	
			Midfoot Posterior	--	--	--	--	--	--	--	
			Midfoot Anterior	2.2500	1.0000	2.2500	--	--	--	--	
			Metatarsals 1-2	12.3750	--	--	1.0552	13.0582	0.9969	12.3365	
			Metatarsals 3-5	24.7500	--	--	1.1946	29.5656	1.0148	25.1166	
			Toe 1	2.2500	1.0000	2.2500	--	--	--	--	
			Toe 2	1.1250	1.0000	1.1250	--	--	--	--	
			Toes 3-5	4.5000	1.0000	4.5000	--	--	--	--	

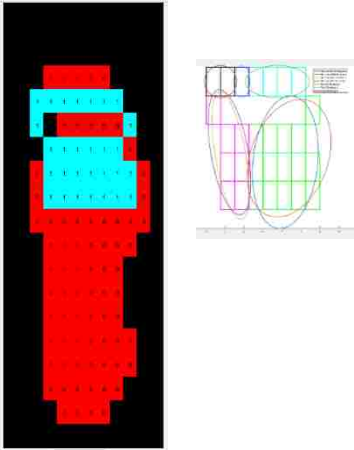
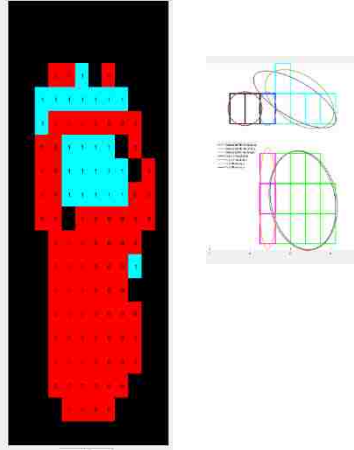
Time instant	Images: <ul style="list-style-type: none"> • Threshold insole – 1 is active sensor, 0 is inactive. • Ellipses fitted to the active sensors 	Anatomical Location	Sensor Area (cm)	Normalized Area					
				Rectangle		Boundaries		Neighbors	
				Norm. Area	Area (cm ²)	Norm. Area	Area (cm ²)	Norm. Area	Area (cm ²)
47		Heel	--	--	--	--	--	--	--
		Midfoot Posterior	--	--	--	--	--	--	--
		Midfoot Anterior	--	--	--	--	--	--	--
		Metatarsals 1-2	12.3750	--	--	1.0552	13.0582	0.9969	12.3365
		Metatarsals 3-5	24.7500	--	--	1.1946	29.5656	1.0148	25.1166
		Toe 1	2.2500	1.0000	2.2500	--	--	--	--
		Toe 2	1.1250	1.0000	1.1250	--	--	--	--
		Toes 3-5	4.5000	1.0000	4.5000	--	--	--	--
48		Heel	--	--	--	--	--	--	--
		Midfoot Posterior	--	--	--	--	--	--	--
		Midfoot Anterior	--	--	--	--	--	--	--
		Metatarsals 1-2	12.3750	--	--	1.0552	13.0582	0.9969	12.3365
		Metatarsals 3-5	23.6250	--	--	1.2490	29.5080	1.0191	24.0756
		Toe 1	2.2500	1.0000	2.2500	--	--	--	--
		Toe 2	1.1250	1.0000	1.1250	--	--	--	--
		Toes 3-5	4.5000	1.0000	4.5000	--	--	--	--

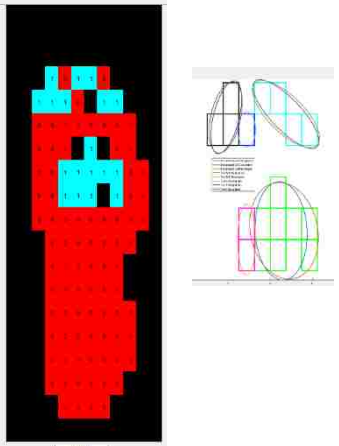
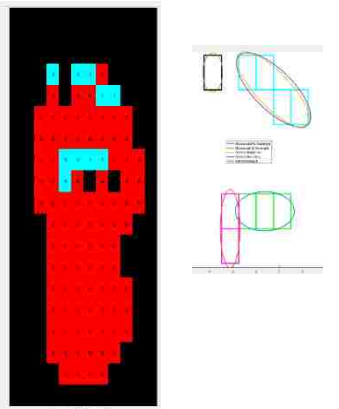
Time instant	Images: <ul style="list-style-type: none"> • Threshold insole – 1 is active sensor, 0 is inactive. • Ellipses fitted to the active sensors 	Anatomical Location	Sensor Area (cm)	Normalized Area					
				Rectangle		Boundaries		Neighbors	
				Norm. Area	Area (cm ²)	Norm. Area	Area (cm ²)	Norm. Area	Area (cm ²)
49		Heel	--	--	--	--	--	--	--
		Midfoot Posterior	--	--	--	--	--	--	--
		Midfoot Anterior	--	--	--	--	--	--	--
		Metatarsals 1-2	12.3750	--	--	1.0552	13.0582	0.9969	12.3365
		Metatarsals 3-5	23.6250	--	--	1.2490	29.5080	1.0191	24.0756
		Toe 1	2.2500	1.0000	2.2500	--	--	--	--
		Toe 2	1.1250	1.0000	1.1250	--	--	--	--
		Toes 3-5	4.5000	1.0000	4.5000	--	--	--	--
50		Heel	--	--	--	--	--	--	
		Midfoot Posterior	--	--	--	--	--	--	--
		Midfoot Anterior	--	--	--	--	--	--	--
		Metatarsals 1-2	12.3750	--	--	1.0552	13.0582	0.9969	12.3365
		Metatarsals 3-5	20.2500	--	--	1.1938	24.1741	1.0236	20.7279
		Toe 1	2.2500	1.0000	2.2500	--	--	--	--
		Toe 2	1.1250	1.0000	1.1250	--	--	--	--
		Toes 3-5	4.5000	1.0000	4.5000	--	--	--	--

Time instant	Images: <ul style="list-style-type: none"> • Threshold insole – 1 is active sensor, 0 is inactive. • Ellipses fitted to the active sensors 	Anatomical Location	Sensor Area (cm)	Normalized Area					
				Rectangle		Boundaries		Neighbors	
				Norm. Area	Area (cm ²)	Norm. Area	Area (cm ²)	Norm. Area	Area (cm ²)
51		Heel	--	--	--	--	--	--	--
		Midfoot Posterior	--	--	--	--	--	--	--
		Midfoot Anterior	--	--	--	--	--	--	--
		Metatarsals 1-2	12.3750	--	--	1.0552	13.0582	0.9969	12.3365
		Metatarsals 3-5	19.1250	--	--	1.2126	23.1918	1.0193	19.4940
		Toe 1	2.2500	1.0000	2.2500	--	--	--	--
		Toe 2	1.1250	1.0000	1.1250	--	--	--	--
		Toes 3-5	4.5000	1.0000	4.5000	--	--	--	--
52		Heel	--	--	--	--	--	--	
		Midfoot Posterior	--	--	--	--	--	--	--
		Midfoot Anterior	--	--	--	--	--	--	--
		Metatarsals 1-2	12.3750	--	--	1.0552	13.0582	0.9969	12.3365
		Metatarsals 3-5	18.0000	--	--	1.2701	22.8613	1.0180	18.3231
		Toe 1	2.2500	1.0000	2.2500	--	--	--	--
		Toe 2	1.1250	1.0000	1.1250	--	--	--	--
		Toes 3-5	4.5000	1.0000	4.5000	--	--	--	--

Time instant	Images: <ul style="list-style-type: none"> • Threshold insole – 1 is active sensor, 0 is inactive. • Ellipses fitted to the active sensors 	Anatomical Location	Sensor Area (cm)	Normalized Area					
				Rectangle		Boundaries		Neighbors	
				Norm. Area	Area (cm ²)	Norm. Area	Area (cm ²)	Norm. Area	Area (cm ²)
53		Heel	--	--	--	--	--	--	--
		Midfoot Posterior	--	--	--	--	--	--	--
		Midfoot Anterior	--	--	--	--	--	--	--
		Metatarsals 1-2	11.2500	--	--	1.1085	12.4708	0.9994	11.2430
		Metatarsals 3-5	18.0000	--	--	1.2701	22.8613	1.0180	18.3231
		Toe 1	2.2500	1.0000	2.2500	--	--	--	--
		Toe 2	1.1250	1.0000	1.1250	--	--	--	--
		Toes 3-5	4.5000	1.0000	4.5000	--	--	--	--
54		Heel	--	--	--	--	--	--	
		Midfoot Posterior	--	--	--	--	--	--	--
		Midfoot Anterior	--	--	--	--	--	--	--
		Metatarsals 1-2	10.1250	--	--	1.1588	11.7332	0.9974	10.0985
		Metatarsals 3-5	19.1250	--	--	1.1969	22.8913	1.0171	19.4518
		Toe 1	2.2500	1.0000	2.2500	--	--	--	--
		Toe 2	1.1250	1.0000	1.1250	--	--	--	--
		Toes 3-5	4.5000	1.0000	4.5000	--	--	--	--

Time instant	Images: <ul style="list-style-type: none"> • Threshold insole – 1 is active sensor, 0 is inactive. • Ellipses fitted to the active sensors 	Anatomical Location	Sensor Area (cm)	Normalized Area					
				Rectangle		Boundaries		Neighbors	
				Norm. Area	Area (cm ²)	Norm. Area	Area (cm ²)	Norm. Area	Area (cm ²)
55		Heel	--	--	--	--	--	--	--
		Midfoot Posterior	--	--	--	--	--	--	--
		Midfoot Anterior	--	--	--	--	--	--	--
		Metatarsals 1-2	11.2500	--	--	1.0622	11.9497	0.9974	11.2206
		Metatarsals 3-5	18.0000	--	--	1.2510	22.8915	1.0593	19.0674
		Toe 1	2.2500	1.0000	2.2500	--	--	--	--
		Toe 2	1.1250	1.0000	1.1250	--	--	--	--
		Toes 3-5	4.5000	1.0000	4.5000	--	--	--	--
56		Heel	--	--	--	--	--	--	--
		Midfoot Posterior	--	--	--	--	--	--	--
		Midfoot Anterior	--	--	--	--	--	--	--
		Metatarsals 1-2	11.2500	--	--	1.0622	11.9497	0.9974	11.2206
		Metatarsals 3-5	18.0000	--	--	1.2510	22.5187	1.0593	19.0674
		Toe 1	2.2500	1.0000	2.2500	--	--	--	--
		Toe 2	1.1250	1.0000	1.1250	--	--	--	--
		Toes 3-5	4.5000	1.0000	4.5000	--	--	--	--

Time instant	Images: <ul style="list-style-type: none"> • Threshold insole – 1 is active sensor, 0 is inactive. • Ellipses fitted to the active sensors 	Anatomical Location	Sensor Area (cm)	Normalized Area					
				Rectangle		Boundaries		Neighbors	
				Norm. Area	Area (cm ²)	Norm. Area	Area (cm ²)	Norm. Area	Area (cm ²)
57		Heel	--	--	--	--	--	--	--
		Midfoot Posterior	--	--	--	--	--	--	--
		Midfoot Anterior	--	--	--	--	--	--	--
		Metatarsals 1-2	7.8750	--	--	1.3087	10.3060	1.0921	8.6002
		Metatarsals 3-5	16.8750	--	--	1.2288	20.7360	1.1199	18.8980
		Toe 1	2.2500	1.0000	2.2500	--	--	--	--
		Toe 2	1.1250	1.0000	1.1250	--	--	--	--
		Toes 3-5	4.5000	1.0000	4.5000	--	--	--	--
58		Heel	--	--	--	--	--	--	--
		Midfoot Posterior	--	--	--	--	--	--	--
		Midfoot Anterior	--	--	--	--	--	--	--
		Metatarsals 1-2	3.3750	1.0000	3.3750	--	--	--	--
		Metatarsals 3-5	12.3750	--	--	1.0618	13.1396	1.0043	12.4278
		Toe 1	2.2500	1.0000	2.2500	--	--	--	--
		Toe 2	1.1250	1.0000	1.1250	--	--	--	--
		Toes 3-5	5.6250	--	--	1.2620	7.0986	1.1709	6.5861

Time instant	Images: <ul style="list-style-type: none"> • Threshold insole – 1 is active sensor, 0 is inactive. • Ellipses fitted to the active sensors 	Anatomical Location	Sensor Area (cm)	Normalized Area					
				Rectangle		Boundaries		Neighbors	
				Norm. Area	Area (cm ²)	Norm. Area	Area (cm ²)	Norm. Area	Area (cm ²)
59		Heel	--	--	--	--	--	--	--
		Midfoot Posterior	--	--	--	--	--	--	--
		Midfoot Anterior	--	--	--	--	--	--	--
		Metatarsals 1-2	2.2500	1.0000	2.2500	--	--	--	--
		Metatarsals 3-5	9.0000	--	--	1.3095	11.7853	1.0159	9.1434
		Toe 1	3.3750	--	--	1.1500	3.8813	1.0248	3.4588
		Toe 2	1.1250	1.0000	1.1250	--	--	--	--
		Toes 3-5	4.5000	--	--	1.2564	5.6537	1.1087	4.9893
60		Heel	--	--	--	--	--	--	--
		Midfoot Posterior	--	--	--	--	--	--	--
		Midfoot Anterior	--	--	--	--	--	--	--
		Metatarsals 1-2	2.2500	1.0000	2.2500	--	--	--	--
		Metatarsals 3-5	3.3750	1.0000	3.3750	--	--	--	--
		Toe 1	1.1250	1.0000	1.1250	--	--	--	--
		Toe 2	--	--	--	--	--	--	--
		Toes 3-5	4.5000	--	--	1.2564	5.6537	1.1087	4.9893

Appendix H – Variable boundaries used for model optimization

Tables H.1 lists the lower and upper bounds used for the material characteristics of all regions and all insole sizes. Figures H.1 to H.7 show the boundaries for the geometric variables that were based on previous tissue thickness measurements (Thomas et al., 2004; Uzel et al., 2006; Valiant, 1984; Zheng et al., 2000) and were tuned to minimize the differences between the experimental and model ground reaction forces.

Table H. 1. The lower and upper bounds of the material variables.

	\bar{k} (N/mm ³)	n	\bar{c} (Ns/mm ³)	m
Lower	0.1	0.01	0.3	1
Upper	0.24	0.03	0.6	1.3

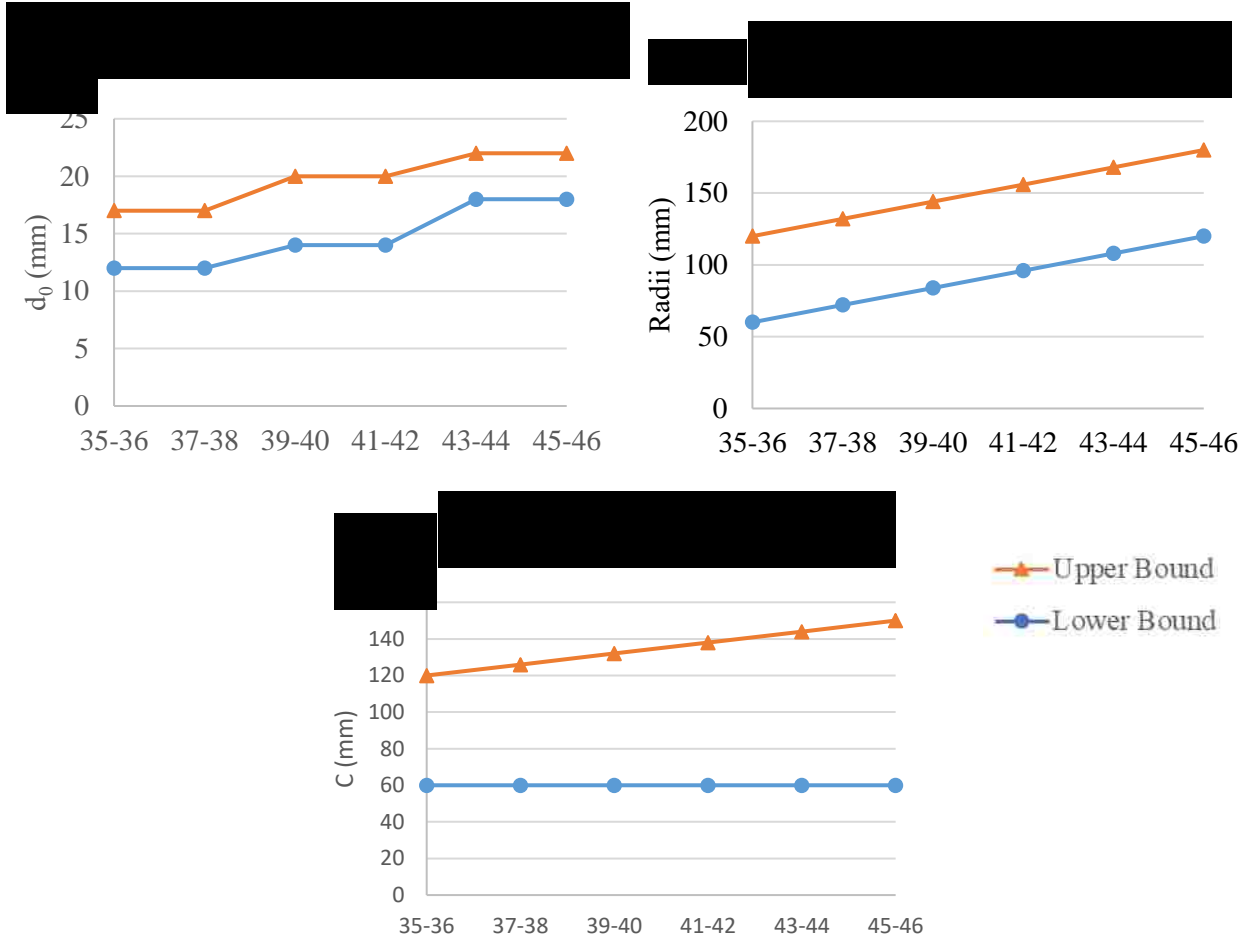


Fig. H. 1. The upper (orange triangles) and lower (blue circles) bounds of the geometric variables for the Heel and all insole sizes: (a) tissue thickness (d_0), (b) radii in the x and y axis (A and B), and (c) radius in the z-axis (C).

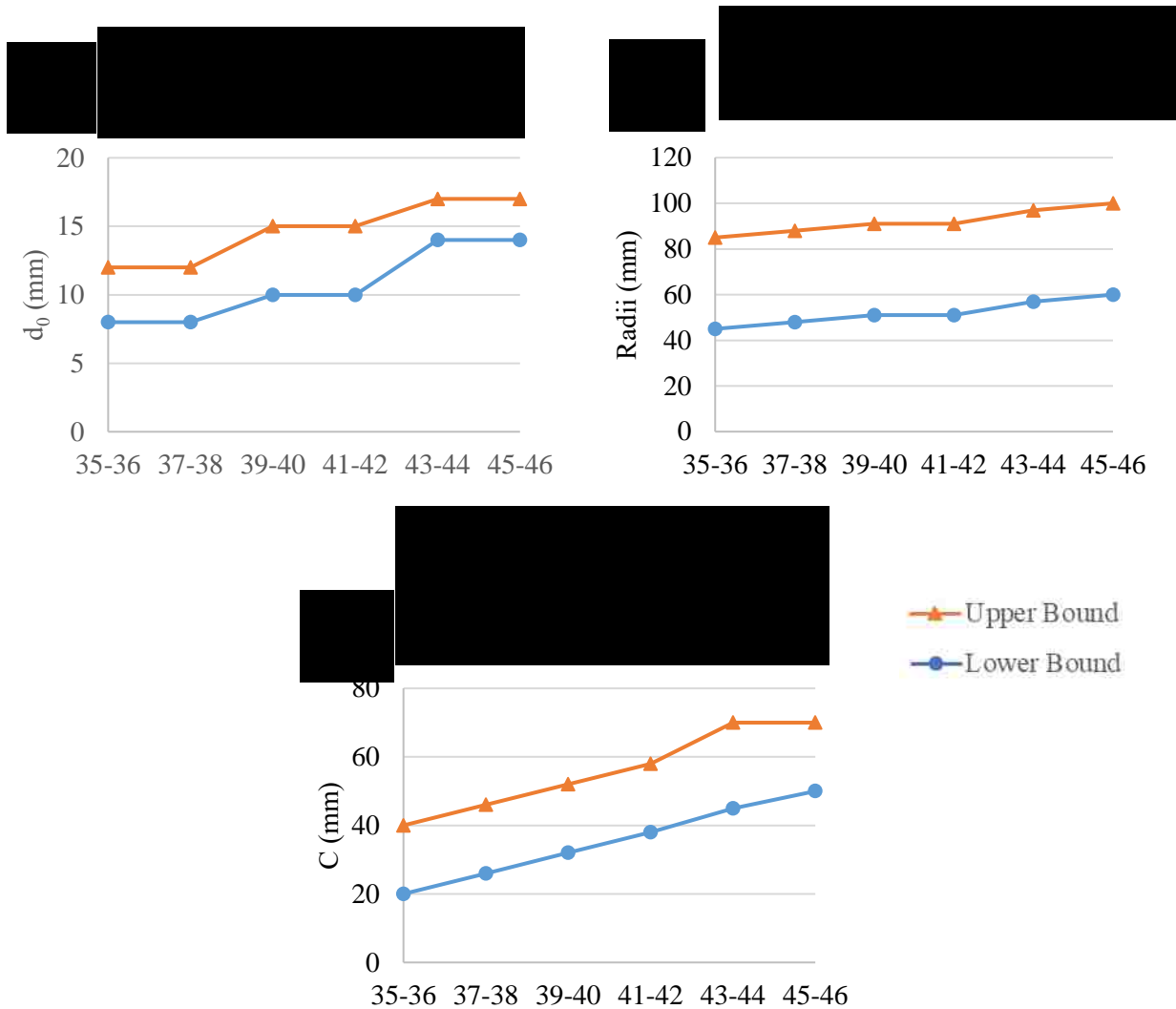


Fig. H. 2. The upper (orange triangles) and lower (blue circles) bounds of the geometric variables for the Midfoot Posterior and Midfoot Anterior: (a) tissue thickness (d_0), (b) radii in the x and y axes (A and B), and (c) radius in the z-axis (C). The bounds are for all insole sizes.

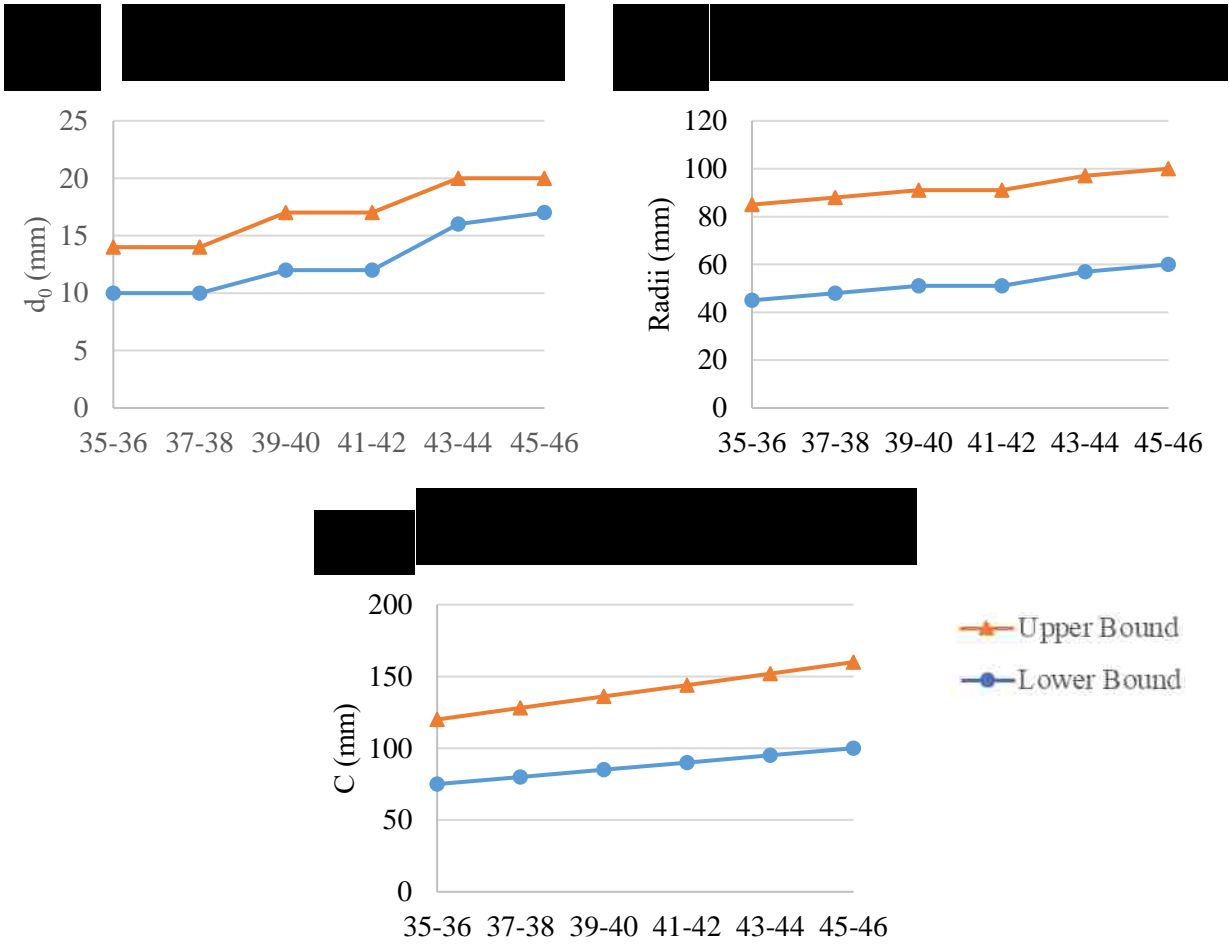


Fig. H. 3. The upper (orange triangles) and lower (blue circles) bounds of the geometric variables for the Metatarsals 1-2 and all insole sizes: (a) tissue thickness (d_0), (b) radii in the x and y axes (A and B), and (c) radius in the z-axis (C).

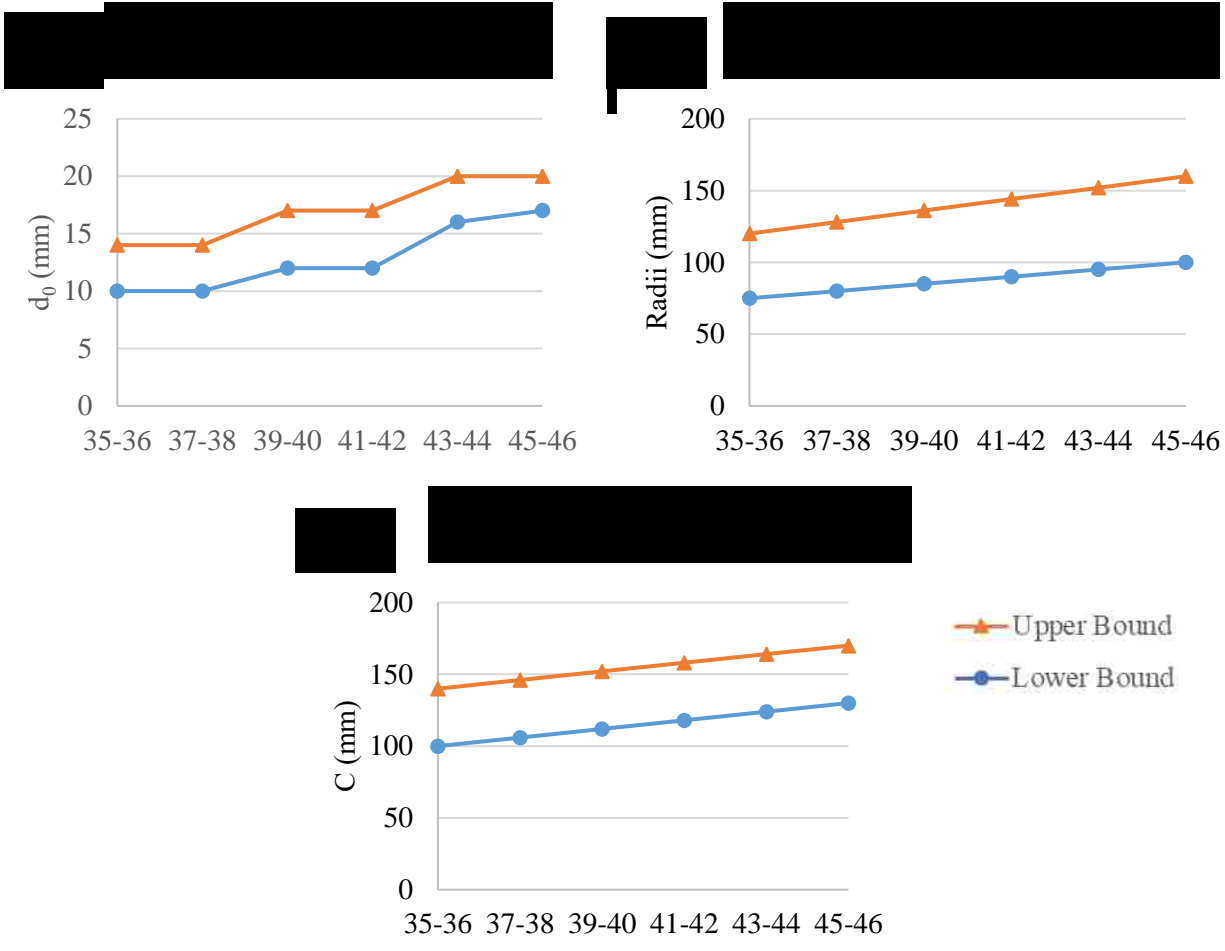


Fig. H. 4. The upper (orange triangles) and lower (blue circles) bounds of the geometric variables for the Metatarsals 3-5 and all insole sizes: (a) tissue thickness (d_0), (b) radii in the x and y axes (A and B), and (c) radius in the z-axis (C).

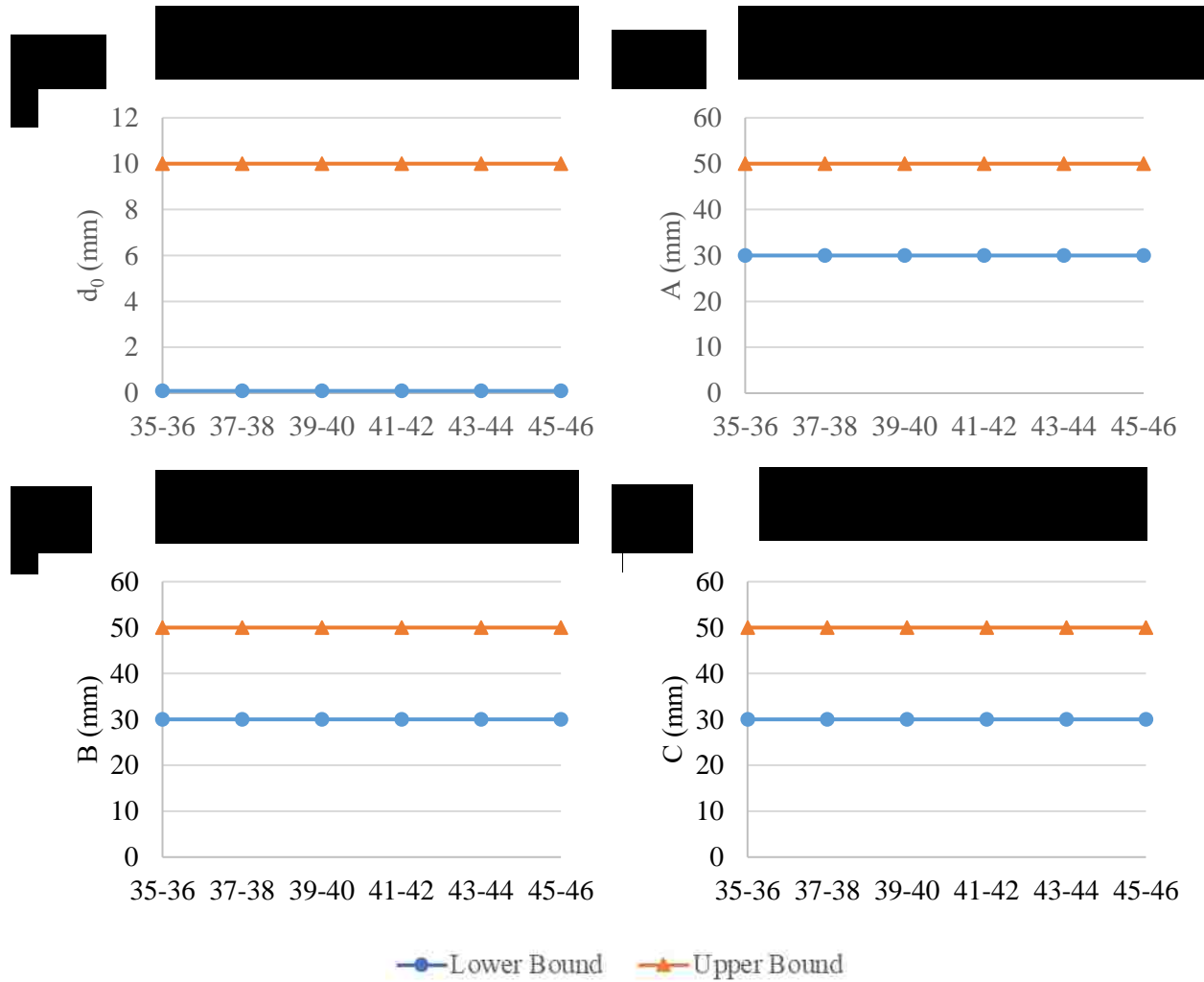


Fig. H. 5. The upper (orange triangles) and lower (blue circles) bounds of the geometric variables for the Hallux and all insole sizes: (a) tissue thickness (d_0), (b) radius in the x-axis (A), (c) radius in the y-axis (B), and (d) radius in the z-axis (C).

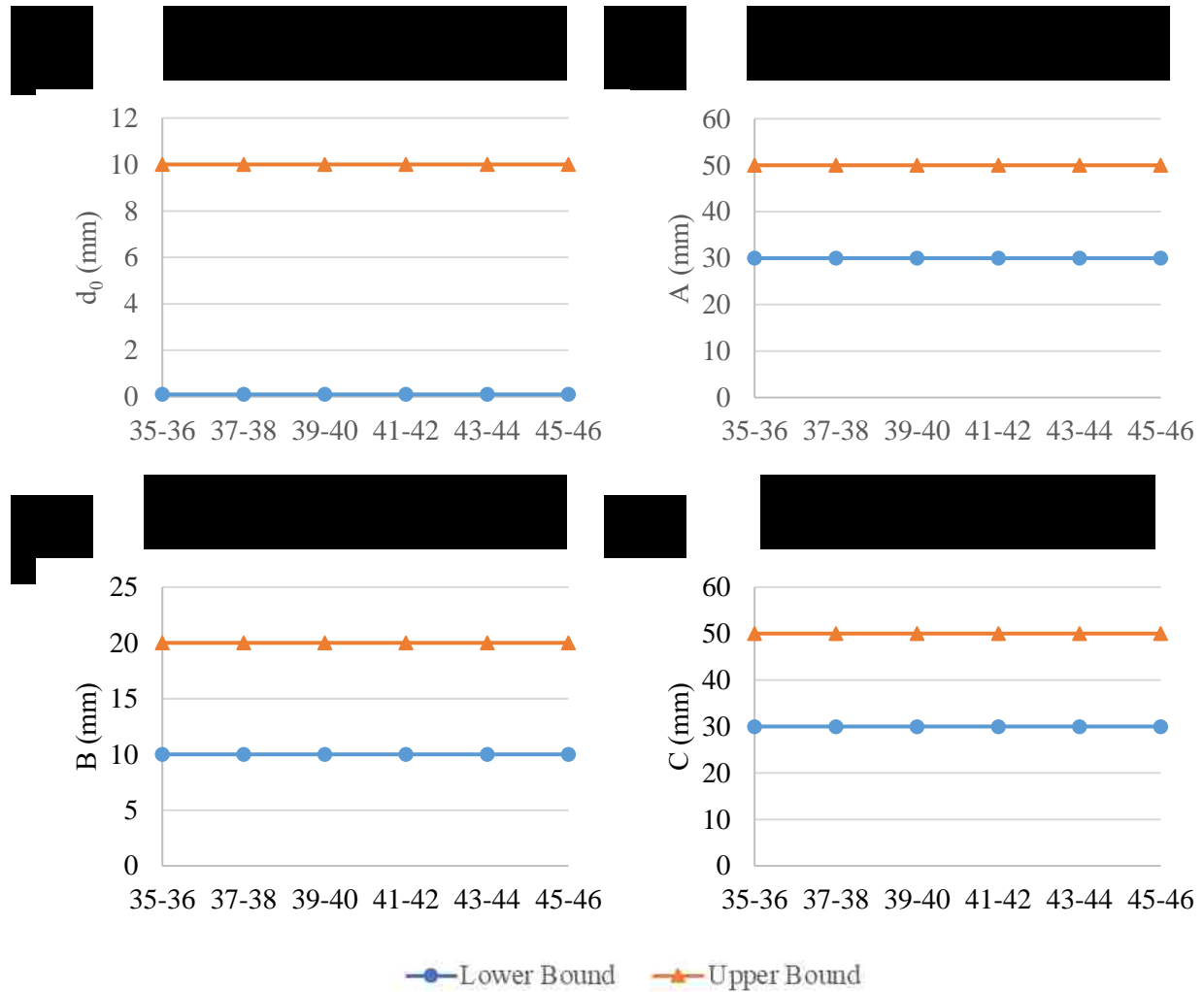


Fig. H. 6. The upper (orange triangles) and lower (blue circles) bounds of the geometric variables for the Toe 2 and all insole sizes: (a) tissue thickness (d_0), (b) radii in the x-axis (A), (c) radius in the y-axis (B), and (d) radius in the z-axis (C).

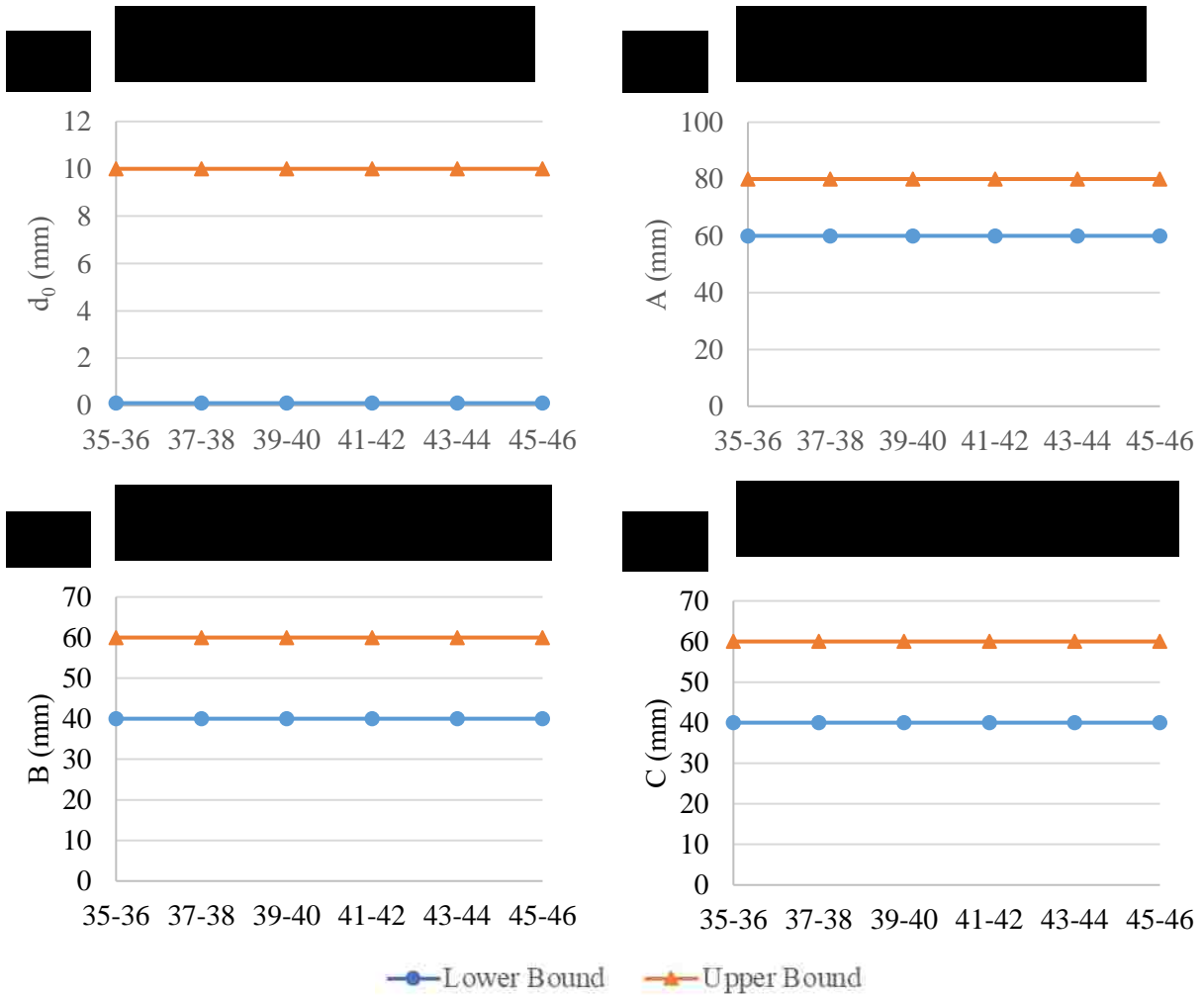


Fig. H. 7. The upper (orange triangles) and lower (blue circles) bounds of the geometric variables for the Toes 3-5 and all insole sizes: (a) tissue thickness (d_0), (b) radii in the x-axis (A), (c) radius in the y-axis (B), and (d) radius in the z-axis (C).

Appendix I – Variable and NRMSE results from model application

The variable and NRMSE average and standard deviation results for each anatomical area, separated by insole size. Each table below (Table I.1 – I.6) present the results for each respective insole size.

Table I. 1. The ellipsoid variable results for each anatomical region of insole size 35-36. Shown as average (standard deviation).

	d₀ (mm)	A (mm)	B (mm)	C (mm)	\bar{k} (N/mm ³)	\bar{c} (N·s/mm ³)	n	m	NRMSE (%)
Heel	16.8 (0.5)	108.8 (10.7)	107.3 (9.9)	70.6 (10.5)	0.208 (0.029)	0.010 (0.000)	0.177 (0.093)	1.18 (0.03)	25.7 (2.8)
Midfoot Posterior	10.8 (1.2)	78.6 (5.1)	78.7 (5.0)	33.0 (4.7)	0.187 (0.046)	0.019 (0.008)	0.106 (0.019)	1.13 (0.06)	12.9 (3.9)
Midfoot Anterior	10.7 (1.4)	70.7 (15.2)	70.7 (15.2)	31.8 (5.4)	0.189 (0.038)	0.022 (0.005)	0.208 (0.182)	1.12 (0.07)	12.8 (5.0)
Met. 1-2	11.5 (0.2)	83.5 (6.1)	83.5 (6.1)	101.6 (10.5)	0.171 (0.021)	0.020 (0.004)	0.567 (0.138)	1.13 (0.01)	10.6 (3.6)
Met. 3-5	11.3 (0.8)	119.9 (12.2)	120.4 (12.8)	121.5 (7.9)	0.161 (0.030)	0.023 (0.006)	0.418 (0.158)	1.06 (0.05)	17.5 (3.8)
Hallux	6.0 (2.6)	39.2 (6.0)	38.6 (6.0)	41.5 (5.8)	0.230 (0.016)	0.011 (0.002)	0.342 (0.209)	1.15 (0.04)	17.0 (6.9)
Toe 2	7.5 (1.8)	46.5 (1.2)	16.2 (2.0)	35.5 (3.5)	0.154 (0.043)	0.014 (0.002)	0.251 (0.139)	1.14 (0.05)	16.8 (7.3)
Toes 3-5	8.2 (2.3)	76.5 (3.4)	56.4 (3.8)	47.4 (5.1)	0.184 (0.046)	0.017 (0.006)	0.259 (0.186)	1.11 (0.05)	14.0 (12.9)

Table I. 2. The ellipsoid variable results for each anatomical region of insole size 37-38. Shown as average (standard deviation).

	d_0 (mm)	A (mm)	B (mm)	C (mm)	\bar{k} (N/mm ³)	\bar{c} (N·s/mm ³)	n	m	NRMSE (%)
Heel	16.4 (0.9)	80.2 (3.9)	80.7 (4.6)	69.9 (8.5)	0.117 (0.027)	0.011 (0.001)	0.294 (0.116)	1.18 (0.03)	25.5 (4.2)
Midfoot Posterior	11.4 (0.6)	77.2 (10.8)	78.4 (11.2)	31.8 (4.3)	0.185 (0.038)	0.016 (0.006)	0.148 (0.068)	1.17 (0.03)	10.5 (3.0)
Midfoot Anterior	10.4 (1.4)	75.8 (9.6)	76.0 (9.4)	38.9 (6.4)	0.183 (0.045)	0.022 (0.006)	0.142 (0.069)	1.13 (0.06)	12.4 (3.6)
Met. 1-2	11.8 (1.1)	97.4 (12.8)	96.6 (12.9)	109.8 (15.5)	0.182 (0.032)	0.020 (0.006)	0.442 (0.164)	1.12 (0.06)	13.0 (5.5)
Met. 3-5	11.6 (0.9)	139.7 (7.0)	141.0 (5.9)	116.5 (9.7)	0.140 (0.022)	0.023 (0.005)	0.311 (0.132)	1.08 (0.06)	15.8 (5.5)
Hallux	6.8 (2.2)	37.4 (5.4)	38.6 (5.1)	41.0 (4.4)	0.216 (0.030)	0.013 (0.004)	0.310 (0.148)	1.16 (0.05)	16.3 (5.4)
Toe 2	7.2 (1.4)	43.7 (2.2)	17.6 (1.5)	36.3 (3.3)	0.144 (0.032)	0.012 (0.003)	0.310 (0.119)	1.11 (0.05)	29.4 (15.1)
Toes 3-5	7.9 (1.4)	72.4 (5.7)	52.7 (5.5)	48.3 (3.9)	0.183 (0.040)	0.015 (0.006)	0.262 (0.133)	1.12 (0.05)	13.7 (4.3)

Table I. 3. The ellipsoid variable results for each anatomical region of insole size 39-40. Shown as average (standard deviation).

	d_0 (mm)	A (mm)	B (mm)	C (mm)	\bar{k} (N/mm ³)	\bar{c} (N·s/mm ³)	n	m	NRMSE (%)
Heel	19.3 (1.1)	93.7 (4.8)	99.5 (7.8)	64.4 (4.2)	0.120 (0.024)	0.011 (0.002)	0.340 (0.127)	1.15 (0.05)	27.1 (2.7)
Midfoot Posterior	13.7 (1.3)	81.4 (10.4)	80.8 (10.6)	40.9 (5.4)	0.185 (0.051)	0.017 (0.007)	0.147 (0.077)	1.14 (0.03)	11.7 (2.8)
Midfoot Anterior	12.5 (1.2)	76.3 (10.3)	76.3 (10.3)	45.6 (4.1)	0.160 (0.035)	0.023 (0.005)	0.242 (0.077)	1.08 (0.07)	10.5 (4.1)
Met. 1-2	13.8 (1.7)	109.3 (15.5)	109.3 (15.5)	110.4 (9.1)	0.160 (0.044)	0.020 (0.009)	0.432 (0.165)	1.10 (0.08)	16.3 (5.7)
Met. 3-5	14.8 (1.2)	127.9 (12.0)	128.4 (11.5)	130.4 (11.6)	0.200 (0.029)	0.018 (0.006)	0.578 (0.112)	1.10 (0.06)	16.3 (6.6)
Hallux	7.9 (2.4)	41.6 (7.2)	42.0 (6.3)	40.4 (3.0)	0.194 (0.026)	0.015 (0.006)	0.252 (0.176)	1.13 (0.06)	16.9 (4.1)
Toe 2	7.6 (1.3)	42.7 (3.0)	17.6 (1.3)	38.4 (3.3)	0.148 (0.043)	0.012 (0.004)	0.287 (0.157)	1.14 (0.06)	28.6 (21.3)
Toes 3-5	8.0 (1.5)	73.0 (4.2)	52.8 (4.8)	46.3 (2.3)	0.181 (0.033)	0.018 (0.006)	0.345 (0.197)	1.15 (0.04)	12.2 (3.7)

Table I. 4. The ellipsoid variable results for each anatomical region of insole size 41-42. Shown as average (standard deviation).

	d_0 (mm)	A (mm)	B (mm)	C (mm)	\bar{k} (N/mm ³)	\bar{c} (N·s/mm ³)	n	m	NRMSE (%)
Heel	18.7 (0.9)	117.6 (19.9)	117.0 (19.3)	68.0 (5.4)	0.161 (0.040)	0.010 (0.000)	0.265 (0.168)	1.17 (0.04)	26.0 (8.2)
Midfoot Posterior	14.7 (0.6)	68.2 (4.7)	68.4 (4.7)	43.6 (6.2)	0.213 (0.031)	0.012 (0.005)	0.360 (0.088)	1.17 (0.05)	10.5 (2.3)
Midfoot Anterior	14.1 (0.7)	71.1 (6.5)	71.4 (7.0)	42.9 (4.3)	0.193 (0.033)	0.014 (0.003)	0.367 (0.105)	1.13 (0.03)	10.0 (1.7)
Met. 1-2	14.0 (0.9)	108.2 (13.4)	111.2 (15.8)	129.5 (7.9)	0.149 (0.025)	0.025 (0.002)	0.419 (0.147)	1.07 (0.03)	13.6 (3.2)
Met. 3-5	13.8 (0.8)	137.4 (7.9)	137.4 (7.9)	139.0 (6.2)	0.151 (0.020)	0.024 (0.002)	0.417 (0.096)	1.06 (0.02)	15.6 (3.7)
Hallux	9.0 (1.0)	39.7 (4.0)	39.2 (3.2)	38.5 (3.9)	0.220 (0.025)	0.014 (0.003)	0.342 (0.161)	1.16 (0.05)	15.4 (3.8)
Toe 2	6.5 (1.8)	44.4 (2.8)	18.3 (1.1)	38.2 (3.1)	0.140 (0.041)	0.010 (0.001)	0.263 (0.068)	1.14 (0.06)	18.4 (4.1)
Toes 3-5	6.5 (2.6)	75.2 (3.2)	55.5 (3.8)	51.4 (5.6)	0.209 (0.024)	0.014 (0.005)	0.172 (0.084)	1.11 (0.04)	18.0 (5.8)

Table I. 5. The ellipsoid variable results for each anatomical region of insole size 43-44. Shown as average (standard deviation).

	d_0 (mm)	A (mm)	B (mm)	C (mm)	\bar{k} (N/mm ³)	\bar{c} (N·s/mm ³)	n	m	NRMSE (%)
Heel	21.9 (0.3)	140.6 (24.3)	142.3 (25.8)	89.1 (14.9)	0.186 (0.056)	0.010 (0.000)	0.170 (0.090)	1.20 (0.00)	18.4 (3.4)
Midfoot Posterior	16.0 (1.3)	91.5 (7.4)	92.4 (7.3)	52.4 (9.4)	0.186 (0.032)	0.022 (0.010)	0.128 (0.051)	1.14 (0.08)	9.0 (3.0)
Midfoot Anterior	15.9 (0.9)	85.9 (7.3)	85.9 (7.3)	54.1 (7.3)	0.167 (0.046)	0.021 (0.005)	0.160 (0.094)	1.13 (0.07)	11.8 (5.0)
Met. 1-2	16.8 (0.8)	129.1 (11.5)	129.1 (11.5)	145.0 (6.6)	0.141 (0.028)	0.024 (0.006)	0.348 (0.183)	1.05 (0.03)	11.1 (4.2)
Met. 3-5	18.2 (0.9)	142.8 (13.8)	142.8 (13.8)	145.0 (13.7)	0.152 (0.024)	0.025 (0.003)	0.415 (0.062)	1.07 (0.02)	16.0 (3.5)
Hallux	5.0 (2.3)	39.7 (4.9)	37.5 (4.0)	45.0 (5.2)	0.219 (0.019)	0.014 (0.004)	0.236 (0.149)	1.11 (0.06)	16.8 (2.4)
Toe 2	6.7 (1.5)	41.6 (2.2)	17.1 (1.0)	38.3 (1.9)	0.133 (0.016)	0.013 (0.002)	0.209 (0.041)	1.13 (0.03)	14.4 (4.7)
Toes 3-5	7.7 (2.1)	71.9 (3.0)	51.9 (3.1)	52.3 (6.6)	0.197 (0.044)	0.015 (0.006)	0.164 (0.044)	1.13 (0.07)	16.9 (7.6)

Table I. 6. The ellipsoid variable results for each anatomical region of insole size 45-46. Shown as average (standard deviation).

	d_0 (mm)	A (mm)	B (mm)	C (mm)	\bar{k} (N/mm ³)	\bar{c} (N·s/mm ³)	n	m	NRMSE (%)
Heel	22.0 (0.0)	163.4 (13.6)	161.0 (13.4)	78.6 (12.4)	0.225 (0.016)	0.010 (0.000)	0.100 (0.001)	1.17 (0.03)	21.1 (5.6)
Midfoot Posterior	15.0 (1.0)	92.5 (7.5)	92.5 (7.5)	65.2 (4.8)	0.149 (0.019)	0.025 (0.001)	0.100 (0.000)	1.09 (0.09)	16.8 (2.2)
Midfoot Anterior	15.5 (1.1)	80.2 (7.6)	80.2 (7.6)	65.6 (7.7)	0.202 (0.038)	0.020 (0.007)	0.141 (0.071)	1.06 (0.04)	12.2 (5.7)
Met. 1-2	17.3 (0.3)	107.3 (5.0)	107.3 (5.0)	154.1 (4.1)	0.146 (0.033)	0.025 (0.003)	0.444 (0.111)	1.02 (0.03)	11.1 (3.6)
Met. 3-5	18.3 (0.2)	143.0 (8.9)	143.0 (8.9)	158.4 (8.2)	0.159 (0.008)	0.024 (0.001)	0.426 (0.051)	1.08 (0.01)	18.5 (1.2)
Hallux	3.5 (2.1)	35.9 (3.0)	33.4 (3.0)	41.1 (7.0)	0.197 (0.023)	0.015 (0.001)	0.319 (0.154)	1.15 (0.04)	18.0 (5.5)
Toe 2	4.4 (1.6)	44.6 (1.5)	17.9 (0.8)	36.1 (4.2)	0.148 (0.034)	0.013 (0.005)	0.208 (0.006)	1.12 (0.02)	15.8 (5.7)
Toes 3-5	5.4 (2.4)	76.7 (3.0)	56.6 (2.9)	55.3 (3.9)	0.196 (0.016)	0.017 (0.004)	0.165 (0.089)	1.08 (0.05)	10.6 (2.3)

References

- Abaqus, 2007. Hyperelastic behavior of rubberlike materials - Model prediction of material behavior versus experimental data, in: Abaqus Analysis User's Manual.
- Aerts, P., Ker, R.F., De Clercq, D., Ilesley, D.W., Alexander, R.M.N., 1995. The mechanical properties of the human heel pad: A paradox resolved. *J. Biomech.* 28, 1299–1308. [https://doi.org/10.1016/0021-9290\(95\)00009-7](https://doi.org/10.1016/0021-9290(95)00009-7)
- Alavi, A., Sibbald, R.G., Mayer, D., Goodman, L., Botros, M., Armstrong, D.G., Woo, K., Boeni, T., Ayello, E. a, Kirsner, R.S., 2014. Diabetic foot ulcers: Part I. Pathophysiology and prevention. *J. Am. Acad. Dermatol.* 70, 1.e1-18; quiz 19-20. <https://doi.org/10.1016/j.jaad.2013.06.055>
- Amenta, N., 2011. Shape Analysis with the Delaunay Triangulation Shape of a Point Set Surface Reconstruction [WWW Document]. UC Davis ECS 226 Comput. Geom. URL <http://web.cs.ucdavis.edu/~amenta/w11/DTapp.pdf> (accessed 11.1.18).
- American Podiatric Medical Association, Kelton Research, 2009. Down At Their Heels: Heel Pain Tops America's List of Persistent Foot Ailments.
- Ankersen, J., Birkbeck, A.E., Thomson, R.D., Vanezis, P., 1999. Puncture resistance and tensile strength of skin simulants. *Proc. Inst. Mech. Eng. Part H J. Eng. Med.* 213, 493–501.
- Archer, K.R., Castillo, R.C., MacKenzie, E.J., Bosse, M.J., 2006. Gait Symmetry and Walking Speed Analysis Following Lower-Extremity Trauma. *Phys Ther* 86, 1630–40. <https://doi.org/10.2522/ptj.20060035>
- Aruntammanak, W., Aunhathaweesup, Y., Wongseree, W., Leelasantitham, A., Kiattisin, S., 2013. Diagnose flat foot from foot print image based on neural network, in: BMEiCON 2013 - 6th Biomedical Engineering International Conference. <https://doi.org/10.1109/BMEiCon.2013.6687684>
- Atlas, E., Yizhar, Z., Gefen, A., 2008. The Diabetic Foot Load Monitor: A Portable Device for Real-Time Subject-Specific Measurements of Deep Plantar Tissue Stresses During Gait. *J. Med. Device.* 2, 011005. <https://doi.org/10.1115/1.2891241>
- Atlas, E., Yizhar, Z., Khamis, S., Slomka, N., Hayek, S., Gefen, A., 2009. Utilization of the foot load monitor for evaluating deep plantar tissue stresses in patients with diabetes: proof-of-concept studies. *Gait Posture* 29, 377–82. <https://doi.org/10.1016/j.gaitpost.2008.10.055>
- Behforootan, S., Chatzistergos, P.E., Chockalingam, N., Naemi, R., 2017a. A clinically applicable non-invasive method to quantitatively assess the visco-hyperelastic properties of human heel pad, implications for assessing the risk of mechanical trauma. *J. Mech. Behav. Biomed. Mater.* 68, 287–295. <https://doi.org/10.1016/j.jmbbm.2017.02.011>
- Behforootan, S., Chatzistergos, P.E., Chockalingam, N., Naemi, R., 2017b. A Simulation of the Viscoelastic Behaviour of Heel Pad During Weight-Bearing Activities of Daily Living. *Ann. Biomed. Eng.* 45, 2750–2761. <https://doi.org/10.1007/s10439-017-1918-1>
- Brown, P., McPhee, J., 2018. A 3D ellipsoidal volumetric foot–ground contact model for forward dynamics. *Multibody Syst. Dyn.* 42, 447–467. <https://doi.org/10.1007/s11044-017-9605-4>
- Brown, R., 2007. FITELLIPSE: Least squares ellipse fitting.
- Buchelly, F.J., Mayorca, D., Ballarin, V., Pastore, J., 2016. Digital image processing techniques applied to pressure analysis and morphological features extraction in footprints. *J. Phys. Conf. Ser.* 705.

<https://doi.org/10.1088/1742-6596/705/1/012020>

- Bucki, M., Luboz, V., Perrier, A., Champion, E., Vuillerme, N., Payan, Y., 2016. Clinical workflow for personalized foot pressure ulcer prevention. *Med. Eng. Phys.* 1–9. <https://doi.org/10.1016/j.matchemphys.2008.10.020>
- Budhabhatti, S.P., Erdemir, A., Petre, M., Sferra, J., Donley, B., Cavanagh, P.R., 2007. Finite Element Modeling of the First Ray of the Foot: A Tool for the Design of Interventions. *J. Biomech. Eng.* 129, 750. <https://doi.org/10.1115/1.2768108>
- Cavanagh, P.R., Simoneau, G.G., Ulbrecht, J.S., 1993. Ulceration, unsteadiness, and uncertainty: the biomechanical consequences of diabetes mellitus. *J. Biomech.* 26 Suppl 1, 23–40.
- Chen, B., Bates, B.T., 2000. Comparison of F-Scan in-sole and AMTI forceplate system in measuring vertical ground reaction force during gait. *Theory Pract.* 3985, 43–53. <https://doi.org/10.1080/095939800307601>
- Chen, W.-M., Lee, S.-J., Lee, P.V.S., 2014. The in vivo plantar soft tissue mechanical property under the metatarsal head: implications of tissues' joint-angle dependent response in foot finite element modeling. *J. Mech. Behav. Biomed. Mater.* 40, 264–74. <https://doi.org/10.1016/j.jmbbm.2014.09.007>
- Chen, W.-M., Lee, T., Lee, P.V.-S., Lee, J.W., Lee, S.-J., 2010. Effects of internal stress concentrations in plantar soft-tissue—A preliminary three-dimensional finite element analysis. *Med. Eng. Phys.* 32, 324–331. <https://doi.org/10.1016/j.medengphy.2010.01.001>
- Cheung, J.T.M., Zhang, M., Leung, A.K.L., Fan, Y.B., 2005. Three-dimensional finite element analysis of the foot during standing - A material sensitivity study. *J. Biomech.* 38, 1045–1054. <https://doi.org/10.1016/j.jbiomech.2004.05.035>
- Chokhandre, S., Halloran, J.P., van den Bogert, A.J., Erdemir, A., 2012. A three-dimensional inverse finite element analysis of the heel pad. *J. Biomech. Eng.* 134, 031002. <https://doi.org/10.1115/1.4005692>
- Chong, A.K., Al-baghdadi, J.A.A., Milburn, P., 2014. Matching 3D Plantar Model with the Force and Pressure Data of the Loading Phase of Gait 704–708.
- Chu, W.C., Lee, S.H., Chu, W., Wang, T.J., Lee, M.C., 1995. The Use of Arch Index to Characterize Arch Height: A Digital Image Processing Approach. *IEEE Trans. Biomed. Eng.* 42, 1088–1093. <https://doi.org/10.1109/10.469375>
- DeBerardinis, J., Dufek, J.S., Trabia, M.B., Lidstone, D.E., 2018. Assessing the validity of pressure-measuring insoles in quantifying gait variables. *J. Rehabil. Assist. Technol. Eng. Special Co.* 1–12.
- DeBerardinis, J., Trabia, M., Dufek, J.S., 2016. Review of Foot Plantar Pressure—Focus on the Development of Foot Ulcerations. *Open Access J. Sci. Technol.* 3. <https://doi.org/10.11131/2016/101158>
- Erdemir, A., Viveiros, M.L., Ulbrecht, J.S., Cavanagh, P.R., 2006. An inverse finite-element model of heel-pad indentation. *J. Biomech.* 39, 1279–1286. <https://doi.org/10.1016/j.jbiomech.2005.03.007>
- Fascione, J.M., Crews, R.T., Wrobel, J.S., 2012. Dynamic footprint measurement collection technique and intrarater reliability: ink mat, paper pedography, and electronic pedography. *J. Am. Podiatr. Med. Assoc.* 102, 130–138. <https://doi.org/10.7547/1020130>
- Fernandez, J.W., Ul Haque, M.Z., Hunter, P.J., Mithraratne, K., 2012. Mechanics of the foot Part 1: a

- continuum framework for evaluating soft tissue stiffening in the pathologic foot. *Int. j. numer. method. biomed. eng.* 28, 1056–70. <https://doi.org/10.1002/cnm.2494>
- Fong, D.T.P., Chan, Y.Y., Hong, Y., Yung, P.S.H., Fung, K.Y., Chan, K.M., 2008. Estimating the complete ground reaction forces with pressure insoles in walking. *J. Biomech.* 41, 2597–2601. <https://doi.org/10.1016/j.jbiomech.2008.05.007>
- Fontanella, C.G., Favaretto, E., Carniel, E.L., Natali, A.N., 2014. Constitutive formulation and numerical analysis of the biomechanical behaviour of forefoot plantar soft tissue. *Proc. Inst. Mech. Eng. Part H J. Eng. Med.* 228, 942–51. <https://doi.org/10.1177/0954411914551852>
- Forner Cordero, A., Koopman, H.J.F.M., Van Der Helm, F.C.T., 2004. Use of pressure insoles to calculate the complete ground reaction forces. *J. Biomech.* 37, 1427–1432. <https://doi.org/10.1016/j.jbiomech.2003.12.016>
- Gefen, A., 2003. Plantar soft tissue loading under the medial metatarsals in the standing diabetic foot. *Med. Eng. Phys.* 25, 491–499. [https://doi.org/10.1016/S1350-4533\(03\)00029-8](https://doi.org/10.1016/S1350-4533(03)00029-8)
- Gefen, A., 2002. Stress analysis of the standing foot following surgical plantar fascia release. *J. Biomech.* 35, 629–637. [https://doi.org/10.1016/S0021-9290\(01\)00242-1](https://doi.org/10.1016/S0021-9290(01)00242-1)
- Gefen, A., Megido-Ravid, M., Itzchak, Y., 2001. In vivo biomechanical behavior of the human heel pad during the stance phase of gait. *J. Biomech.* 34, 1661–5.
- Gilchrist, L.A., Winter, D.A., 1996. A two-part, viscoelastic foot model for use in gait simulations. *J. Biomech.* 29, 795–798. [https://doi.org/10.1016/0021-9290\(95\)00141-7](https://doi.org/10.1016/0021-9290(95)00141-7)
- Grigoriadis, G., Newell, N., Carpanen, D., Christou, A., Bull, A.M.J., Masouros, S.D., 2017. Material properties of the heel fat pad across strain rates. *J. Mech. Behav. Biomed. Mater.* 65, 398–407. <https://doi.org/10.1016/j.jmbbm.2016.09.003>
- Gu, Y., Li, J., Ren, X., Lake, M.J., Zeng, Y., 2010. Heel skin stiffness effect on the hind foot biomechanics during heel strike. *Skin Res. Technol.* 16, 291–6. <https://doi.org/10.1111/j.1600-0846.2010.00425.x>
- Güler, H.C., Berme, N., Simon, S.R., 1998. A viscoelastic sphere model for the representation of plantar soft tissue during simulations. *J. Biomech.* 31, 847–853. [https://doi.org/10.1016/S0021-9290\(98\)00085-2](https://doi.org/10.1016/S0021-9290(98)00085-2)
- Hass, J., Weir, M.D., Thomas, G.B.J., Heil, C., 2016. Substitutions in Multiple Integrals, in: Hoag, C., Lynch, D., Hoffman, W., Casha, S., Al., E. (Eds.), *University Calculus: Early Transcendentals*. Pearson, London, pp. 806–808.
- Isvilanonda, V., Iaquinto, J.M., Williams, E.D., Cavanagh, P.R., Haynor, D.R., Chu, B., Ledoux, W.R., 2013. In vivo patient-specific material properties of the subcalcaneal fat: an inverse finite element analysis, in: *37th Annual Conference of the American Society of Biomechanics*. pp. 1–2.
- Johnson, A.R., Quigley, C.J., Freese, C.E., 1995. A Viscohyperelastic Finite-element Model For Rubber. *Comput. Methods Appl. Mech. Eng.* 127, 163–180.
- Ker, R., 1996. The time-dependent mechanical properties of the human heel pad in the context of locomotion. *J. Exp. Biol.* 199, 1501–1508.
- Klaesner, J.W., Hastings, M.K., Zou, D., Lewis, C., Mueller, M.J., 2002. Plantar tissue stiffness in patients with diabetes mellitus and peripheral neuropathy. *Arch. Phys. Med. Rehabil.* 83, 1796–1801. <https://doi.org/10.1053/apmr.2002.35661>

- Koch, M., Lunde, L.K., Ernst, M., Knardahl, S., Veiersted, K.B., 2016. Validity and reliability of pressure-measurement insoles for vertical ground reaction force assessment in field situations. *Appl. Ergon.* 53, 44–51. <https://doi.org/10.1016/j.apergo.2015.08.011>
- Kwan, R.L.C., Zheng, Y.P., Cheing, G.L.Y., 2010. The effect of aging on the biomechanical properties of plantar soft tissues. *Clin. Biomech.* 25, 601–605. <https://doi.org/10.1016/j.clinbiomech.2010.04.003>
- Ledoux, W.R., Blevins, J.J., 2007. The compressive material properties of the plantar soft tissue. *J. Biomech.* 40, 2975–2981. <https://doi.org/10.1016/j.jbiomech.2007.02.009>
- Ledoux, W.R., Meaney, D.F., Hillstrom, H.J., 2005. A Quasi-Linear, Viscoelastic, Structural Model of the Plantar Soft Tissue With Frequency-Sensitive Damping Properties. *J. Biomech.* 126, 831. <https://doi.org/10.1115/1.1824133>
- Levins, A.D., Skinner, H.B., 1998. Adaptive Gait Responses to Plantar Heel Pain. *J. Rehabil. Res. Dev.* 35, 289–293.
- Lidstone, D.E., Deberardinis, J., Dufek, J.S., Trabia, M.B., 2019. Electronic Measurement of Plantar Contact Area Walking using an Adaptive Thresholding Method for Medilogic(R) Pressure-Measuring Insoles. *Foot* 39, 1–10. <https://doi.org/10.1016/j.foot.2019.01.009>
- Lidstone, D.E., Porcher, L.M., Deberardinis, J., Dufek, J.S., Trabia, M.B., n.d. Concurrent Validity of an Automated Footprint Detection Algorithm to Measure Plantar Contact Area during Walking. *J. Am. Podiatr. Med. Assoc.*
- Logan, B.M., 2012. *McMinn's Color Atlas of Foot and Ankle Anatomy*, 2nd ed. Saunders.
- MathWorks, 2018a. *fmincon* [WWW Document]. Documentation. URL <https://www.mathworks.com/help/optim/ug/fmincon.html>
- MathWorks, 2018b. *Choosing the Algorithm* [WWW Document]. Documentation. URL <https://www.mathworks.com/help/optim/ug/choosing-the-algorithm.html>
- Medilogic GmbH, 2017. *FAQ - Medilogic GmbH* [WWW Document]. URL <http://www.medilogic.com/en/information-portal/faq/> (accessed 1.31.17).
- Millard, M., Kecskeméthy, A., 2015. A 3D foot-ground model using disk contacts. *Mech. Mach. Sci.* 26, 161–169. https://doi.org/10.1007/978-3-319-10723-3_17
- Miller-Young, J.E., Duncan, N.A., Baroud, G., 2002. Material properties of the human calcaneal fat pad in compression experiment and theory. *J. Biomech.* 35, 1523–1531.
- Mithraratne, K., Ho, H., Hunter, P.J., Fernandez, J.W., 2012. Mechanics of the foot Part 2: A coupled solid-fluid model to investigate blood transport in the pathologic foot. *Int. j. numer. method. biomed. eng.* 28, 1071–81. <https://doi.org/10.1002/cnm.2493>
- Mohammed, M.A.P., 2014. Visco-hyperelastic model for soft rubber-like materials. *Sains Malaysiana* 43, 451–457.
- Naemi, R., Chatzistergos, P., Sundar, L., Chockalingam, N., Ramachandran, A., 2016. Differences in the mechanical characteristics of plantar soft tissue between ulcerated and non-ulcerated foot. *J. Diabetes Complications* 30, 1293–1299. <https://doi.org/10.1016/j.jdiacomp.2016.06.003>
- Nakamura, S., Crowninshield, R.D., Cooper, R.R., 1981. An analysis of soft tissue loading in the Foot — A preliminary report. *Bull. Prosthet. Res.* 18, 27–34.
- Natali, A.N., Fontanella, C.G., Carniel, E.L., 2012. *Computer Methods in Biomechanics and Biomedical*

- Engineering Constitutive formulation and numerical analysis of the heel pad region. *Comput. Methods Biomech. Biomed. Engin.* 15, 37–41.
- Natali, A.N., Fontanella, C.G., Carniel, E.L., 2010. Constitutive formulation and numerical analysis of the heel pad region. *Med. Eng. Phys.* 32, 516–522. <https://doi.org/10.1080/10255842.2010.539561>
- Ogden, R.W., 1972. Large Deformation Isotropic Elasticity - On the Correlation of Theory and Experiment for Incompressible Rubberlike Solids Author (s): R . W . Ogden Source : Proceedings of the Royal Society of London . Series A , Mathematical and Physical Published by : Proc. R. Soc. Lond. A. *Math. Phys. Sci.* 326, 565–584.
- Ogden, R.W., Saccomandi, G., Sgura, I., 2004. Fitting hyperelastic models to experimental data. *Comput. Mech.* 34, 484–502. <https://doi.org/10.1007/s00466-004-0593-y>
- Ong, F.R., Wong, T.S., 2005. Analysis of dynamic foot pressure distribution and ground reaction forces. *Proc. SPIE - Int. Soc. Opt. Eng.* 5852, 681–686. <https://doi.org/10.1117/12.621768>
- Pai, S., Ledoux, W.R., 2012. The shear mechanical properties of diabetic and non-diabetic plantar soft tissue. *J. Biomech.* 45, 364–70. <https://doi.org/10.1016/j.jbiomech.2011.10.021>
- Pàmies-Vilà, R., Font-Llagunes, J.M., Lugrís, U., Cuadrado, J., 2014. Parameter identification method for a three-dimensional foot-ground contact model. *Mech. Mach. Theory* 75, 107–116. <https://doi.org/10.1016/j.mechmachtheory.2014.01.010>
- Petre, M., Erdemir, A., Panoskaltsis, V.P., Spirka, T. a, Cavanagh, P.R., 2013. Optimization of nonlinear hyperelastic coefficients for foot tissues using a magnetic resonance imaging deformation experiment. *J. Biomech. Eng.* 135, 61001–12. <https://doi.org/10.1115/1.4023695>
- Riley, P.O., Paolini, G., Della Croce, U., Paylo, K.W., Kerrigan, D.C., 2007. A kinematic and kinetic comparison of overground and treadmill walking in healthy subjects. *Gait Posture* 26, 17–24. <https://doi.org/10.1016/j.gaitpost.2006.07.003>
- Robinson, C.C., Balbinot, L.F., Silva, M.F., Achaval, M., 2013. Plantar Pressure Distribution Patterns of Individuals with Prediabetes. <https://doi.org/10.1177/193229681300700503>
- Rome, K., Webb, P., Unsworth, A., Haslock, I., 2001. Heel pad stiffness in runners with plantar heel pain. *Clin. Biomech.* 16, 901–905. [https://doi.org/10.1016/S0268-0033\(01\)00081-X](https://doi.org/10.1016/S0268-0033(01)00081-X)
- Sarraffian, S.K., 1993. *Anatomy of the Foot and Ankle: Descriptive, Topographic, Functional*, 2nd ed. J.B. Lippincott Company, Philadelphia.
- Scott, S.H., Winter, D.A., 1993. Biomechanical model of the human foot: Kinematics and kinetics during the stance phase of walking. *J. Biomech.* 26, 1091–1104. [https://doi.org/10.1016/S0021-9290\(05\)80008-9](https://doi.org/10.1016/S0021-9290(05)80008-9)
- Selgrade, B.P., Chang, Y.-H., 2015. Locomotor control of limb force switches from minimal intervention principle in early adaptation to noise reduction in late adaptation. *J. Neurophysiol.* 113, 1451–1461. <https://doi.org/10.1152/jn.00246.2014>
- Shergold, O.A., Fleck, N.A., Radford, D., 2006. The uniaxial stress versus strain response of pig skin and silicone rubber at low and high strain rates. *Int. J. Impact Eng.* 32, 1384–1402.
- Shourijeh, M.S., McPhee, J., 2013. Efficient Hyper-Volumetric Contact Dynamic Modelling of the Foot within Human Gait Simulations, in: *Proceedings of the ASME 2013 International Design Engineering Technical Conferences and Computer and Information in Engineering Conference*. pp. 1–8.

- Shourijeh, M.S., McPhee, J., 2015. Foot–ground contact modeling within human gait simulations: from Kelvin–Voigt to hyper-volumetric models. *Multibody Syst. Dyn.* 35, 393–407. <https://doi.org/10.1007/s11044-015-9467-6>
- Sopher, R., Nixon, J., McGinnis, E., Gefen, A., 2011. The influence of foot posture, support stiffness, heel pad loading and tissue mechanical properties on biomechanical factors associated with a risk of heel ulceration. *J. Mech. Behav. Biomed. Mater.* 4, 572–582. <https://doi.org/10.1016/j.jmbbm.2011.01.004>
- Spears, I.R., Miller-Young, J.E., 2006. The effect of heel-pad thickness and loading protocol on measured heel-pad stiffness and a standardized protocol for inter-subject comparability. *Clin. Biomech.* 21, 204–12. <https://doi.org/10.1016/j.clinbiomech.2005.09.017>
- Stebbins, M.J., 2012. Obtaining Material Properties of the Plantar Soft Tissue for a Patient-Specific Finite Element Model of the Foot.
- Strickland, N., 2012. Compute double integrals in polar coordinates [WWW Document]. URL <http://neil-strickland.staff.shef.ac.uk/courses/MAS243/lectures/handout07.pdf>
- Su, K.H., Kaewwichit, T., Tseng, C.H., Chang, C.C., 2016. Automatic footprint detection approach for the calculation of arch index and plantar pressure in a flat rubber pad. *Multimed. Tools Appl.* 75, 9757–9774. <https://doi.org/10.1007/s11042-015-2796-x>
- Telfer, S., Woodburn, J., Turner, D.E., 2014. Measurement of functional heel pad behaviour in-shoe during gait using orthotic embedded ultrasonography. *Gait Posture* 39, 328–332. <https://doi.org/10.1016/j.gaitpost.2013.07.118>
- Thomas, V.J., Patil, K.M., Radhakrishnan, S., 2004. Three-dimensional stress analysis for the mechanics of plantar ulcers in diabetic neuropathy. *Med. Biol. Eng. Comput.* 42, 230–235. <https://doi.org/10.1007/BF02344636>
- Tong, J., Lim, C.S., Goh, O.L., 2003. Technique to study the biomechanical properties of the human calcaneal heel pad. *Foot* 13, 83–91. [https://doi.org/10.1016/S0958-2592\(02\)00149-9](https://doi.org/10.1016/S0958-2592(02)00149-9)
- Treloar, L., 1943. The physics of rubber elasticity. *Nature* 151.
- Trindade, B.M., Ono, Y., Lemaire, E.D., Almohimeed, I., 2014. Development of a wearable ultrasonic sensor and method for continuous monitoring of mechanical properties of plantar soft tissue for diabetic patients, in: *IEEE International Ultrasonics Symposium, IUS*. pp. 2112–2115. <https://doi.org/10.1109/ULTSYM.2014.0526>
- Urry, S.R., Wearing, S.C., 2001. A comparison of footprint indexes calculated from ink and electronic footprints. *J. Am. Podiatr. Med. Assoc.* 91, 203–209.
- Uzel, M., Cetinus, E., Ekerbicer, H.C., Karaoguz, A., 2006. Heel Pad Thickness and Athletic Activity in Healthy Young Adults: A Sonographic Study. *J. Clin. Ultrasound* 34, 231–236. <https://doi.org/10.1002/jcu>
- Valiant, G.A., 1984. A Determination of the Mechanical Characteristics of the Human Heel Pad In Vivo. The Pennsylvania State University.
- Wearing, S.C., Hooper, S.L., Dubois, P., Smeathers, J.E., Dietze, A., 2014. Force-Deformation Properties of the Human Heel Pad during Barefoot Walking. *Med. Sci. Sports Exerc.* 46, 1588–94. <https://doi.org/10.1249/MSS.0000000000000281>
- Wojtyra, M., 2003. Multibody Simulation Model of Human Walking. *Mech. Based Des. Struct. Mach.*

31, 357–379. <https://doi.org/10.1081/SME-120022855>

Yarnitzky, G., Yizhar, Z., Gefen, a., 2006. Real-time subject-specific monitoring of internal deformations and stresses in the soft tissues of the foot: A new approach in gait analysis. *J. Biomech.* 39, 2673–2689. <https://doi.org/10.1016/j.jbiomech.2005.08.021>

Zheng, Y., Choi, Y.K., Wong, K., Chan, S., Mak, A.F., 2000. Biomechanical Assessment of Plantar Foot Tissue in Diabetic Patients using an Ultrasound Indentation System. *Ultrasound Med. Biol.* 26, 1–20.

Zheng, Y.P., Huang, Y.P., Zhu, Y.P., Wong, M., He, J.F., Huang, Z.M., 2012. Development of a foot scanner for assessing the mechanical properties of plantar soft tissues under different bodyweight loading in standing. *Med. Eng. Phys.* 34, 506–511. <https://doi.org/10.1016/j.medengphy.2011.11.005>

Curriculum Vitae

Jessica DeBerardinis
deberardinis.jessica@gmail.com

Education

University of Nevada Las Vegas – Las Vegas, NV: GPA: 3.77

- Mechanical Engineering Ph.D., Post-Baccalaureate Track (Direct Ph.D. Program)
 - Dissertation Title: Developing a Plantar Tissue Stiffness Model
- Expected Graduation:

University of Utah – Salt Lake City, UT: GPA: 3.613

- Biomedical Engineering BS – Spring 2014

Experience

Skills

- Matlab – including extensive programming and Optimization, Computer vision, System Identification, and Image Analysis Toolboxes.
- Solidworks
- SPSS and R statistics – including analysis of variations, significance analysis, and correlation analysis
- Motion Capture System: Vicon Nexus 2.6
- High speed video collection: Phantom 640
- Gait analysis with pressure-measuring insoles: Medilogic
- Fibroblast cell culturing and imaging prototype bioreactors and fluorescent microscopy.
- Familiarity with machining processes, product design, and quality control.
- Familiarity with the Internal Review Board process to write, revise, and approve informed consents and protocols for human research

Professional Experience

Graduate Assistant, University of Nevada, Las Vegas – 2014 - 2018

- Led various teams of graduate and undergraduate students to design and implement experiments and analyze the results of those experiments.
- Identified and reviewed literature pertaining to research
- Designed and implemented experiments to collect data pertaining to: material characteristics of pressure-measuring insoles; the loads and deformations experienced by plantar tissue during walking; diabetic plantar pressure and the development of diabetic plantar ulcers.
- Developed mathematical models and assessed the validity of these models in Matlab

Team Leader, Bioengineering Design Class – 2014

- Became familiar with the process of design as regulated by the FDA and utilized this process to develop a medical device.

- Designed a medical device that would remove ingested narcotic packages efficiently without damaging the packaging of the narcotic package or harming the patient.
- Able to design, prototype our device, and verify that the prototype met specifications within one year.
- Was a team leader and led my team through the design process. Was responsible for the design plan, weekly meetings and updates, leading all design reviews, and ensuring all deadlines were met.

Engineer, BSD Medical Corporation – 2012-2014

- Wrote, released, and performed protocols and procedures pertaining to the testing, packaging, and use of the company's microwave ablation products.
- Designed and released new products and parts of products through engineering change orders (ECO's)
- Performed and reported various testing related to product verification and other product related testing.
- Designed and conducted a research project to investigate the effects of interfacing materials on the microwave ablation zone and presented that research in the Bioengineering Senior Undergraduate Research Symposium, April 2014.
- Attended clinical cases as a product consultant.

Undergraduate Research Assistant, Hitchcock Lab USTAR – 2011-2012

- Designed, manufactured, and tested new prototypes of bioreactors for growing cells in perfused environment.
- Tests included leakage tests, hydraulic permeability tests, and sterility tests.
- Also designed and tested new protein coating procedures for the polyurethane scaffold used to grow the cells.
- Presented and published research in 2012 Undergraduate Research Symposium

Lab Technician and Data Entry, Albion Laboratories, Inc. – 2007-2012

- Prepared and analyzed plant and soil samples using quality control protocols involving a UV Vis, elemental analyzer, pH meter, analytical balances.
- Supervised a plant analysis laboratory and organized the daily preparation and testing of samples.
- Supervised another coworker as they prepared and tested samples.
- Digitized journal articles and test results into the R&D database.

Publications

Peer Reviewed

Jessica DeBerardinis, Mohamed B. Trabia, Janet S. Dufek, Yann Le Gall, Nicolas Da Silva Sacoto, *Enhancing accuracy of the vertical component of ground reaction force during walking using pressure-measuring insoles*, Under review for the Journal of Rehabilitation and Assistive Technologies Engineering

Jessica DeBerardinis, Janet S. Dufek, Mohamed B. Trabia, *A Viscoelastic Ellipsoidal Model of the Mechanics of Plantar Tissues*, Under review at the Journal of Biomechanics

Jessica DeBerardinis, Conner Neilsen, Daniel Lidstone, Janet S. Dufek, Mohamed B. Trabia, *The Validity of Two Techniques for Center of Pressure Measurements*, Under Review at the Journal of Rehabilitation and Assistive Technologies Engineering

Daniel Lidstone, Jessica DeBerardinis, Janet S. Dufek, Mohamed B. Trabia, *Improved Accuracy of Plantar Contact Area Measurements from Pressuring Measuring Insole Using and Adaptive Sensor Thresholding Method*, The Foot, Vol. 39, pgs. 1-10, 2019

Daniel Lidstone, Louise Porcher, Jessica DeBerardinis, Mohamed B. Trabia, Janet S. Dufek, *Concurrent Validity of an Automated Footprint Detection Algorithm to Measure Plantar Contact Area during Walking*, The Journal of the American Podiatric Medical Association, Epub Nov. 2018.

Jessica DeBerardinis, Mohamed B. Trabia, Janet S. Dufek, Daniel Lidstone, *Assessing the validity of pressure-measuring insoles in quantifying gait variables*, Journal of Rehabilitation and Assistive Technologies Engineering, Vol 5, pgs 1-12, 2018.

Jessica DeBerardinis, Mohamed B. Trabia, Janet S. Dufek, *Review of Foot Plantar Pressure - Focus on the Development of Foot Ulcerations*, The Open Access Journal of Science and Technology, Vol. 3 2016

James Kennedy, Asad Rauf, Jessica Ashmead, John Lackey, Robert Hitchcock, *Perfused Tissue Model for Evaluation of Changes in Bulk Properties*, Journal of Medical Devices, Vol. 6, No. 1, 2012

Not Peer Reviewed

Jessica Ashmead, Robert Hitchcock *Development of a Bioreactor as a Platform for Cardiac Tissue Model*, University of Utah Undergraduate Research Abstracts, Vol. 12, 2012

Conferences and Symposiums

Podium Presentations

Daniel E. Lidstone, Louise M. Porcher, Jessica DeBerardinis, Mohamed B. Trabia, and Janet S. Dufek, *Concurrent Validity of an Automatic Technique to Calculate Plantar Contact Area at Mid-Stance during Gait*, 2017 Annual Meeting of the American Society of Biomechanics, Boulder CO, Aug 2017

Jessica DeBerardinis, David Samson, Mohamed Trabia, Janet Dufek, *The Effect of Walking Speed on the Dynamic Reliability and Validity of Pressure-Measuring Insoles*, Annual Meeting of the Mountain West Clinical Translational Research – Infrastructure Network, Las Vegas, NV, June 2015

Jessica DeBerardinis, *The Effects of Interfacing Materials on Microwave Ablation Zones*, Bioengineering Senior Undergraduate Research Symposium, Salt Lake City, UT, April 2014

Jessica Ashmead, Hitchcock Robert, *Development of an Advanced Platform for Cardiac Tissue Modeling*, UROP Symposium, Salt Lake City, UT, April 2012

James Kennedy, Asad Rauf, Jessica Ashmead, John Lackey, Robert Hitchcock, *Perfused Tissue Model for Evaluation of Changes in Bulk Properties*. Design of Medical Devices Conference, Minneapolis, MN, April 2012

Poster Presentations

Jessica DeBerardinis, Conner Neilsen, Daniel Lidstone, Janet S. Dufek, Mohamed B. Trabia, *Validity of Pressure-Measuring Insoles in Quantifying Center of Pressure*, Annual Meeting of the American Society of Biomechanics, August 2018.

Jessica DeBerardinis, Daniel Lidstone, Janet S. Dufek, Mohamed B. Trabia, *Elliptical estimation of Plantar Contact Areas during Walking*, Annual Meeting of the American Society of Biomechanics, August 2018.

Mathew Sunil Varre, Jessica DeBerardinis, Daniel E. Lidstone, Ashley Trotter, Mohamed B. Trabia, Janet S. Dufek, *Estimating Walking Speed using a Single Camera in the Plane of Progression*, Annual Meeting of the American Society of Biomechanics, August 2018.

Mathew Sunil Varre, Daniel E. Lidstone, Jessica DeBerardinis, Ashley Trotter, Mohamed B. Trabia, Janet S. Dufek, *Evaluation of Plantar Pressure Distribution in Prediabetic and Diabetic Individuals*, Southwest Chapter of the American College of Sports Medicine Annual Conference, October 2017

Daniel E. Lidstone, Jessica DeBerardinis, Anthony Ghanem, Ashley Trotter, Mathew Sunil Varre, Mohamed B. Trabia, Janet S. Dufek, *Characterization of Plantar Contact Area Error from Pressure-Measuring Insoles is Reduced using an Adaptive Sensor Threshold Method*, Southwest Chapter of the American College of Sports Medicine Annual Conference, October 2017

Ashley Trotter, Jessica DeBerardinis, Janet S. Dufek, Mohamed B. Trabia, *Reliability and Validity of Center of Pressure Measurements for Medilogic Insoles during Walking*, Undergraduate Research Week, Las Vegas NV, October 2017

Anthony Ghanem, Jessica DeBerardinis, Mohamed Trabia, Janet Dufek, Daniel Lidstone, *Identification of Hysteresis Behavior of Pressure-Measuring Insoles*, 2017 Summer Biomechanics, Bioengineering, and Biotransport Conference, Tucson AZ, June 2017

Jessica DeBerardinis, Daniel Lidstone, Janet S. Dufek, Mohamed B. Trabia, *Determining Gait Symmetry using Pressure-Measuring Insoles*, Gait and Clinical Movement Analysis Society Annual Conference, May 2017.

Daniel Lidstone, Jessica DeBerardinis, Louise M. Porcher, Mohamed B. Trabia, Janet S. Dufek, *Calculating the Area of Compressed Plantar Tissue during Gait*, Gait and Clinical Movement Analysis Society Annual Conference, May 2017.

Schwob Michael, Jessica DeBerardinis, Mohamed Trabia, Janet Dufek, *Identification of a Model Relating and Insole Sensor Signal to Ground Reaction Force*, 6th Annual Graduate Celebration, April 2016.

Michelle Quizon, Westley Davis, Jessica DeBerardinis, Mohamed B. Trabia, Janet S. Dufek, *Validation of the Ability of Pressure-Sensing Insoles to Measure Tissue Compression*, OUR-UNLV Undergraduate Research Showcase, October 2015.

Jeremy Letkiewicz, Jessica DeBerardinis, Mohamed B. Trabia, Janet S. Dufek, *Use of Pressure-Sensing Insoles to Measure Plantar Tissue Compression*, OUR-UNLV Undergraduate Research Showcase, October 2015.

Jessica DeBerardinis, David Samson, Mohamed Trabia, Janet Dufek, *Dynamic Reliability and Validity of Pressure-Measuring Insoles*, Annual Meeting of the American Society of Biomechanics, Columbus, OH, August 2015

Jessica DeBerardinis, David Samson, Mohamed Trabia, Janet Dufek, *Determination of Heel Deformation Using a Two-Camera System*, Annual Meeting of the Southwest Regional Chapter of the American College of Sports Medicine, Costa Mesa, CA, October 2014.

David Samson, Jessica DeBerardinis, Mohamed Trabia, Janet Dufek, *Methodology for Evaluating Heel Deformation Utilizing a Variable Sized Cursor Scan*, Annual Meeting of the Southwest Regional Chapter of the American College of Sports Medicine, Costa Mesa, CA, October 2014.

Awards, Recognitions, and Submissions

- College of Engineering Best Dissertation: 2019
- Barrick Research Fellowship: 2018
- Honorable Mention at the UMC 2018 Research Empowerment Day
- University of Nevada Las Vegas Grad Slam:
 - Regional Competitor: 2019
 - Audience Choice Finalist: 2018
 - Finalist: 2014 and 2016
 - Semifinalist: 2015
- Best Engineering Graduate Poster – 3rd place: 2015
- National Science Foundation Grant: 2015, unfunded
- Force and Motion Scholarship: 2014, unfunded
- Undergraduate Research Scholar Designation: 2014 at the University of Utah
- Competitor in the Invent competition: 2011 at the University of Utah
- Finalist in the TechTitans Competition: 2011
- Honorable Mention at the National Collegiate Inventors Competition: 2011
- Undergraduate Research Opportunities Program Participant: 2011-2012 at the University of Utah